ABSTRACT

Title of Document: LEVERAGING POROUS SILICON CARBIDE TO CREATE SIMULTANEOUSLY LOW STIFFNESS AND HIGH FREQUENCY AFM MICROCANTILEVERS

Sarice Shelton Barkley
Master of Science, 2014

Directed By: Associate Professor Santiago Solares
Department of Mechanical Engineering

Many operative modes of the atomic force microscope (AFM) are optimized by using cantilever probes that have both a low force constant and a high resonance frequency. Due to fabrication limitations, however, this ideal cannot be achieved without resorting to sizes incompatible with standard AFM instrumentation. This project proposes that cantilevers made from electrochemically etched porous silicon carbide (SiC) enjoy reduced force constants without significantly sacrificing frequency or size. The study includes prototype fabrication, as well as parametric experiments on the etching recipe and suggestions to improve the process. Analysis of the mechanical properties of the prototypes proves that introducing porosity to the structure greatly reduces the force constant ($k_{porous} \approx 0.27 k_{bulk}$) while only slightly reducing the resonance frequency ($f_{0,porous} \approx 0.86 f_{0,bulk}$).

LEVERAGING POROUS SILICON CARBIDE TO CREATE SIMULTANEOUSLY LOW STIFFNESS AND HIGH FREQUENCY AFM MICROCANTILEVERS

By

Sarice Shelton Barkley

Thesis submitted to the Faculty of the Graduate School of the
University of Maryland, College Park, in partial fulfillment
of the requirements for the degree of
Master of Science
2014

Advisory Committee:
Associate Professor Santiago Solares, Chair
Associate Professor Teng Li
Associate Professor Peter Chung

Dedication

To my parents,

Eric and Elizabeth Barkley

Acknowledgements

I would like to thank Prof. Santiago Solares, my advisor at the University of Maryland. Your mentoring has provided clarity in cases of both intellectual and emotional confusion. Thank you for your ongoing encouragement and support. As an extension of this, I would like to thank The Group: Alfredo Diaz Gonzalez, Enrique Lopez, Babak Eslami, Ben Warner, and Steve Oursler. Thank you for all of the laughs and guidance.

I would like to extend my deepest gratitude to Dr. Rachel Cannara and Dr. Fred Sharifi, for the innumerable hours of teaching, encouragement, and advice. Thank you for all you've done for me.

Next, I would like to thank Lisa Shimomoto, Dr. Richard Gates, Dr. Christian Long, and others who have assisted me for providing their time and expertise.

I would like to extend my gratitude to the other members of my committee, Prof. Teng Li and Prof. Peter Chung. I gratefully acknowledge funding through the Cooperative Research Agreement between the University of Maryland and the National Institute of Standards and Technology Center for Nanoscale Science and Technology, Award 70NANB10H193, at the University of Maryland.

Finally, I would like to thank my family and friends who have kept me grounded over the past few months. To my parents, brother, and sister: You have never stopped believing in me, supporting me, and inspiring me. Thank you for everything. And to Ben Jones: Thank you for the endless hours of support, advice, explanations, and joy. I love you all.

Table of Contents

List of Figures

List of Tables

Chapter 1: Introduction

1.1 Motivation: Improving the AFM

Since its invention in 1986, the atomic force microscope (AFM) [1] has had an extensive and ongoing impact in academic and industrial research. Beginning with a conceptually intuitive design and a single operative mode, it has evolved with the needs of the scientific community so that today it offers myriad innovative modes of operation that a user can choose from to image and characterize any sample on a nanoscale. This versatility makes it a powerful tool, and for this reason the AFM has found a niche in every sphere of scientific research [2-13]. Developments and improvements continue to appear in journals, yet rather than approaching exhaustion each reimagining opens opportunities for further growth. In this way, the AFM is relevant to modern science and is worthy of continued exploration.

1.2 The Problem: Inseparable probe mechanical properties

A key component of the instrument with need for improvement is the cantilever probe, a microscale resonator fundamental to the mechanism that makes AFM significant to the community. The mechanical properties of the cantilever determine the force range and sensitivity of an AFM experiment. What is considered an ideal combination of mechanical properties for a particular experiment depends on which mode of operation is used. For this reason, AFM cantilevers with a variety of mechanical properties are available commercially. However, current industrial fabrication methods are limited due to coupled relationships of the fundamental

parameters. The consequence is that many modes are theoretically optimized through the use of cantilevers with mechanical properties that are not readily available.

The most problematic example of this is due to the coupled relationship between the force constant k and resonance frequency f_0 of cantilevers. Many AFM modes of operation—such as contact mode, lateral force microscopy, and fast tapping mode—could benefit from the option to independently control these two properties. Unfortunately, modern fabrication methods do not have a way to offer this. The best available solution is cantilevers that are capable of having both low k and high f_0 by utilizing sizes smaller than are detectable by commercial AFMs [14-16]. The result is that researchers must either compromise optimized experimental conditions by choosing probes stiffer or slower than ideal, or purchase expensive additions to standard equipment.

1.3 Proposed Solution: Fabricating cantilevers from porous silicon carbide

One of the fundamental parameters that influence the k and f_0 values of a cantilever is the material's mass density ρ. Little exploration has gone into the impact of reducing the intrinsic ρ of a cantilever material by making it porous. This is largely because introducing porosity to the crystal structure of typical cantilever materials compromises mechanical integrity, and they may easily fail during experiments. However, reducing ρ would impact k and f_0 in opposing ways, allowing the reduction of the former without greatly changing the latter. Furthermore, its reduction does not require compromising cantilever size. This makes it extremely enticing, although seemingly inaccessible.

Silicon carbide (SiC) is a wide band gap semiconductor that has recently gained popularity as a potential material for AFM cantilevers [16-18]. It has many mechanical and electrical properties that are comparable or superior to silicon, the current leading material for AFM cantilevers. These properties include a low bulk mass density ($\rho_{SiC} = 1.4\rho_{Si}$) and a high elastic modulus ($E_{SiC} = 3E_{Si}$), which are parameters relevant to the resonator qualities.

Unlike porous silicon, which is extremely brittle and unusable for high frequency microresonators, porous silicon carbide maintains a rigid foam structure that is expected to retain its bulk robustness. Assuming this is correct, a successful process for reducing the material's mass density could produce cantilevers that have simultaneously low *k* and high f_0, while maintaining sizes compatible with standard AFM equipment. This has not previously been achieved, and so would offer a significant improvement to cantilever fabrication technology and AFM experimental methods.

1.4 Research Objectives

The primary objective of this project is to offer a proof of concept that cantilever mass reduction is a viable option for fabricating low *k*, high f_0 microresonators. Success of this objective would make possible the optimization of many AFM operative modes without sacrificing compatible cantilever sizes and would thus be extremely valuable to the AFM community.

To prove the proposal, the project will address three tasks. First, a process must be developed for generating porous structures in wafers of bulk SiC that maximize mass reduction while maintaining structural robustness. Pores will be

produced using an electrochemical etching process. Secondly, the mass reduction as a result of pore formation must be accurately quantified. This will be done using high resolution imaging with a scanning electron microscope (SEM) and focused ion beam (FIB). Thirdly, AFM cantilever probes must be formed from porous and bulk SiC. Mechanical properties of these cantilevers must be measured and compared to analogous cantilevers formed from bulk SiC. The proposal will be considered successful if one of the porous cantilevers' mechanical properties k or f_0 is improved compared to that of the bulk cantilevers' while simultaneously improving or maintaining the other property.

A secondary objective is to develop a process for creating porous SiC that is accessible to standard laboratory facilities. The electrochemical etching process should be reproducible with minimal dependence on specialized equipment. As will be demonstrated, the majority of the process can be done in-house with only a few steps requiring more advanced fabrication tools. These more advanced tools are available at most fabrication laboratories, including those at the University of Maryland.

Chapter 2: Background

2.1 The Atomic Force Microscope

2.1.1 History and modern relevance

When Binnig, Quate, and Gerber invented the atomic force microscope (AFM) [1], they revolutionized nanoscale characterization for the scientific community. It was originally intended to improve upon one of Binnig's earlier inventions, the scanning tunneling microscope (STM) [19], by expanding high resolution imaging capabilities to insulating samples. Today, the AFM is used for this and much more, and has become an essential tool for any laboratory concerned with sub-continuum properties.

The success of the tool is understandable. When it was proposed, it offered many unique capabilities that were impossible for other imaging tools available. For example, its most influential contemporaries, optical and electron microscopes, could only project a two-dimensional image. As a member of the scanning probe microscope family, the AFM provides an added dimension to its images. The AFM was also superior because it eliminated constraints on size and application that burdened its predecessors. At the time of the AFM's invention, optical microscopy could not achieve sufficient resolution to image below the diffraction limits of visible light, which has wavelengths ranging from 300 – 700 nm. This restriction became impractical as the scientific community strove to understand surfaces on the atomic scale. When electron microscopes were invented, this restriction was effectively eliminated by imaging with electrons instead of photons, thus achieving sub-

nanometer resolution. However, the concept requires that the sample be under vacuum and at least somewhat conductive. This precluded the imaging of biological samples without extensive preparation, which could fundamentally alter what was trying to be studied. Physical microscopes such as profilometers and the AFM are not restricted in these ways and can theoretically achieve atomic resolution on any sample, regardless of electrical properties and without the need for vacuum conditions. This expanded the availability of high resolution imaging for applications like biological and medical research [20-22].

Additionally, the fundamental concept of the AFM is elegant in its simplicity, making it easy to expand upon and improve. Furthermore, in addition to imaging, it is capable of measuring material properties and surface forces with nanoscale resolution. Therefore, since its invention in 1986, enthusiastic researchers have developed dozens of applications and modes of operation beyond its original purpose [2-13]. This has extended its impact to effectively every modern field of scientific research, making it one of the most versatile nanocharacterization tools available.

The point is not really to advertise, but to assert the significance of AFM in the scientific community. It is thus worthwhile to continue seeking ways to improve upon methods and instrumentation, and a significant idea can have a far-reaching impact.

This project suggests an improvement upon the AFM cantilever. This is a fundamental component of the AFM with direct influence on its capabilities. The success of this proposal is therefore expected to be an improvement for myriad AFM

applications, with classic contact mode [1], sensitive lateral force microscopy [5], and fast tapping modes [26] particularly in mind.

2.1.2 Basic Mechanics

Before going further it is helpful to establish a basic introduction to the instrumental mechanics. The AFM is made of a few key components: the piezoelectric scanners, a form of feedback control, and the force sensor. The most typical setup is depicted in figure 2.1.

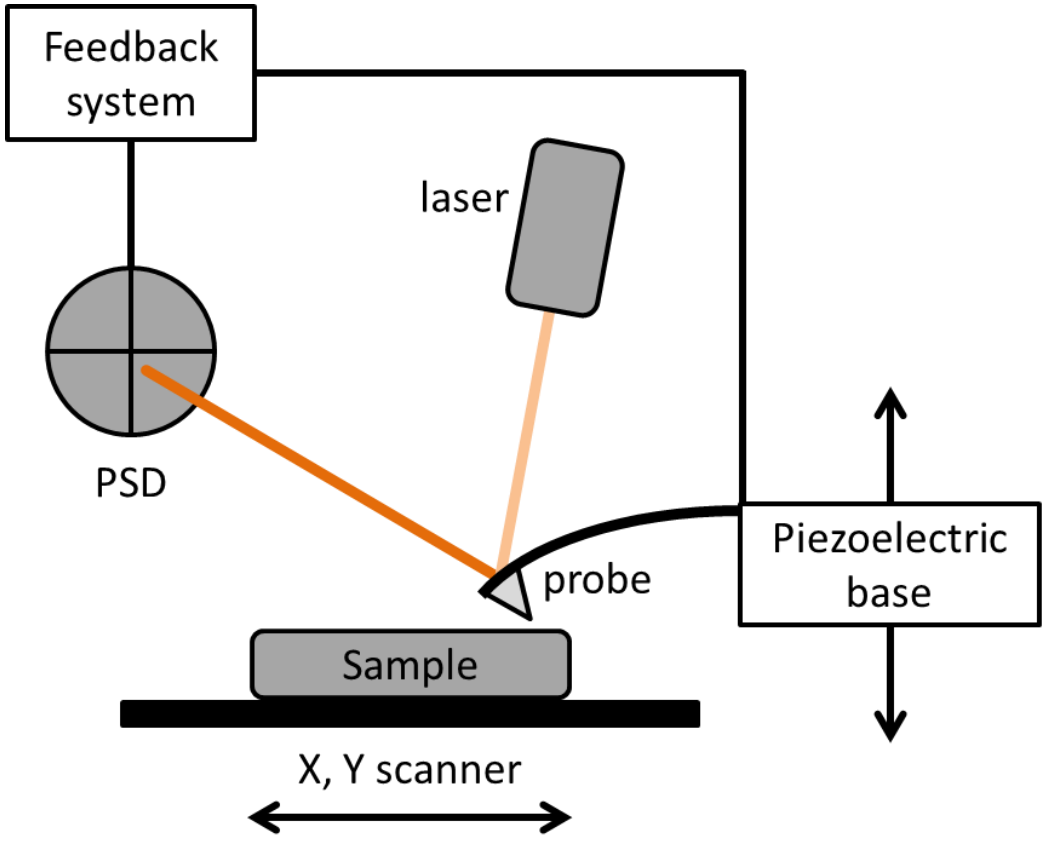

Figure 2.1: Schematic of a standard AFM. It consists of a cantilever probe, piezoelectric scanners at the sample stage and cantilever base, a laser that reflects onto a photo-sensitive diode array (PSD), and a feedback system.

In simple terms, the AFM can be thought of as a tactile microscope (as opposed to an optical one). Its most defining feature is a physical probe that is used to

"feel out" a sample, creating a map of nanoscale surface features and mechanical properties much like our fingers do on the macroscale. This makes it a member of the scanning probe microscope family, along with its predecessor the STM and other profilometers. The principle of this mechanism requires a finger (the probe), a way to move the finger (the piezoelectric scanners), and a way to interpret the response of the finger (the laser on the photosensitive diode array in conjunction with the feedback system).

For typical AFM setups, this probe is a cantilevered beam on the order of a hundred micrometers in length that is fashioned with a sharp, conical tip extending from the free end. The tip has an effective radius that ranges from a few nanometers to several micrometers. The base of this cantilever and the sample stage are controlled by piezoelectric actuators, which approach the probe to the sample in a highly controlled way. Lastly, a laser is reflected off of the free end of the cantilever and onto a photo-sensitive diode array (PSD) connected to a feedback system. This technique is known as an optical lever sensor (OLS), and it is used to monitor the minute deflections of the cantilever as it interacts with the sample. Attractive and repulsive forces act on the tip as it approaches and makes contact with the surface. These forces bend the cantilever torsionally and flexurally, deflecting the laser spot to different positions on the PSD laterally and vertically (figure 2.2). The relative position of the reflected laser spot on the PSD array corresponds to a voltage. The change in voltage across the array as the cantilever deflects the laser is transmitted to the feedback system and converted into a distance using the PSD's known optical

lever sensitivity, which has units of V/m. This distance is representative of how the tip-sample forces shift the probe from its equilibrium position.

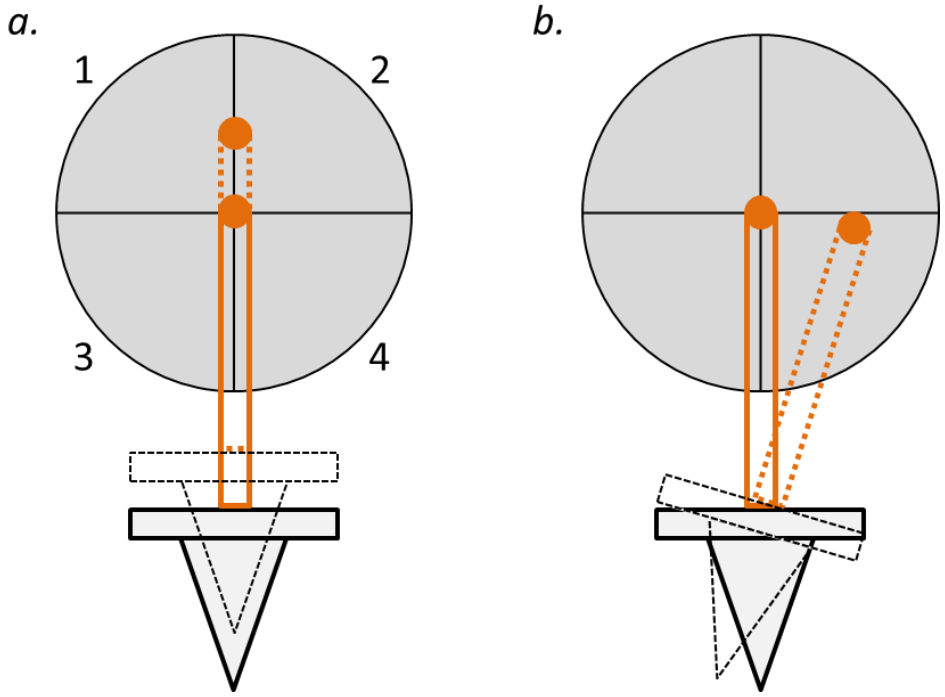

Figure 2.2: The optical lever sensor on a photo-sensitive diode array (PSD). Flexural movements of the probe correspond to vertical changes in the reflected laser's positon (a) and torsional movements correspond to lateral changes (b).

This system is an application of Hooke's Law:

$$F = -k \cdot \Delta x \tag{2.1}$$

The goal is to translate the probe's response into a force, which can be used to extract sample properties. The OLS quantifies the probe's change from its equilibrium position, Δx. Therefore, in order to translate the OLS measurement into a force, the probe's force constant *k* must be well known.

In this way, it is crucial to fully understand the dynamics of the cantilever supporting the probe. The most important mechanical properties of the cantilever dynamics are the force constant *k*, resonance frequency f_0, and quality factor *Q*. The

force constant is needed to quantify forces, as described above. Additionally, it determines sensitivity to sample features and interaction forces between the tip and sample. The latter two determine experimental parameter optimization (particularly in dynamic modes), scanning speed, and signal processing.

The force constant, resonance frequency, and quality factor are properties inherent to the AFM cantilever. They directly control the behavior of the probe, which is the source of information in AFM experiments. As a consequence, the capabilities of an experiment are defined by the limits of the cantilever's dynamics. For example, an experiment conducted in constant contact with the sample requires a relatively soft cantilever, in order to maintain high resolution and to preserve the probe and the sample. On the other hand, an experiment run in a dynamic mode must be able to oscillate the probe at high frequency to achieve high resolution and fast scanning times, and as such requires a cantilever with a high resonance. In this way, optimizing the cantilever properties to a particular AFM experiment is critical to the experiment's quality. However, what is considered optimal varies depending on the operative mode. The next section introduces three common operative modes and how their results depend on the dynamics of the cantilever.

2.2 Modes of Operation

The AFM enjoys dozens of operative modes that make it relevant to as many scientific fields [2-13]. Each of these modes is theoretically improved by taking advantage of cantilevers with specific mechanical properties. The following section describes a few of these modes that are improved specifically by using a cantilever

that has a combination of high f_0 and low k. The cantilevers proposed in this project would thus be applicable to these modes, as well as others not described.

2.2.1 Contact Mode

The original and most intuitive operative mode is contact mode [1], in which the probe comes into true contact with the sample. The cantilever is then dragged along the surface, and its flexural and torsional response to changes in sample height directly produces a topographical map of a surface.

Low force constant cantilevers are preferred in this mode for two reasons. First, the OLS depends on sufficient deflection of the cantilever to quantify changes on the PSD signal. The softer the cantilever, the more sensitive the probe is to small changes on the surface. In this way, softer cantilevers allow higher achievable resolution. Additionally, if a cantilever is too stiff, high interaction forces will quickly wear away or even break the tip. The image is highly dependent on tip shape; therefore, a worn or broken tip reduces the achievable resolution and compromises the accuracy of the images [27, 28]. High impact forces also run the risk of altering or ruining the sample [29]. For these reasons, contact mode experiments must use cantilevers with low k.

It is also preferable that contact mode cantilevers have high resonance frequencies. Environmental noise tends to exist mostly at low frequencies [30]. A low f_0 can bleed into these other low frequencies, reducing the quality factor Q and consequentially the sampling rates. This is due to noise in the feedback. In contact mode, the feedback tracks the forces read by the PSD and changes the height of the sample stage accordingly in an effort to keep the cantilever at a constant deflection.

However, noise in the feedback results in a non-constant deflection. As a consequence, the cantilever sees a non-constant force. This is a well-known phenomenon, so many AFMs implement a Fourier transform-based filter to remove this phantom force [31]. The Fourier transform translates the image from real space to frequency space and removes unwanted components. Unfortunately, if the Fourier transform of this non-constant force overlaps with the resonance frequency of the cantilever, the cantilever will get excited and vibrate. This is undesirable in contact mode. The lower the cantilever's f_0 is, the more likely the small variation in the contact forces will overlap with it. The faster one scans, the more this excitation influences the results. Thus, to mitigate these effects, the experiment must be run at slower scanning speeds.

In general for AFM, slower scanning speeds are not only inconvenient because they take longer; many samples experience some drift, affecting the image and measurement quality. Additionally, many biological samples deteriorate and require fast scan times to properly capture. Therefore, to maintain fast scan times, a cantilever with a sufficiently high f_0 must be used.

For all of these benefits of high resolution, low wear, and fast scan times, contact mode cantilevers can be optimized by having mechanical properties that are a combination of low k and high f_0.

2.2.2 Lateral Force Microscopy

Lateral force microscopy (LFM) is a modified version of contact mode [5]. In classic contact mode, the vertical deflection of the cantilever, measured as the difference in signal between the top and the bottom halves of the PSD, is primarily

used to study the sample. LFM, in contrast, focuses on the lateral signal taken from the difference between the left and right halves of the PSD. This minor distinction provides the user with information about the friction properties of the sample, which cannot be seen by the flexural mode. For reasons similar to contact mode, LFM is optimized by implementing cantilevers with low k and high f_0.

Sensitivity of the cantilever becomes a significant issue in LFM experiments. Cantilever beams by definition are longer than they are wide, and so lateral deflection is significantly less pronounced compared to flexural. For this reason, they theoretically require softer cantilevers to achieve the same sensitivity as an experiment in contact mode. However, in practice, LFM cantilevers often have similar force constants to those used in contact mode [32]. This is because the coupling between k and f_0 suffered by current fabrication methods forces a practical lower limit for k. Since LFM cantilevers must avoid too low a resonance frequency for reasons similar to those for contact mode, k values much softer than those used for contact mode applications are impractical.

Instead, alternative ways to strengthen the probe's lateral signal are implemented. These tricks include altering the geometry of the cantilever to emphasize the torsional mode or coating the tip with a material to create a larger tip-sample interaction area [32, 33]. However, deviating from uniform cantilever geometries requires a more complex model to analyze the dynamics. Moreover, applying a coat increases the tip's effective radius, thus reducing the achievable lateral resolution. Therefore, existing solutions are still not ideal, and as such LFM

experiments would benefit from cantilevers that can be made softer than those available without further reducing their resonance frequency.

2.2.3 Non-contact and Tapping Mode

The previous two examples described AFM operative modes that are improved by cantilevers with lower force constants, but in practice must compromise ideal *k* values to avoid having too low resonance frequencies. In this section dynamic modes are introduced, which have the opposite problem. These modes measure the dynamic oscillation of the cantilever, as opposed to the static deflection. Thus they are optimized by utilizing cantilevers with high f_0, in order to oscillate very quickly. However, the accompanying stiffness is typically very high, which can be impractical for certain cases [34].

The original purpose of the AFM was to offer high resolution imaging capabilities to nonconducting samples. Such a tool was a powerful advancement for the biological and medical fields, which were otherwise forced to dehydrate and coat samples in a conductive material in order to take images using electron microscopy, potentially contaminating or ruining them. However, the constant dragging of the original AFM mode occasionally applied unintentionally high forces to the sample due to capillary action at the tip-sample interface in ambient conditions [31]. This was not ideal for soft samples, such as biological tissues or polymers, as the high forces ran the risk of altering or tearing the sample. Additionally, applying a constant force to a soft sample could overpower surface features, eliminating them and thus resulting in an inaccurate representation of the sample.

To address this, Martin et al. developed non-contact mode AFM (NC-AFM) in 1987 [35]. As its name implies, the cantilever does not make direct contact with the sample in this mode. Instead, the cantilever is excited near its resonance frequency. Far away from the sample, the cantilever experiences no interaction forces and sustains its equilibrium resonance behavior (figure 2.3). Near the sample, attractive van der Waals forces shift the cantilever's resonance peak. The feedback loop watches these shifts and moves the cantilever to maintain either a constant amplitude (amplitude modulation, or AM-AFM) or constant frequency (frequency modulation, or FM-AFM). Thus, by tracking the change in tip-sample interaction forces, a topographical map of the sample surface can be created. Minimal contact between the tip and sample preserves both, allowing longer lifetimes and sustaining accuracy. However, measurable sample quantities are limited to topography in ambient conditions. Furthermore, theoretically ideal experimental parameters for NC-AFM can be difficult to achieve, and more so to maintain.

Tapping mode AFM is an alternative dynamic mode that offers a solution to some of these issues [26]. Tapping mode, also known as intermittent-contact mode (IC-AFM), similarly oscillates the cantilever near its resonance while maintaining a set amplitude or frequency. The distinction between the two is that this technique allows the probe to make contact with the sample, passing into the repulsive regime of the interaction forces (figure 2.3). Because the tip and sample make contact, more wear is associated with this method than with NC-AFM; however it is still relatively low compared to contact mode. Moreover, the contact allows measurement of sample properties besides topography in ambient conditions.

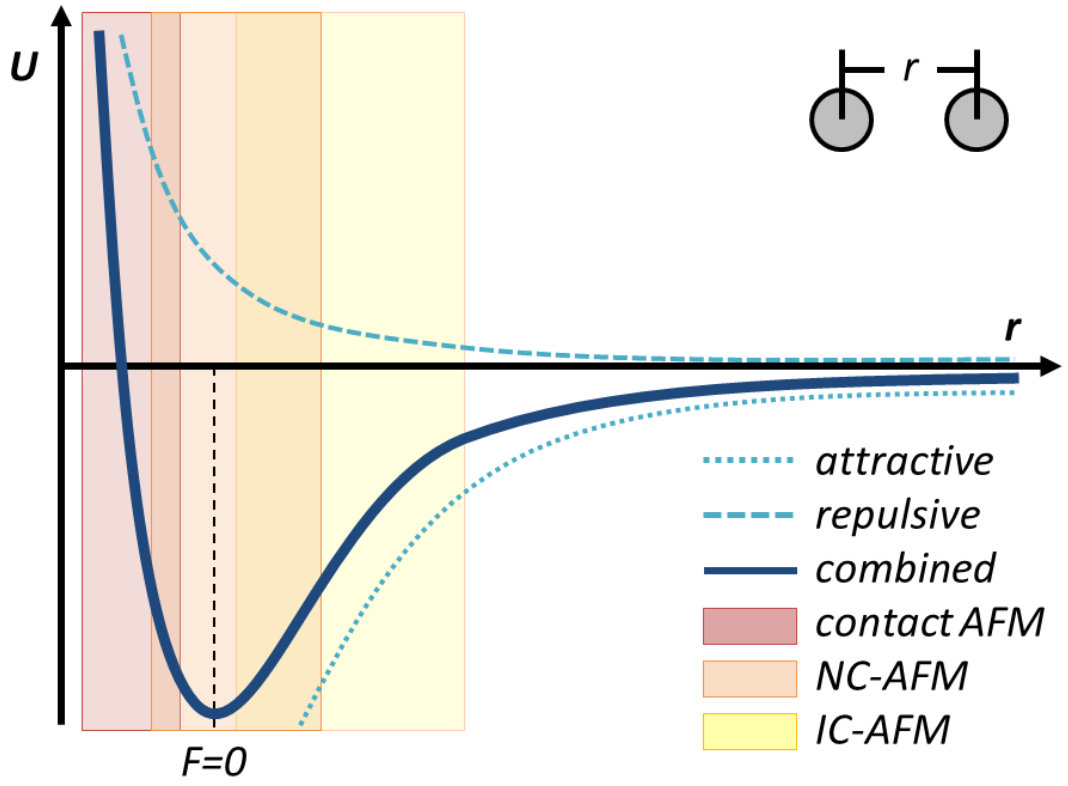

Figure 2.3: The potential well for the system takes a form similar to a Lennard-Jones potential, which approximates the interaction between atoms as a combination of van der Waals attraction forces and Pauli repulsion forces. In contact mode AFM, the probe is held in the repulsive regime. Non-contact mode (NC-AFM) attempts to hold the probe in the attractive regime. Tapping mode (IC-AFM) experiences a combination of the two.

In dynamic modes a high resonance frequency is essential for fast scanning and high resolution. This is because, intuitively, bringing the tip to the sample more times per second captures information in smaller increments. Also, because more signal processing is required, the results are less direct compared to contact mode measurements and thus tend to be slower. Finally, scanning at higher frequencies overcomes environmental noise that muddies the lower edge of the spectrum, as previously discussed. Sources of this low frequency interference include building vibrations, which typically range from 1 to 10 Hz, and acoustic vibrations, which can reach kHz range. There is additionally a phenomenon known as $1/f$ noise associated

with the AFM electronics, meaning at lower frequencies there is significant contribution to the signal that is not relevant to the interaction between the tip and the sample. Thus, the cantilever must be driven at high frequencies so that its response is clearly isolated from background noise. For these reasons of resolution, speed, and accuracy, dynamic modes tend to use cantilevers with high f_0.

As a direct consequence of this, the force constants of these cantilevers are also very high. In some ways high *k* cantilevers are preferable in dynamic modes, particularly for NC-AFM. A stiff cantilever is less likely to get stuck into contact with the sample. This occurs when the gradient of the force attracting the probe to the sample overcomes the cantilever's stiffness. However, in IC-AFM, the impact forces between the tip and sample increases with *k* so that, although the tip is making only intermittent contact with the sample, each tap inflicts high forces. Each of these taps potentially causes damage to the tip or sample. Whether this damage is gradual or sudden, these impacts often result in a sample that cannot be salvaged and a tip that can no longer be used. For this reason, tapping mode AFM cantilevers would benefit from being able to independently control *k* for high f_0.

It is significant to note that NC-AFM most often uses FM-AFM and IC-AFM most often uses AM-AFM. However, this is simply a trend and not a rule, and as such the terms cannot be used interchangeably. Care will be taken in future references to differentiate between FM- and AM-AFM.

In summary, contact mode, lateral force microscopy, and tapping mode are a few examples that illustrate how the mechanical properties of a cantilever influence

the quality of an AFM experiment and how there is a need in the field for a method to independently control the force constant and resonance frequency of the cantilever.

2.3 Commercial cantilevers

This section describes standard specifications of commercially available cantilevers, how they are typically made, and why k and f_0 cannot be independently controlled.

2.3.1 Standard probe specifications

The probe used in an AFM can theoretically be anything with the dynamics of a spring-like cantilever; in fact, early AFM probes were made from tungsten wire, and the original probe was made by gluing a diamond shard to the end of a thin strip of gold [1, 31]. Today, the conventional AFM probe takes the form of a rectangular silicon cantilever with a sharp tip at the free end and a larger chip supporting the clamped end, illustrated in figure 2.4. This chip can then be easily set into the piezoelectric actuator, which mechanically drives the probe at high frequencies. The chip has industrially standardized dimensions of approximately 3.5 x 1.6 x 0.5 mm to eliminate issues of compatibility across AFMs. It is usually made from silicon.

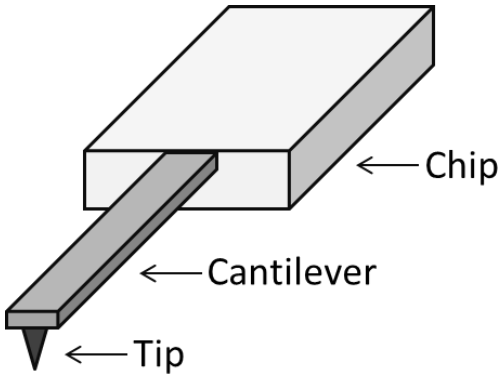

Figure 2.4: An illustration of the chip-cantilever-tip style probes most typical for AFM.

The tip at the free end is the true probe in the system, as it is what physically interacts with the sample. There is a variety of available tip specifications to accommodate different applications. Such options include the material, sharpness, or fabrication method, among others. The tip's effective radius can have a large range of anywhere from nanometers to microns. Intuitively, a sharper tip allows better achievable spatial resolution [36]. But sharpness is inevitably dulled with use. Therefore, it is preferable that the tips be made from a hard material that suffers low wear. However, this must also be balanced by cost—the probes are considered a disposable component of the tool and are replaced frequently. For this reason diamond tips are not necessarily common, and are reserved for experiments where hardness is crucial. Instead, the most common materials for AFM tips are silicon nitride (Si_3N_4) and silicon (Si) [31]. Si_3N_4 is used to fabricate probes with low force constants. They are usually fashioned monolithically from a Si_3N_4 cantilever (any component of the probe that can be formed monolithically from another reduces the number of joints and thus potential points for failure or excessive energy loss. It also ensures perfect clamping for a monolithically formed cantilever, which is a significant assumption made in the theory applied to analyze the cantilever's behavior. Therefore, monolithic probe components are preferred). However, the fabrication process of Si_3N_4 cantilevers tends to generate probes that retain some internal stress, which results in curvature along their primary axis at equilibrium. This curvature alters the cantilever's dynamics from what is expected in an unpredictable way and so is undesirable. Si tips are sharper than Si_3N_4 ones, and Si cantilevers have less of a problem with this internal stress. The entire chip-cantilever-tip can also be

easily fabricated monolithically. However, silicon tips are relatively brittle and thus have less of a lifespan. Still, silicon is the most common material used to fabricate optical lever-based AFM force sensors.

Silicon carbide (SiC) has recently been proposed as another promising tip and cantilever material [16-18]. It is already considered a leading semiconductor for its robustness in harsh environments, which may be relevant to some AFM applications, such as high temperature AFM [37]. It also offers high chemical stability and potential for tunable electrical conductivity. But even for more common applications, the low wear and low stiction of SiC would produce robust tips. It additionally has a relatively low mass density ($\rho_{SiC} = 1.4\rho_{Si}$) and high elastic modulus ($E_{SiC} = 3E_{Si}$), which are favored material properties for their influence in raising the cantilever's resonance frequency. This project takes advantage of these properties and others to create modified SiC cantilevers.

The AFM is capable of being so diverse largely because there are so few restrictions on the probe. Because of this, the probe can be altered extensively to make possible or improve upon a particular application. For example, a tip can be coated with a conductive material for electric force microscopy or a magnetic material for magnetic force microscopy [6, 9]. Additionally the cantilever's shape can be modified to change its dynamic response, as in the case of V-shaped cantilevers used to mitigate twisting along the primary axis and T-shaped cantilevers used to emphasize it [33, 38]. With this versatility in mind, this project aims to form low *k*, high f_0 cantilevers out of porous material, which has only been narrowly explored due to limited success finding a porous material that is suitably stable.

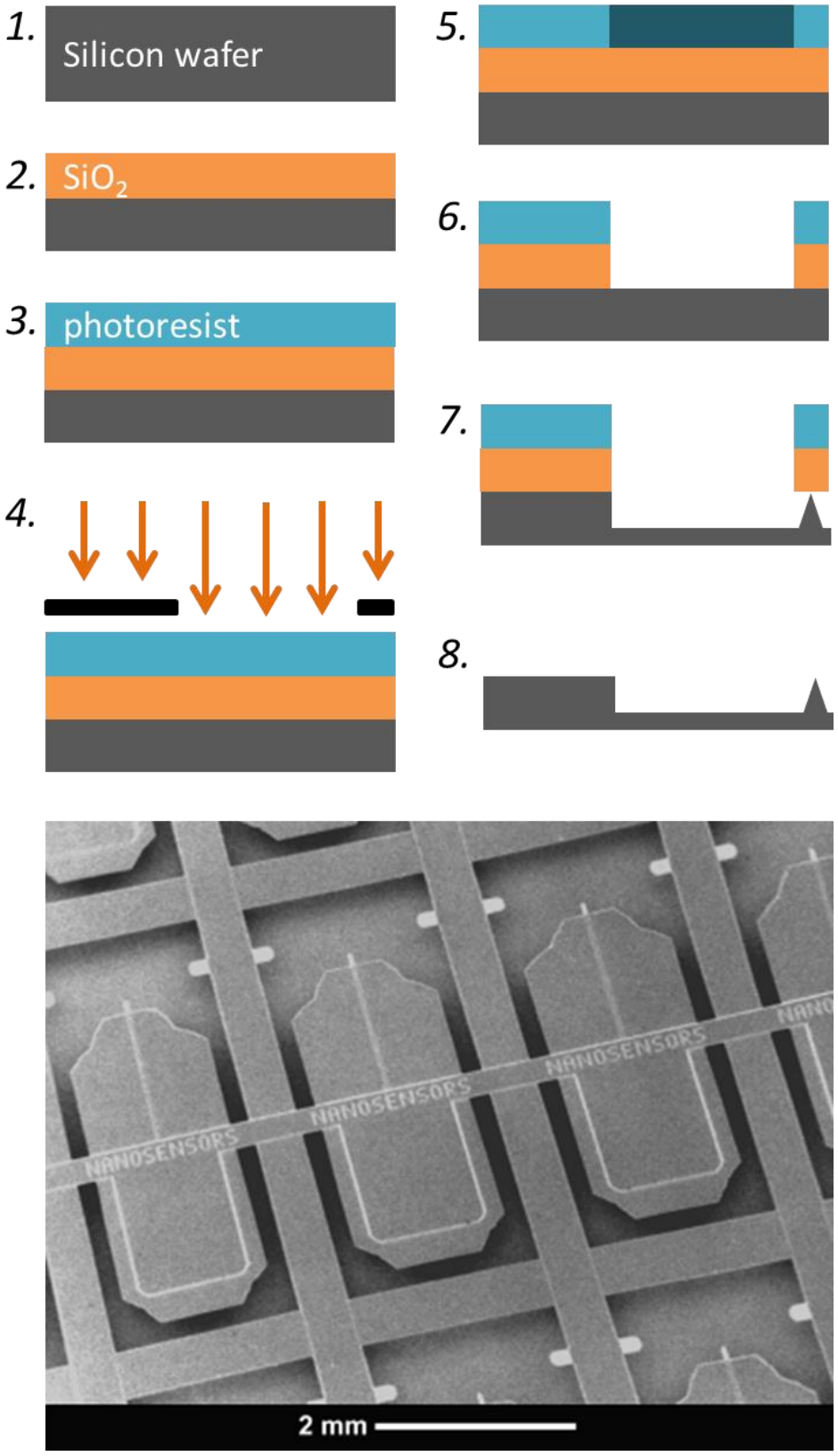

Figure 2.5: The Wolter fabrication process, described below. Image of probe array from [39].

2.3.2 Fabrication methods of industrial cantilevers

The original AFM probes fashioned from foil and diamond shards were sufficient but lacked consistency. As the AFM became more popular, the need grew for more and better probes. This need was met in 1990 by Olaf Wolter, who developed a method by combining semiconductor manufacturing and wet etching technologies to create the first batch-fabricated AFM probes [40].

The original Wolter lever method has since evolved to accommodate specific needs, but the concept remains the same. Today, the typical process for creating Si AFM probes begins with oxidizing both faces of the Si wafer to create a protective layer of silicon dioxide (SiO_2). Then, photoresist is deposited on each side, which can be patterned so that only specified areas are vulnerable to etchant. The wafer can then be etched in a highly controlled way to form the chip, cantilever, and tip structures. Figure 2.5 illustrates the process. A batch of over 1000 probes can be made from a single 6-inch silicon wafer this way [39]. Similar techniques could be implemented to produce bulk or porous SiC AFM probes.

2.3.3 Mechanical properties of industrial cantilevers

Commercially available cantilevers strive to offer a range of mechanical properties to accommodate the needs of different experiments [41]. However, k is directly coupled with f_0, making this difficult. For example, contact mode cantilevers tend to be soft and slow, with force constants less than 1 N/m and resonance frequencies below 100 kHz. Dynamic mode cantilevers, on the other hand, are stiff and fast, with force constants greater than 10 N/m and resonance frequencies of

several hundreds of kHz and even up to MHz range. As was explained in section 2.2, this trend can be non-ideal for many applications.

A few cantilevers are available that have low k (0.02-0.2 N/m) and high f_0 (1-2 MHz) [14, 15]. To achieve this, the cantilevers are very small: 9.0 × 2.0 × 0.1 μm. However, AFM laser spot sizes are typically on the order of 10 × 30 μm. Smaller spot sizes of 3 × 9 μm are available with added modules. Cantilevers that are much smaller than the laser spot size, such as the ones described, are undetectable by the AFM. In order to detect them, expensive additions must be purchased and installed. This project proposes an option to avoid this issue altogether by offering an alternative way to independently modify k and f_0 that does not require compromising the size of the cantilever.

For effectively all AFM applications, signal processing and scan speeds drive the ideal cantilever towards having as high a resonance frequency as possible. Resonance frequency, as a function of fundamental parameters, is given as

$$f_0 = \frac{1}{2\pi}\sqrt{\frac{k}{m_{eff}}} = \frac{1}{2\pi}\sqrt{\frac{3 \cdot E \cdot I(L,w,t)}{L^3 \cdot (0.24 \cdot \rho \cdot V(L,w,t))}} \tag{2.2}$$

where m_{eff} represents the distributed mass of a tipless cantilever, $0.24\rho V$. The area moment of inertia I and volume V are determined by the cantilever's geometry in terms of its dimensions length L, width w, and thickness t. The elastic modulus E and mass density ρ are then the material properties determined by the material from which the cantilever is formed.

Today's state-of-the-art high f_0 cantilevers are produced by a collaborative effort between the Photonics and Nanostructures Laboratory and the Center for

Materials Elaboration and Structural Studies [16]. Their cantilevers are made out of bulk SiC for its low mass density and high elastic modulus. After thus maximizing the contribution of material properties to f_0, the remaining modifiable parameters are the cantilever's dimensions. These are minimized to leverage the strong inverse relationship on L and $V(L, w, t)$. The resultant cantilevers are capable of reaching 150 MHz using sizes as small as 4.0 × 1.2 × 0.5 μm. However, they are incredibly stiff and are dimensionally incompatible with standard AFMs. Thus they are expensive to detect and impractical for use outside of NC-AFM imaging.

2.4 Restatement of project proposal

This project proposes to use porous silicon carbide to create cantilevers with low force constants while maintaining relatively high resonance frequencies. Silicon carbide is an ideal material for this endeavor for several reasons. First of all, bulk SiC is already considered an advantageous AFM probe material for its material properties like low wear and low stiction [16-18]. Therefore, SiC is established in the literature and in industrial fabrication equipment, so that minimal modification to existing processes is required. Secondly, while other popular AFM cantilever materials such as silicon become unstable after introducing porosity, it is believed that proper fabrication of porous silicon carbide will produce a rigid foam structure that will maintain the robust qualities of bulk SiC, such that it will be able to withstand high force impacts and high frequency oscillations necessary for use as an AFM cantilever.

Success of this project will greatly benefit the AFM community. Many commonly used operational modes of AFM must currently sacrifice resolution, speed, and other important experimental parameters as a consequence of the coupled

relationship between k and f_0. By providing an alternative method to independently modify these mechanical properties, future experiments in these modes will have more control over the dynamics dictating the experiment, and thus higher quality results. This is especially significant since this particular combination of low k and high f_0 has been up to this point unattainable outside of miniscule cantilevers incompatible with standard AFM equipment.

Chapter 3: Theory

3.1 The cantilever dynamics

It is advantageous to understand well the cantilever dynamics when attempting to improve them. This section provides a discussion of the dynamics from several perspectives. We will start with a point-mass analysis, which simplifies the probe to a point-mass oscillator. Then, we will apply an Euler-Bernoulli model to capture the dynamics of the larger cantilever system. Finally, we will include a compilation of the most relevant parametric relationships and a discussion of how they will direct our goals and influence our results.

3.1.1 Point-mass analysis

The dynamic properties of the cantilever are most simply described by reducing the probe and sample to a point-mass in a damped, single-degree-of-freedom vibratory system, such as is shown in figure 3.1.

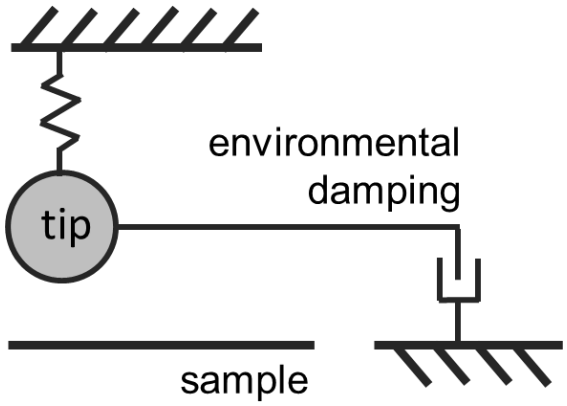

Figure 3.1: The point-mass model for the tip and sample.

Although it appears to be oversimplified, this model faithfully captures the dynamics of the tip interacting with the sample, which can be extended to good

approximation to the behavior of the cantilever as a whole. The equation of motion for this system is

$$m_{eff}\ddot{u} + c\dot{u} + ku = F(u,t) \tag{3.1}$$

Here, $u(t)$ is the position of the tip and overdots indicate temporal derivatives. The effective mass m_{eff} is again used to represent the distributed mass of the cantilever. Viscous damping is quantified using the coefficient *c* and the stiffness in the system derives from the force constant *k* of the cantilever.

The forcing term $F(u,t)$ is the sum of externally applied loads on the probe and includes not only the driving force from the piezoelectric actuators, but also the forces due to the interaction of the tip and the sample. However, from far away, these interaction forces are negligible. Thus we can begin the analysis by applying a solely time-dependent forcing function $F(t) = A_0 \sin(\omega t)$. This force is representative of the tip's reaction to the displacement applied by the piezoelectric actuators at the cantilever's base. Forcing the cantilever such that $\omega \approx \omega_0$is the basis of dynamic AFM modes. To analyze the system response, we solve equation 3.1 for $u(t)$ in steady state to get

$$u(t) = u_0(\omega)\sin(\omega t - \phi) \tag{3.2}$$

where

$$u_0(\omega) = \frac{A_0}{\sqrt{(k - m_{eff}\omega^2)^2 + c^2\omega^2}} = \frac{A_0/m_{eff}}{\sqrt{(\omega_0^2 - \omega^2)^2 + (\omega\omega_0/Q)^2}} \tag{3.3}$$

and

$$\tan(\phi) = \frac{c\omega}{k - m_{eff}\omega^2} \tag{3.4}$$

Here, the angular resonance frequency $\omega_0 = 2\pi f_0 = \sqrt{k/m_{eff}}$ and the quality factor $Q = m_{eff}\omega_0/c$ are introduced. The quality factor is used as a way to quantify the relative width of the resonance peak and will be explained in greater depth later in section 3.1.3.

The significance of this result is to see from equation 3.3 that as the driving frequency ω approaches the cantilever's resonance frequency ω_0, the response of u_0 becomes very high and is tempered only by the environmental and internal damping inherent to physical systems. Sensitivity of dynamic AFM modes depends on a high amplitude response of the cantilever near its resonance frequency. The amount of damping, expressed by the quality factor, is augmented by contributions from nearby frequency peaks, dulling the response of the driven probe. Therefore, in order to excite a large response at the tip, it is preferred to have a resonance frequency significantly above the peaks due to external noise that occupy the lower end of the frequency spectrum.

At this point we have considered the response of the probe due to a solely time-dependent driving force when isolated from the sample. There is additionally, however, a spatial-dependent force at close distances. As the tip of the probe approaches the sample, attractive van der Waals and Pauli repulsive forces (recall from figure 2.3) shift the resonance frequency of the tip—specifically, reducing the frequency when the tip is in the attractive regime and increasing it in the repulsive regime. It is this resonance shift that allows surface forces to be analyzed. To show this, we begin by writing the force on the tip as that of a spring displaced from its

equilibrium position ($u_0$without external forcing), $F_{sp}(u) = -k(u - u_0)$. Knowing that $F = -\nabla U$, the potential energy of the deformed spring is written as

$$U = \frac{1}{2}k(u - u_0)^2 \tag{3.5}$$

from which we see that

$$\frac{\partial^2 U}{\partial u^2} = k \tag{3.6}$$

Now the contribution due to the tip-sample interaction forces can be included and expanded in a Taylor series about the tip's equilibrium position ($u_0{}^*$ with external forcing) in the following way:

$$\begin{aligned} F(u) &= F_{sp}(u) + F_{TS}(u) \\ &\approx -k(u_0{}^* - u_0) + F_{TS}(u_0{}^*) + \left(k - \frac{\partial F_{TS}(u_0{}^*)}{\partial u}\right)(u - u_0{}^*) + \cdots \end{aligned} \tag{3.7}$$

The first two terms cancel, such that the overall forcing simplifies to

$$F(u) \approx -\left(k - \frac{\partial F_{TS}(u_0{}^*)}{\partial u}\right)(u - u_0{}^*) \tag{3.8}$$

Therefore, the effective spring constant of the system in the presence of tip-sample forces is

$$k_{eff} = k - \frac{\partial F_{TS}(u_0{}^*)}{\partial u} \tag{3.9}$$

This result implies that attractive interaction between the tip and the sample opposes the restoring force, corresponding to a positive gradient and decreasing the effective spring constant. Conversely, a repulsive interaction leads to a larger effective spring

constant. This in turn shifts the effective resonance frequency, which is one of the fundamental concepts of dynamic AFM.

It is from this result that the cantilever experiences a "snap" into contact with the sample, due to the gradient of the interaction forces overcoming the stiffness of the cantilever. If the cantilever has a relatively low inherent force constant, the force gradient required to overcome it is small and the tip strikes the sample. This snap into contact potentially damages the tip and the sample. For this reason, NC-AFM cantilevers should be stiff (to prevent snapping into contact by requiring a very high a force gradient) and IC-AFM cantilevers should be softer (to mitigate snap-in force, thus preserving tip and sample).

3.1.2 Euler-Bernoulli analysis

While approximating the probe as a point-mass is useful to derive much of the cantilever's behavior, it fails to capture the motion of the cantilever as an extended body. The most significant consequence of this is the loss of information in regards to the cantilever's higher modes of vibration and the significance of the particular boundary conditions. By applying an Euler-Bernoulli beam model, we can express the shape and frequency of these higher eigenmodes and discuss the influence of assuming perfect clamping [42].

The Euler-Bernoulli model assumes a long, narrow beam. Thus it is applicable to AFM cantilevers, which are often longer than they are wide by at least a factor of ten. For our application we assume a beam of uniform properties, including mass per unit length ρ_L(as opposed to the volumetric density denoted by ρ), elastic modulus E, area moment of inertia I, and cross-sectional area A.

The equation of motion for a uniform beam is

$$EI\frac{\partial^4 w(x,t)}{\partial x^4} + \rho_L A\frac{\partial^2 w(x,t)}{\partial t^2} = F(x,t) \tag{3.10}$$

where different coordinates have been applied to distinguish this analysis from the point-mass. The four boundary conditions for a cantilevered beam are

1. $w(0,t) = 0$, stating that the base of the beam does not experience deflection.
2. $w'(0,t) = 0$, stating that the slope of the base is zero.
3. $w''(L,t) = 0$, modeling the theory's assumption that there is no bending moment at the cantilever's free end.
4. $w'''(L,t) = 0$, modeling the theory's assumption that there is no shearing force acting at the cantilever's free end.

To solve the equation of motion, the solution is separated into purely spatial and purely temporal expressions. Applying boundary conditions to the spatial expression $Y(x)$ yields the eigenfunctions of the form

$$Y_r(x) = A_r\left[\sin\beta_r x - \sinh\beta_r x - \frac{\sin\beta_r L + \sinh\beta_r L}{\cos\beta_r L + \cosh\beta_r L}(\cos\beta_r x + \cosh\beta_r x)\right], \quad r = 1, 2, \ldots \tag{3.11}$$

where β_r comes from the characteristic equation as

$$\beta_r = \sqrt[4]{\frac{{\omega_r}^2\rho_L}{EI}}, \qquad r = 1, 2, \ldots \tag{3.12}$$

These eigenfunctions give the shapes of the cantilever modes, as shown in figure 3.2. The first three natural frequencies given by β_r are

$$\omega_1 = 3.52\sqrt{\frac{EI}{\rho_L L^4}},\ \omega_2 = 22.04\sqrt{\frac{EI}{\rho_L L^4}}, \omega_3 = 61.70\sqrt{\frac{EI}{\rho_L L^4}}$$

(3.13)

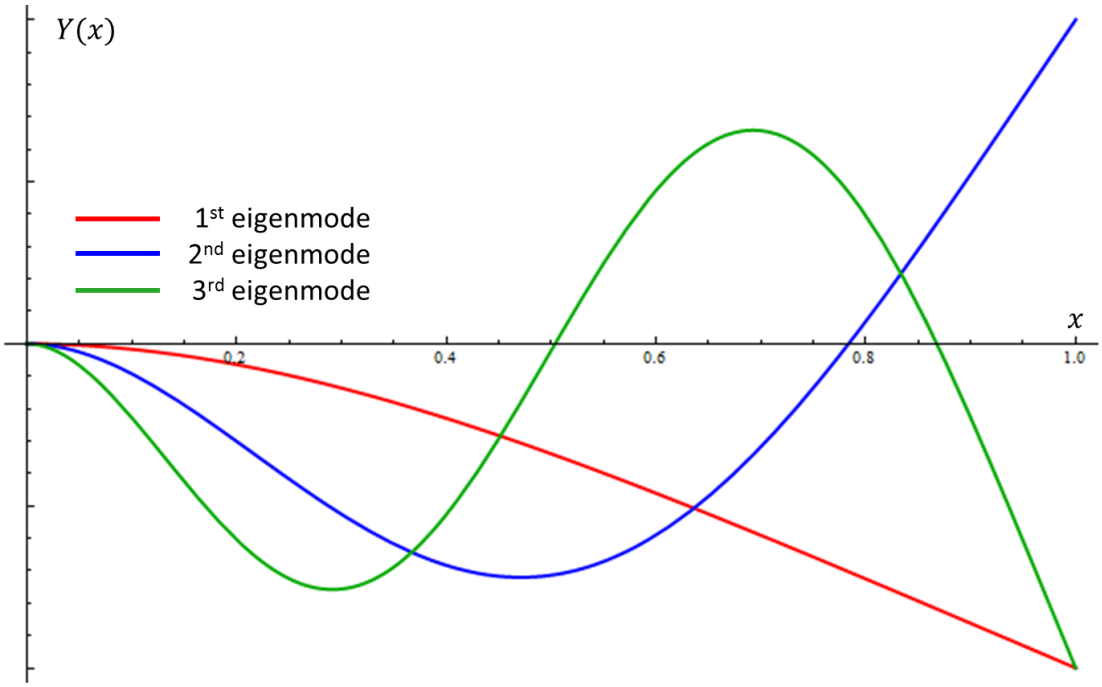

Figure 3.2: The first three eigenmodes for a cantilever beam.

The significance of this analysis is that these results are based on the assumption of a perfectly clamped beam. In the case of an imperfectly clamped beam, the resonance frequencies of the higher modes will not be where the theory predicts—namely, imperfect clamping results in a softer effective force constant, thus reducing the natural frequencies. This concept was used to check the quality of the clamping for the fabricated cantilevers. If the resonance peaks of higher modes are lower than predicted by the theory, the cantilever is imperfectly clamped.

3.1.3 Mechanical properties

The mechanical properties of the cantilever dictate its response to forcing. The three most significant properties are the force constant *k*, the resonance frequency f_0, and the quality factor *Q*. Again, these properties depend on a few fundamental properties, including the cross-sectional area. In the following discussion of these properties, the relevant cross-section will be explicitly stated as rectangular or equilaterally triangular (figure 3.3). The latter is considered because it applies to the cantilevers made in this project. The former is considered because it is more commonly used in practice and theory, and therefore helpful as a point of reference and as a future goal.

The force constant, also referred to as the spring constant or the stiffness of the cantilever, measures the mechanical compliance of the structure in response to an applied force. Rearranging Hooke's relation for a spring (equation 2.1), we can determine the deflection at the end of the cantilever by

$$\Delta x = -\frac{L^3}{3EI}F \tag{3.14}$$

where we have substituted in the equation for *k* in terms of fundamental parameters. From this it is clear that small lengths such as those used to create high frequency cantilevers result in small deflections, reducing the cantilever's sensitivity to small surface features. The area moment of inertia *I* depends on the cantilever's cross section. In the case of a rectangular cross section, the flexural moment is

$$I_{rect} = \frac{wt^3}{12} \tag{3.15}$$

which can be used to find

$$k_{rect} = \frac{Ewt^3}{4L^3} \tag{3.16}$$

In the case of an equilaterally triangular cross section, these equations are instead

$$I_{tri} = \frac{w^4}{32\sqrt{3}} \tag{3.17}$$

and

$$k_{tri} = \frac{\sqrt{3}Ew^4}{32L^3} \tag{3.18}$$

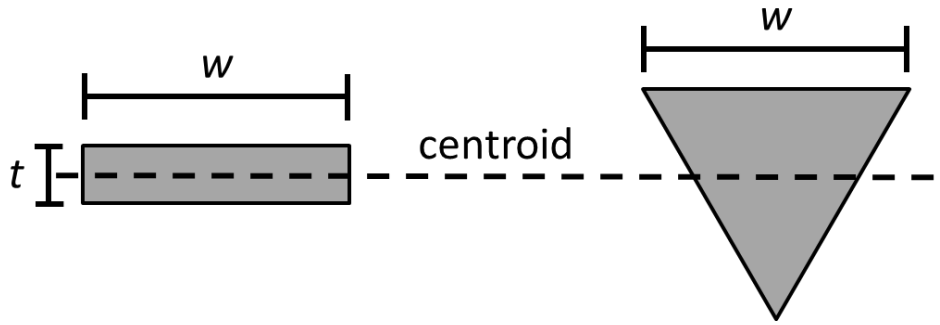

Figure 3.3: The dimensions and centroids of the two considered cross-sections.

Additionally, there are moments and force constants associated with the torsional and lateral modes. As was described in section 2.2.2, lateral force microscopy (LFM) is an example of an AFM mode that takes advantage of these other degrees of freedom to take unique measurements. The difference between the force constants of these modes of motion comes from the differences in the area moments of inertia due to the motion being about a different axis. For a rectangular cantilever, the moments are

$$I_x = \frac{wt^3}{12} \qquad I_y = \frac{w^3t}{12} \tag{3.19}$$

Since the cantilever's width is often much greater than its thickness, this leads to much higher force constants about the y-axis. In fact, the stiffness of this mode is so much higher than the flexural force constant that many applications consider lateral motion of the cantilever to be effectively negligible. On the other hand, due to the symmetry of an equilateral triangular cross section, the lateral and flexural force constants are identical. This is another advantage of rectangular cross-sections, if motion along other modes is undesirable.

The resonance frequency also plays a significant role in the dynamics. In the interest of signal processing, an ongoing goal of cantilever fabrication is to achieve as high a resonance frequency as possible while still balancing the needs of other parameters. The resonance frequency of the lowest vibrational mode rewritten from equation 2.2 is given by

$$f_0 = 0.56\sqrt{\frac{E \cdot I(L,w,t)}{L^3 \cdot \rho \cdot V(L,w,t)}} \tag{3.20}$$

assuming a tipless cantilever with no external forces. By inspection, the most effective way to raise the frequency is by scaling down the volume, which takes advantage of the heavy dependence on L. However, k is similarly heavily dependent on L. It is for this reason that k and f_0 are so problematically coupled that commercial cantilevers are rarely both soft and fast.

The inspiration for this project comes from the fact that the mass density ρ of the cantilever is the only property available that can be used to potentially lower k while maintaining f_0. This is because reducing ρ, which raises f_0, simultaneously

reduces the elastic modulus E, which reduces both f_0 and k. The counteracting effects on f_0 should mitigate any change while softening k.

The quality factor Q is another significant aspect of the cantilever dynamics. It is a dimensionless parameter that rises from the environmental and internal damping of the system and quantifies the rate of energy transformation in a system. Higher Q indicates a lower rate of energy loss relative to the stored energy of the resonator, meaning that the oscillations die out more slowly. In FM-AFM, less internal energy loss leads to a cantilever that is more sensitive to variations of the tip-sample forces, resulting in a faster system response. In AM-AFM, high Q leads to long transients, and thus a slow system response. Typical values for Q of a silicon cantilever in vacuum range from 10,000 – 100,000. This is reduced to a range of 200 – 400 in ambient conditions.

An alternative perspective is that the quality factor is a measure of the resonant width of the cantilever. In the case of an undamped oscillator, driving the system at its resonance results in an unbounded response, as can be seen from equation 3.3 by removing the term dependent on Q. Internal damping in the system moderates this response, to a degree described by Q. High Q indicates a tight resonant width and low damping. As damping gets larger, the peak becomes more muted, and the width of the peak broader (figure 3.4). Furthermore, nearby resonant peaks leech energy from the cantilever's, further reducing Q. Thus a reasonably high Q generates a cantilever response distinct from external contributions. However, if the resonance frequency is sufficiently high, Q can be low without causing significant issue.

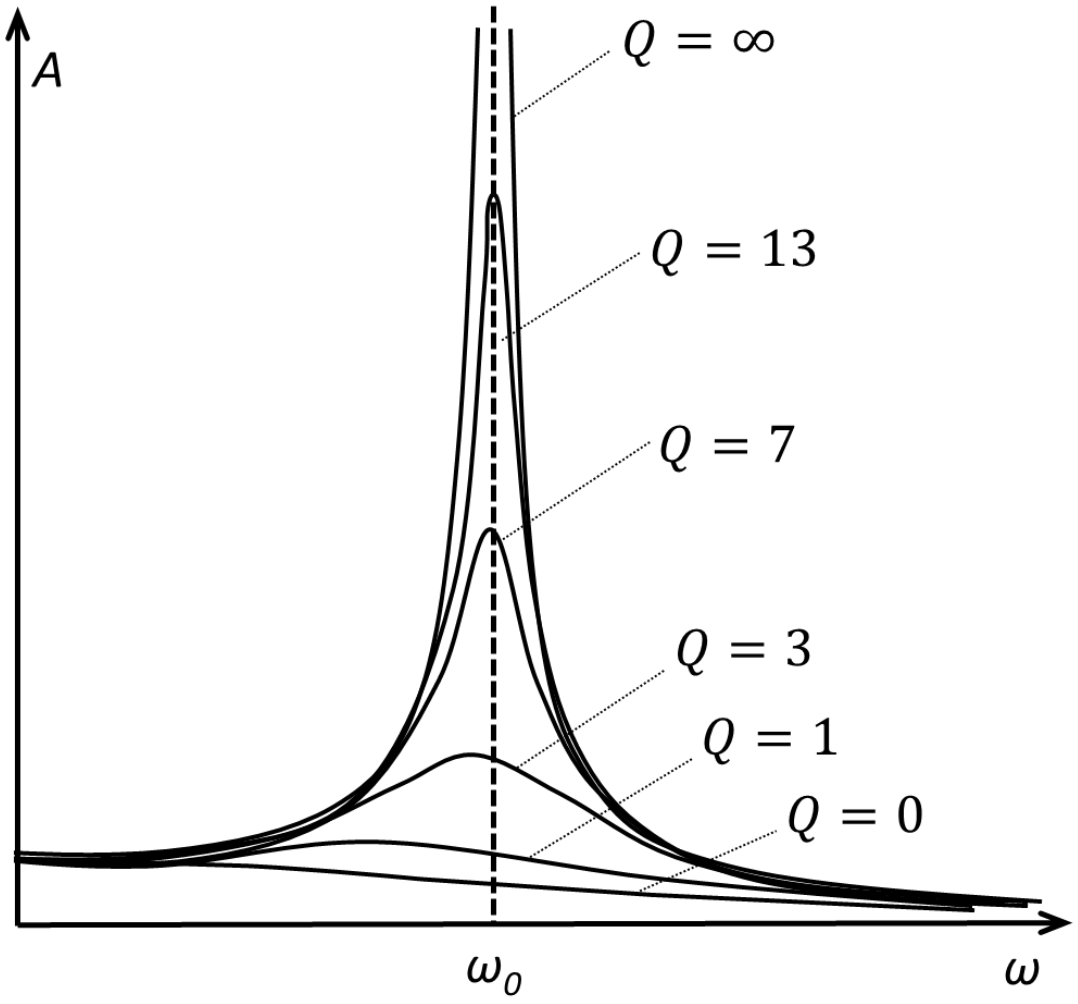

Figure 3.4: The effect of the quality factor *Q* on the amplitude *A* of a resonant response. With lower *Q*, the amplitude of the response is dampened, or in extreme cases nearly eliminated. $Q = \infty$ demonstrates the singularity that arises in the response in the case of no damping according to equation 3.3.

3.2 Electrochemistry

3.2.1 A simplified introduction

Semiconductor electrochemical etching is a complex study with theoretical contributions from many fields, including solid state and condensed matter physics. The following background is not intended to be a thorough exploration of the theory—if the reader is interested in such, the author recommends references [43-45].

However, it is helpful to introduce a few of the most pertinent concepts for our discussion here.

An electrochemical system of the kind used in this project has three key features: the solid electrode, the aqueous electrolyte, and the interface between them. The reaction occurs at the interface of a solid that conducts electrons (whether done well by a metal or poorly by a semiconductor) and an electrolyte that conducts ions. A reducing agent in the solution captures holes in the exposed crystal lattice and is then oxidized in the anodic process. This transfer of electrons to and from ions or molecules is the mechanism known as reduction-oxidation, or more simply redox. It is this process that removes material at the surface and is driven into the volume by the applied voltage.

The electrochemical etching of SiC gained a presence in the literature in the 1990s [46-48]. In 2000, Zangooie et al. produced several studies on the formation of different pore morphologies [49, 50], which is dependent on the values chosen for the myriad parameters directing the reaction. When seeking a particular morphology for an application, familiarity with these dependencies can inform the choices for these parameter values. For the case of a microresonator as desired here, the ideal morphology is a foam. This allows high mass loss while still forming a robust structure. Furthermore, a foam made from subtractive electrochemical etching can be very regular, so that it maintains the validity of the uniformity assumption applied by the theory to the cantilever dynamics.

Electrochemical reactions for producing porous silicon carbide are generally of the form [48, 51]:

$$SiC + 2H_2O + 4h^+ \rightarrow SiO + CO \uparrow + 4H^+ \quad (3.21a)$$

$$SiC + 4H_2O + 8h^+ \rightarrow SiO_2 + CO_2 \uparrow + 8H^+ \quad (3.21b)$$

$$6HF + SiO_2 \rightarrow H_2SiF_6 + 2H_2O \quad (3.21c)$$

In order for pores to propagate through the material the SiC lattice is dissolved. This requires holes h^+ in the lattice, which in the reaction produces SiO and SiO_2. These are dissolved in the solution by the hydrofluoric acid (HF). The gas phase reaction products CO and CO_2 are then released as bubbles (indicated by the arrows), and the reaction continues.

To sustain this reaction, the electrolyte is usually an aqueous hydrofluoric acid (HF) solution [46-52]. Ethanol is often included to help the electrolyte migrate inside the porous features. This eases the release of CO and CO_2 gas bubbles so that they do not get trapped inside the pores, thus encouraging the reaction to continue.

3.2.2 Band theory

To provide a deeper understanding of the chemical processes it is helpful to introduce an atomic perspective of the system. An individual atom has a certain number of electrons according to whichever chemical element it is. These electrons discreetly fill the available spaces of each quantized energy level (figure 3.5). If the electrons order themselves in such a way that each occupied energy level is filled to capacity, all of the electrons are tightly bound and do not easily escape. If a few extra spaces are available in the highest occupied energy level, these outer electrons are only loosely bound and will transfer easily to a more stable state.

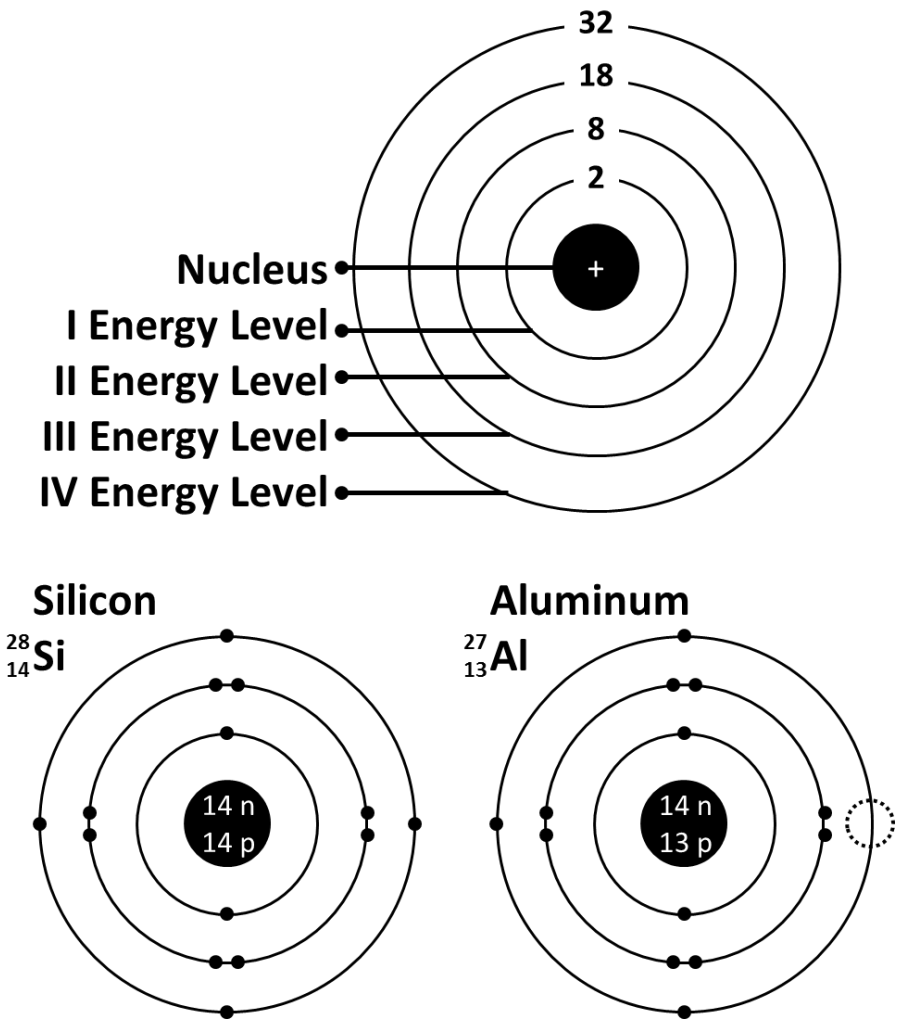

Figure 3.5: The energy levels of individual atoms. As an example, aluminum has one less proton than silicon, so that it leaves one more vacancy in the third energy level.

These energy levels propagate to the larger lattice structure formed by the many atoms that make up a solid. The discrete energy levels of the mass of atoms are so densely packed that they form apparent bands of energy (figure 3.6). The valence band refers to the last energy level to have every available space full. The conduction band then is the energy level after this, which houses whatever electrons are leftover. Electrons can transfer from the valence to the conduction band, depending on the size of the band gap E_g, which gives the amount of energy required to make the jump.

Conductors require little to no energy for this transfer. Insulators require an effectively insurmountable expanse of energy. Semiconductors are somewhere in the middle. In this way, the size of E_g determines conductivity.

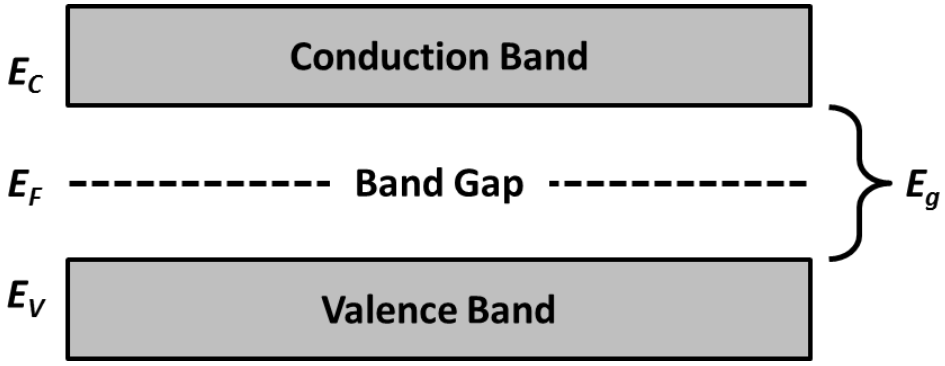

Figure 3.6: The band theory of solids. The energy of the conduction band E_C and of the valence band E_V is separated by the band gap, E_g. The size of E_g determines how much energy is required for electrons to move from the valence to the conduction band.

The Fermi energy level E_F is the electrochemical potential of these electrons. It roughly represents the highest occupied energy level in the valence band at 0 K. In metals, the valence and conduction bands overlap, and the conduction band is not full. This means electrons can transfer easily from the valence to the conduction bands and thus flow freely through the bulk material. This is why metals are conductive. In semiconductors, the conduction band is unfilled and there is a relatively small band gap between the valence and conduction bands. This gap is small enough that some electrons have enough energy to make the transfer, particularly with assistance from thermal energy or by shifting the Fermi level via doping.

Doping is a way to facilitate electron transfer in semiconductors without requiring external energy input. The concept is to inject into the atomic lattice atoms that have an extra hole (acceptors) or electron (donors) in its energy levels compared to the bulk material. This consequently shifts the Fermi level towards the valence or

the conduction band, respectively, diminishing the apparent band gap. In the present case, the samples that are anodized are wafers of heavily doped n-type SiC, meaning there is a large excess of donors and the Fermi level is shifted significantly towards the conduction band (figure 3.7a).

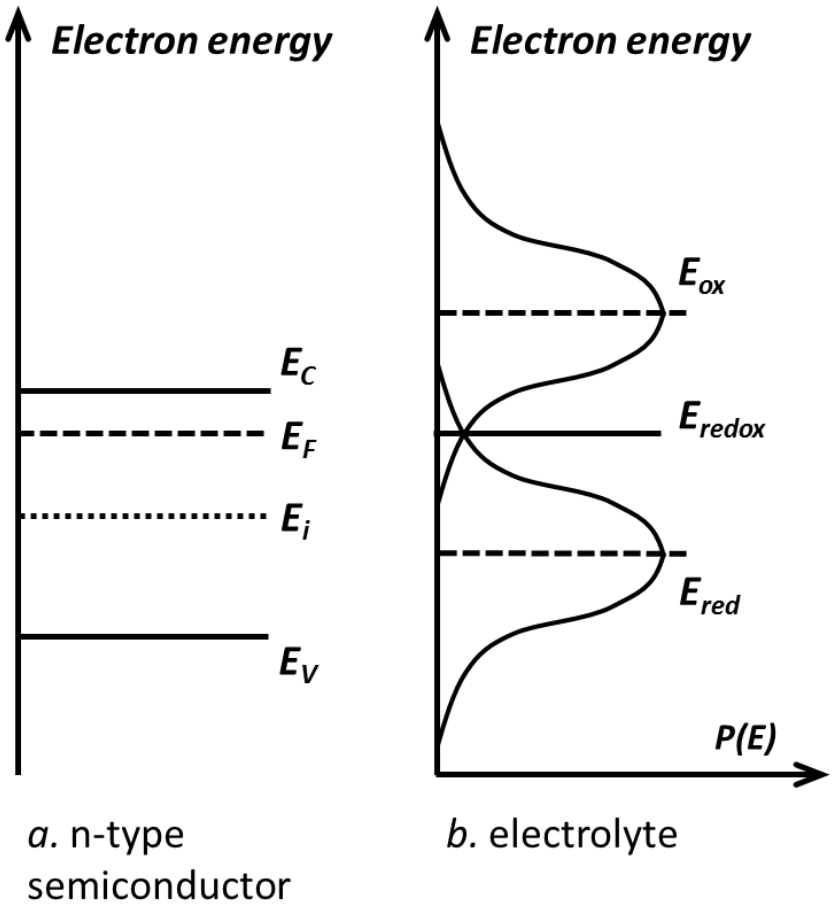

Figure 3.7: Electron energy band diagram for (a) a strongly doped n-type semiconductor, such as the silicon carbide used for this project, and (b) the electrolyte. In (a), doping has shifted the Fermi level E_F significantly towards the conduction band, compared to its intrinsic level E_i of the undoped material. In (b), *P(E)* is the probability that the energy level E_{ox} or E_{red} (describing the tendency of an ion to gain or lose an electron, respectively) has fluctuated to energy *E*. E_{redox} is the average energy value of the two for equal concentrations of reducing and oxidizing agents in the electrolyte, and acts as an effective "electrolyte Fermi level."

In a solution, there are no free electrons. Instead, the diffused ions or molecules perform the electron transfer. The ionic solution has an energy level E_{redox},

which is analogous to the Fermi energy level for the solid. It is the effective energy level at which a reduced ion will lose an electron (energy level E_{red}) or an oxidized ion will gain an electron (energy level E_{ox}). Thus as the ions approach the solid electrode, they may capture electrons from the solid depending on their relative energy levels (figure 3.7b).

If the band gap in the solid is small, the energy required for the electrolyte to capture the electrons is probabilistically easy to reach. Therefore in order to facilitate the removal of material, the amount of energy required for an electron in the solid to escape the valence band should be mitigated via doping. This indicates that the process is dependent on the amount that the semiconductor is doped.

3.2.3 Influence of sample conductivity

Pure single crystal semiconductors exhibit low conductivity due to low carrier density. This hampers electrochemical etching. By doping a semiconductor, more electrons are available for transfer. The number of electrons added through doping can be related to the resistivity of the sample by

$$\log(N_D - N_A) = 16.08 - 1.83 \log R \tag{3.22}$$

for the specific case of n-type 6H SiC [53]. Here $N_D - N_A$ is the difference between the number of donors N_D and number of acceptors N_A, determined by the carrier concentration (i.e. number of electrons available for transfer) per cubic cm and R is the sample's resistivity in Ω·cm.

The electrons and holes that participate in conduction are known as intrinsic carriers. In a pure material, the carrier concentration can be assumed to be effectively constant, as it is an inherent property related to the material's crystal structure.

However, the carrier concentration in a doped material can vary, even within a single ingot of the material. As the carrier concentration affects the electrochemical etching process by determining the resistivity, it is relevant to check the carrier concentration specific to each sample to ensure consistent results. It is for this reason that Hall measurements are taken for the anodized samples, as will be described in sections 4.1.1 and 5.2.1.

The electrochemical process is also affected by the ohmicity of the connection. Ohmic contact refers to how linear the current-voltage (I-V) curve is for an electrical junction between two conductors or semiconductors. It implies that there is no energy barrier for electron transfer at the anodic contact. Conductors are easily linear due to their high conductivity. Semiconductors, in contrast, may result in nonlinear resistivity. In the case of SiC, the Si-face forms an ohmic contact much more easily than the C-face. A nonlinear I-V curve results in qualitative variance of porosity during the electrochemical process, and so is worthwhile to avoid in the interest of producing regular features.

3.3 Porosity

3.3.1 Previous attempts on other materials

Little research has gone into leveraging the reduced mass of porous materials for AFM cantilevers. Porous multilayer-coated tips have been proposed for nanolithographic purposes [54]. However, porosity of the tip does not significantly impact the dynamics of the cantilever. One recently published study demonstrates how a template can be used to grow microcantilevers out of macroporous nickel inverse opal or alumina shell structures for applications in flexible batteries, chemical

sensors, and micromechanical sensors [55]. Template processes offer highly controlled porosity, but can be expensive and difficult to establish compared to electrochemical etching.

Porous silicon is a well-studied and broadly applicable material for its high surface area, bioactivity, and porosity-dependent optical properties [56-60]. Using any of many techniques, one can achieve porosities ranging from 95% to as low as 5% of the original mass. However, despite bulk Si being a favorite material for AFM cantilevers, porous Si is unusable as a contact microresonator. This is a consequence of the atomic structure. Bulk silicon is brittle on its own, but the decimated bonds that hold together porous silicon are much more so. Under the large energy input required to vibrate the structure at high frequencies, it shatters rather than bends. Section 3.3.3 describes this in more detail.

The hesitation to use porous materials for microcantilevers is largely due to the lack of control in the fabrication and porosity's impact on the structure's mechanical strength. However, porous silicon carbide can result in a rigid foam structure that should be stable as a microresonator, as opposed to porous silicon. This is due to the atomic influence of carbon in silicon carbide, which creates a far more compliant crystal structure. Furthermore, modern techniques for introducing porosity such as templating and electrochemical procedures offer sufficient control on the nature of the porous structures that was not previously achievable. In addition to all of this, the material properties of SiC make it an ideal AFM probe material, independent of its potential for including porosity. It is for these reasons that SiC was chosen to demonstrate the potential of introducing porosity to AFM cantilevers.

3.3.2 Quantifying porosity

For this application, the goal is to produce a significant volume of regular, branching porous structures that make up a foam out of which a homogenously porous cantilever can be formed. Qualitatively alternative porous structures include dendritic organizations that do not maintain a structure or irregular pores that significantly hamper assumptions of uniformity. Other examples include relatively dense morphologies that do not efficiently reduce the cantilever's density and highly anisotropic pores, such as columnar structures. Anisotropic morphologies can still be effective, and might be implemented to emphasize or dampen cantilever motion along particular axes. Still, branching foams were considered best for the purposes of this project and porous cantilevers were formed from this morphology. Examples of these alternative morphologies are pictured in figure 3.8.

Porosity characterization is relevant to a range of materials, from sponges to fine powders. Despite the seeming unlikeness across such materials, they share enough theoretical similarity that it is important to be able to compare them in a meaningful manner. In an effort to avoid misuse and improper analysis of porous materials, the National Institute of Standards and Technology (NIST) published standardized definitions of porosity and surface area properties [61]. Terms used in this discussion will be defined by this reference. The relevant porous structure to consider for the present purpose is a porous solid, as opposed to aggregated particulates such as powders. Concepts to be introduced and defined include pore size, pore wall size, and total mass loss.

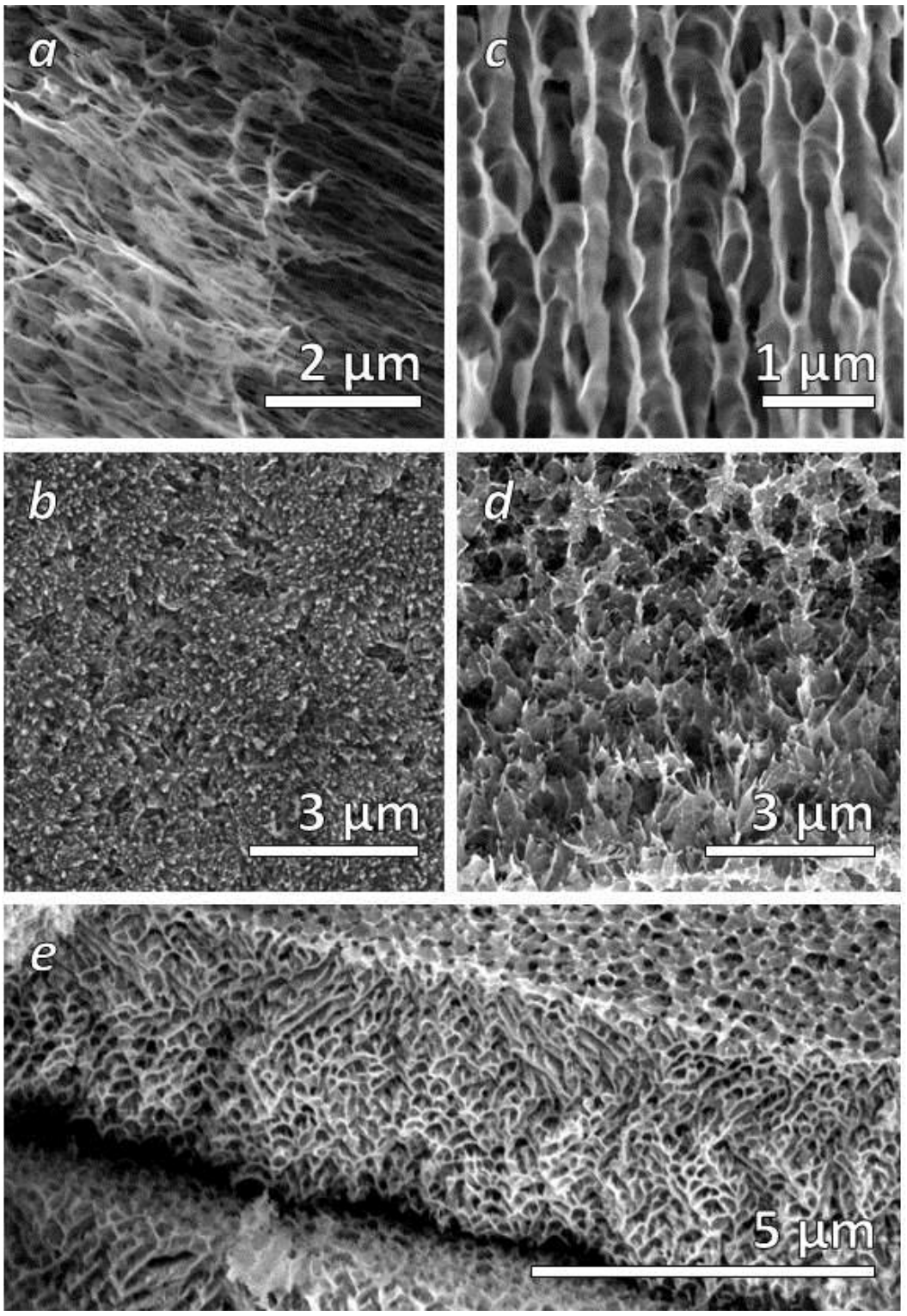

Figure 3.8: A selection of pore morphologies created in the anodization process. Dendrites (a) risk weak structures. Blooms (b) are too dense to be effective. Relatively columnar pores (c) are organized but generate highly anisotropic dynamics. Spikes (d) have thin walls that are more easily crushed when deformed. The branching foam structure (e) is ideal for creating rigid cantilevers of relatively uniform porosity.

Pores can be initially classified by how accessible they are to external fluid. Considering figure 3.9, closed pores (a) are completely inaccessible to external fluids and so do not contribute to processes like fluid flow and gas adsorption. However, they do contribute to macroscopic properties like mass density, elasticity, and others. In contrast, open pores (b), (e), and (f) are accessible to external fluids. These can be further distinguished by whether they are "through," meaning there is an uninterrupted path from one external opening to another like (c), or "blind," in which an open pore terminates at some point within the solid body, as in (b) and (f). Blind pores can further appear in different shapes. For example they can maintain an even diameter until their terminus (f), form a funnel shape (d), or open up into a bulbous shape (b). Finally, closed pores may not actually be true pores, but instead simply divots contributing to surface roughness (g). The convention to differentiating between the two is that a pore is deeper than it is wide.

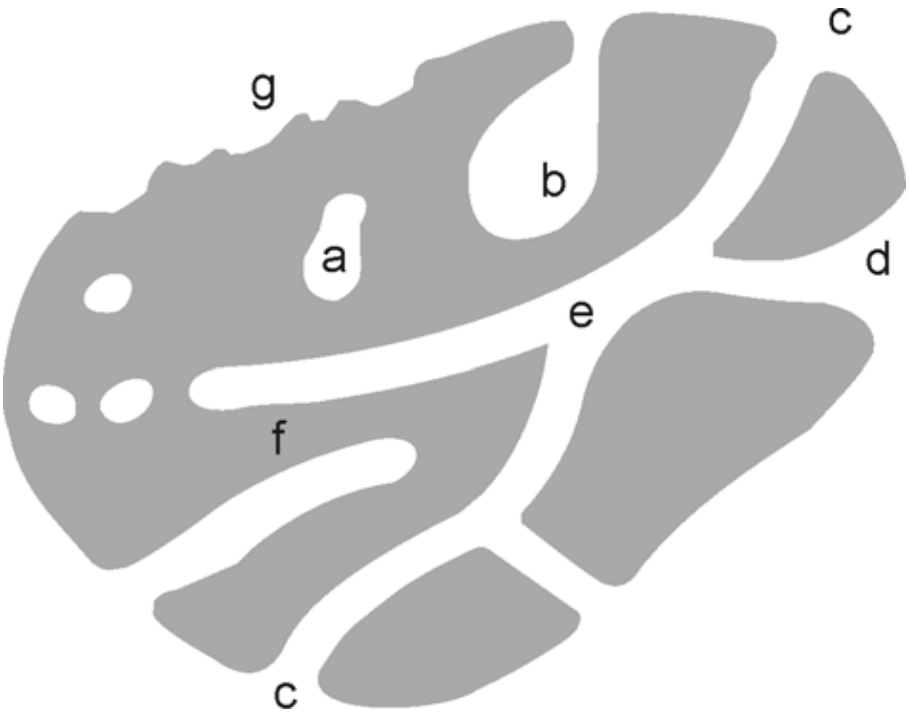

Figure 3.9: Schematic of different pore types. From [61].

The SiC pores formed in the anodization procedure used in this project are open by nature, as it is a subtractive process, meaning the pores are created by the removal of exposed material. Furthermore, they are blind and of constant diameter for the most part, although they may open up in a bulbous form.

The volume fraction of porosity can be quantified by measuring how much of a sample's apparent specific volume is attributed to pores, $\varepsilon = V_p/V$. This value depends heavily on the method used to measure each of these values. To measure V, one can use simple geometrical determination from the known dimensions, or alternatively fluid displacement. To measure V_p there are a few favored methods, including gas adsorption, capillary condensation, fluid displacement, and others. Methods utilizing fluids can only measure open pores, so may result in an underestimation of the true porosity. Another potential risk of underestimation is in cases where the pores are too small for whatever gauge is being used to resolve; for example, the molecular size of an adsorbate or the wavelength of a radiation probe may be too large to reach inside the pores. This project uses high resolution imaging with a SEM for direct characterization of the pores.

Pore size is also difficult to define precisely, since pore shape can be highly variable. This raises debate for which dimension to use that truly describes the size of a pore such that it can also be used to compare to pores of other shapes. To make this easier, an analysis often begins with qualitatively describing a pore as an idealized shape. These shapes are generally kept simple, such as spheres, cylinders, prisms, cavities, windows, or slits. Then, because it is the limiting feature, the smallest dimension of the assumed pore shape is used to measure a pore's size. This

dimension is referred to as the “pore width.” An example of this is to consider a cylindrical pore that goes very deep and has an annular cross-section with the diameter on one axis larger than on the other. The smaller diameter is used to reference this pore’s size, although this does not capture how deeply into the material the pore goes. A further convention in regards to pore size is to refer to pores of widths under 2 nm as micropores, widths between 2 and 50 nm as mesopores, and widths greater than 50 nm as macropores. The term nanopore is also used for pores with widths between 1.5 and 5 nm.

The last measurement of porosity to be described here is known as the pore wall size. This is the average distance between two adjacent pores and provides a way to describe the density and regularity of pores over an area. If the pore wall sizes are generally much smaller than the pore size, the pores are densely occupying the surface. If the standard deviation of pore wall size is also small, the porous features are consistently spaced. In this way, it is important for this application that the pore walls and diameters have a small standard deviation to support the uniformity assumption. Pore wall size itself should be small, but not so thin that they easily buckle and fracture during high frequency oscillations.

3.3.3 Effect on structural strength

This paper has frequently asserted that porous silicon carbide (SiC) is more stable than porous silicon (Si). To theoretically support this claim, it is worthwhile to introduce a few concepts from atomic bonding.

In metals, atoms are capable of hopping to a different site in the lattice. Therefore, deforming metallic bonds simply produces dislocations, which

additionally travel along the lattice. Thus, in order to fracture a metal, the lattice must first be saturated with dislocations. This allows metals to survive significant plastic deformation.

In contrast, covalent solids, such as many ceramics, are only able to deform via stretching of the atomic bonds. However, once the interatomic bonding energy is exceeded, a crack forms in the lattice. Cracks form in metals, but the stress energy density is spread due to dislocation motion. In ceramics, a crack localizes the stress, so that neighboring bonds quickly follow suit. In this way, the strength of covalent solids is entirely dependent on the strength of the atomic bonds. While these bonds are technically stronger than metallic bonds, breaking them inevitably results in cataclysmic failure.

Both SiC and Si are covalent solids. Therefore, neither plastically deforms, and their primary failure mode is due to crack propagation. However, Si – Si bonds are relatively weak ($E_{Si} = 130 - 185\ GPa$). C – C and C – Si bonds tend to be stronger; therefore atomic influence of carbon in the SiC crystal lattice makes it more robust ($E_{SiC} = 450\ GPa$) [62, 63].

It is reasonable to state that the relative strengths of these materials can be extended to their porous forms. This can be seen by reviewing equations 3.21; since the products SiO and CO or SiO_2 and CO_2 are produced in equal measure, it can be assumed that the bonds are dissolved at an equal rate. If more C-bonds were dissolved than Si-bonds, the structure would weaken at a faster rate and possibly be comparable in strength to porous Si, meaning that we achieve no gains by using porous SiC

instead of porous Si. Fortunately, this is not the case. Therefore, while porous SiC is expected to be weaker than bulk SiC, it is still stronger than porous Si.

Ultimately, the mechanical strength is not measured or modeled in this project. However, the cantilevers clearly create a self-supporting structure. Furthermore, the porous structures survive applied forces while measuring their mechanical properties in the AFM, suggesting they are sufficiently robust for AFM cantilever applications.

Considering specifically porous foams, the walls of the pores must be able to withstand the compressing and stretching stresses that result from the cantilever oscillating. Failure is more likely to occur due to compression [64]. Therefore, the two most relevant failure mechanisms for porous silicon carbide foams are elastic buckling and crushing of the pore walls. The critical stresses of these two modes can be found by the equations

Elastic buckling $$\sigma_{EB} = 0.05E_{bulk}(\rho_{porous}/\rho_{bulk})^2 \quad (3.23a)$$

Crushing $$\sigma_F = 0.65\sigma_{F,bulk}(\rho_{porous}/\rho_{bulk})^{3/2} \quad (3.23b)$$

3.3.4 Effect on uniformity assumption

Throughout this paper, the cantilever is referred to as a continuous or uniform structure. It is important to carefully define these terms and to explicitly discuss how porosity impacts uniformity. First, it calls to mind the fundamental assumption of continuum mechanics, which states that there is a continuous distribution of matter that completely fills the space occupied by the object of interest. By assuming this, any spatial dependence of structural properties such as mass density and elasticity can be eliminated, simplifying the analysis [65].

By definition, this is not applicable to porous media. However, if the vacancies present in the material are satisfactorily consistent in nature, the concept of a uniform material can still be applied. It is for this reason that it is significant to ensure that the porous qualities of the foam are consistent.

Chapter 4: Methods and Procedures

This chapter details how we approached the goals of this project. It is organized by two parts: the procedure for anodizing the bulk material and the procedure for creating cantilevers from the resultant porous material. The samples used are 5x5 mm and 10x10 mm wafers of n-type doped 6H polytype bulk silicon carbide (SiC). They have nominal resistivity of 0.02 to 0.2 Ω·cm and are marked to indicate which side is carbon-terminated and which is silicon-terminated.

4.1 Mass reduction

4.1.1 Hall measurements and sample preparation

Preliminary Hall effect measurements were taken to confirm dopant concentration. This ensures consistent anodization conditions. To take these measurements, four ohmically conductive contacts must be formed at each corner. Using a mask to form the contacts, aluminum (Al) is deposited on the Si-face using physical vapor deposition and annealed at 600^{o}C in argon gas. After cleaning using a solvent bath, Hall measurements are taken that check ohmicity and measure bulk carrier concentration.

Next, one side is coated with conductive material to form an ohmically conductive electrical junction. Anodization experiments were run on both Si- and C-terminated faces. To anodize the Si-face, the Hall measurement contacts are first cleaned away using an acid etchant; then, another film of Al can be deposited on the bare C-face. These samples are annealed at 700^{o}C to improve the ohmicity of the contact, as the carbon side is less readily conductive. When anodizing the C-face, the

Hall contacts need not be removed and a thin film can be deposited directly for the anodic contact. Samples are again cleaned in a solvent bath.

Samples are then packaged in preparation for anodization. The package is formed by a piece of acid-resistant tape backing, a thin strip of copper foil, the sample to be anodized, and a second piece of tape with a hole cut in the middle. The sticky sides of the tape pieces face each other to hold the package together. The copper foil provides a conductive pathway between the SiC and the anode. The sample must be laid so that the Al-coated side is in good contact with the copper foil. The hole in the tape exposes an area of the SiC that is to be etched. The purpose of the package is to keep the copper foil in good contact with the conductive side of the sample while also protecting the conductive pathway from being etched away by the acidic electrolyte. To ensure the success of these two goals, air pockets must be eased out from the foil-sample interface and a sufficient amount of tape must line the edge of the exposed SiC so that no acid can leak through. The sample is then prepared for anodization.

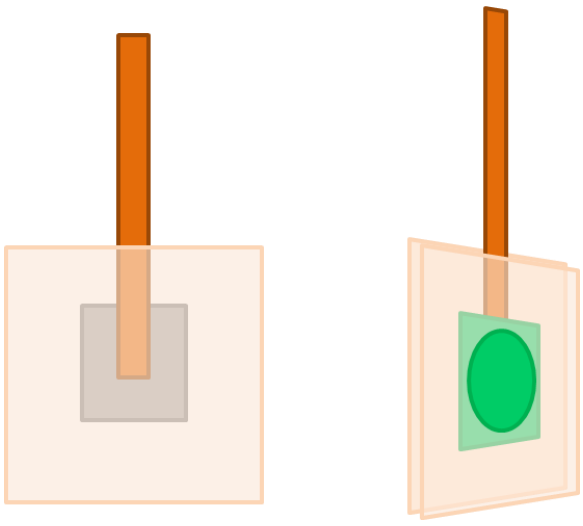

Figure 4.1: An illustration of the anodization package, viewed from the back and front. The aluminum-coated backside (silver) must be in good contact with the copper foil (brown). The final tape package exposes an area of silicon carbide (green) while still protecting the conductive pathway from the acidic electrolyte.

4.1.2 The electrochemical reaction and sample anodization

Semiconductor electrochemistry is sensitive to a large number of parameters and can be a very complex process to control. These parameters include but are not limited to the nature of the electrolyte (ingredients chosen and their relative concentrations), the nature of the sample (the specific crystal structure and the level of doping in each individual piece), and the power driving the reaction (the amount of voltage applied and the quality of the electric junctions). The process can yield a large range of results that can produce entirely different pore morphologies or merely fine changes to the structure qualities.

The parameter values chosen for this project were chosen by conducting a series of experiments to optimize the produced porous material for the application. These tests investigated the influence of the relative concentrations of the electrolyte ingredients, the voltage applied, the duration of the process, and the ohmic quality of the anodic electrical junction. Details of these tests and their results are given in section 5.2.2.

The porous SiC material is created using an electrochemical reaction that is well-established in the literature and is detailed in equations 3.21. In order for pores to propagate through the material, the SiC lattice is dissolved by the electrolyte, which consists of hydrofluoric acid (HF), ethanol, and de-ionized water (DI-H2O). To drive the reaction, the SiC electrode is anodically biased in conjunction with a cathodically biased piece of 99.9% platinum wire mesh.

The recipe for the electrolyte was chosen based on the studies of Kang et al., who established a method of stable field emission using nanoporous SiC [52]. Tests

varying the concentration of HF in the electrolyte concluded that a recipe of roughly 10% HF, 5% ethanol, and 85% DI-H_2O by volume yielded the best results for this application.

To drive the reaction, a circuit was formed and connected to a DC power supply (figure 4.2). Current was held constant at 0.25 A for smaller exposed areas on 5x5 mm pieces and 0.35 A for larger exposed areas on 10x10 mm pieces. To form the foam structure desired for this application, a higher voltage of 20 V is applied. The process is operated at room temperature.

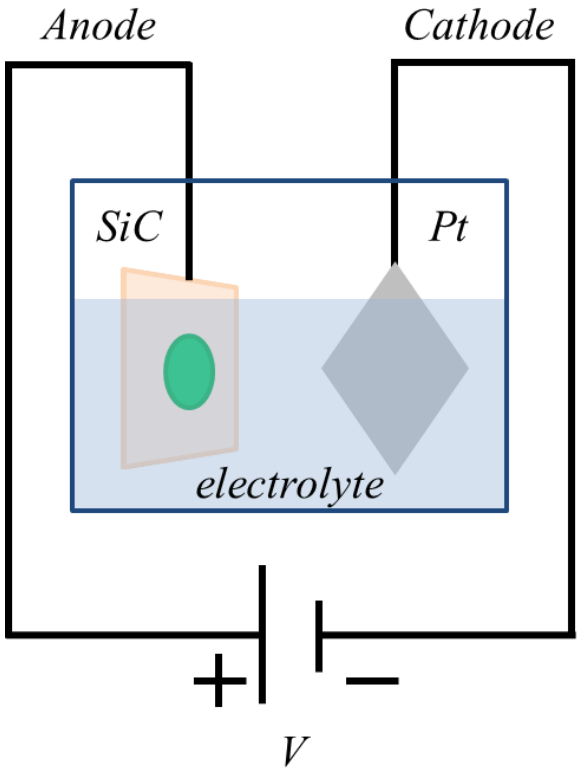

Figure 4.2: A schematic of the circuit formed to drive the electrochemical reaction.

The goal is to produce a significant volume of consistent, branching porous structures from which a homogenously porous cantilever can be formed. This requires carefully choosing the nature of the surface to be etched. Previous studies in the

production of self-organized columnar pores used Si [66, 67], Al_2O_3 [68, 69], and InP [70, 71], which yielded minimum pore diameters of 300 nm, 50 nm, and 200 nm, respectively. These studies of semiconductor etching and others have shown that the etching is almost always anisotropic. Additionally, more ionic polar semiconductors like ZnO [72] and InP show that the etching process varies depending on which face is exposed, indicating that the chemistry is affected by how the face is terminated. This also applies to etching SiC, which not only has different crystal structures to choose from (most common are 3-cubic, 4-hexagonal, or 6-hexagonal) but also different faces (Si- or C-terminated). To create extended porous structures the 6H polytype is used. Tests anodizing both faces (detailed in section 5.2.2) concluded that the C-terminated face produced more homogeneous structures, which is preferred for this application.

Despite the electrochemical process being sensitive to many parameters as described here, it has also proven to be a highly reproducible process. In fact, two completely independent systems established over the course of this project produced self-consistent results.

4.1.3 Reduced mass quantification

As described in section 3.3.2, there are many ways to quantify porosity. To choose one for this project, there are several things to be considered. First of all, it would be inappropriate to apply the average mass loss of the entire volume to the microscale cantilevers; the porous features likely vary over the anodized volume and the cantilever porosity must be specifically understood. Secondly, the material chosen to make a cantilever must form a cohesive structure in order to withstand high

frequency oscillations, so it is preferred that the material is visualized. Thirdly, similar processes have demonstrated that the porosity is depth-dependent [52], so this must be well understood to avoid nonhomogeneous cantilevers.

To satisfy these considerations, this project took advantage of a scanning electron microscope (SEM) combined with a focused ion beam (FIB) to directly visualize and measure the amount of material removed as a function of depth. The power of this technique is that the FIB is able to remove layers of material to reveal how the pores propagate through the volume and the SEM is able to take extremely high resolution images (~2 nm) from which properties of the porosity can be precisely quantified. This technique is superior to many of the previously mentioned examples because it is highly specific, which satisfies the need for understanding well the porous material forming each cantilever.

An additional feature of this method is that it is possible to create a true map of the porous volume. Software designed for the FIB is capable of taking images at specified increments over the course of a mill and stitching them together to form a three-dimensional image. With this technique, the mass lost in an anodization experiment can be completely and accurately quantified. While the software could not be used, mass reduction measurements for this project implemented this concept. Images were taken and porosity measured at incrementally greater depths to establish a complete understanding of the porous volume. This is a destructive exercise, so cantilevers cannot be visualized this way. However, it provides a thorough understanding of the areas immediately surrounding a cantilever, so that the

measurements can be extended to the cantilever itself with a level of certainty not afforded by other methods.

To analyze the images captured we used the image analysis program ImageJ. The image was thresholded to depict the vacancies as black and the surviving material as white. Since the images often include the back walls of the pores, care was taken when thresholding to isolate the back material from the superficial layer (demonstrated in figure 4.3). This way, only the most superficial layer contributes to the mass loss measurement and the image represents a two-dimensional slice of the porous material. The mass loss can then be quantified by comparing the summation of the black pixels to the white. In addition to mass loss, the diameters of the pores and the pore walls were measured. Consistency in these measurements indicates a homogeneous structure.

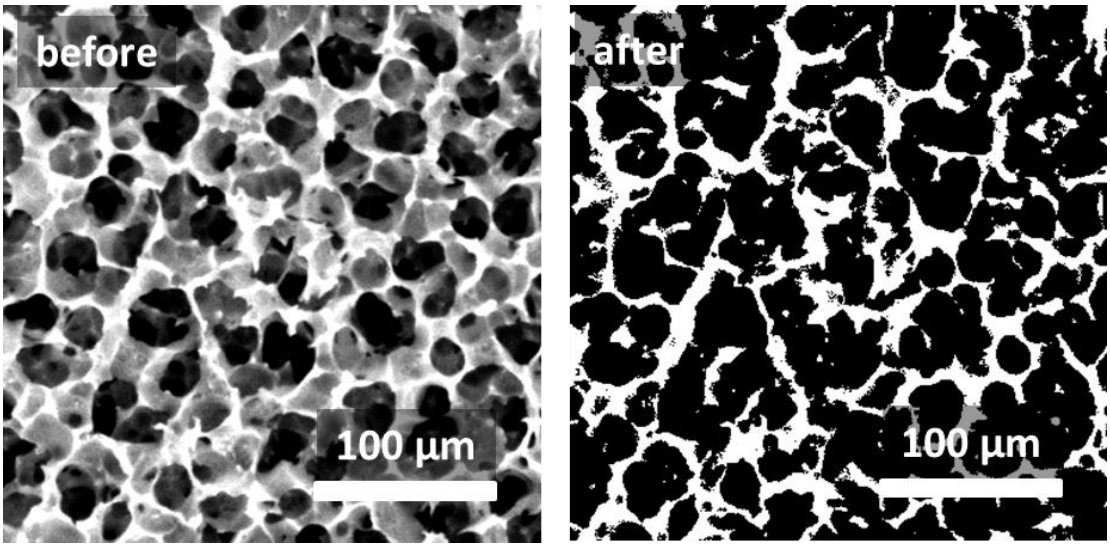

Figure 4.3: The images are thresholded to isolate the most superficial layer of material and calculate mass loss. This example depicts 76% mass loss.

The previously mentioned depth-dependence of the porosity is due to a characteristic “crust” layer of relatively dense porous material at the surface that

extends 5 to 15 μm into the volume. This phenomenon is believed to be a consequence of the surface chemistry associated with using deionized water in the electrolyte [52].

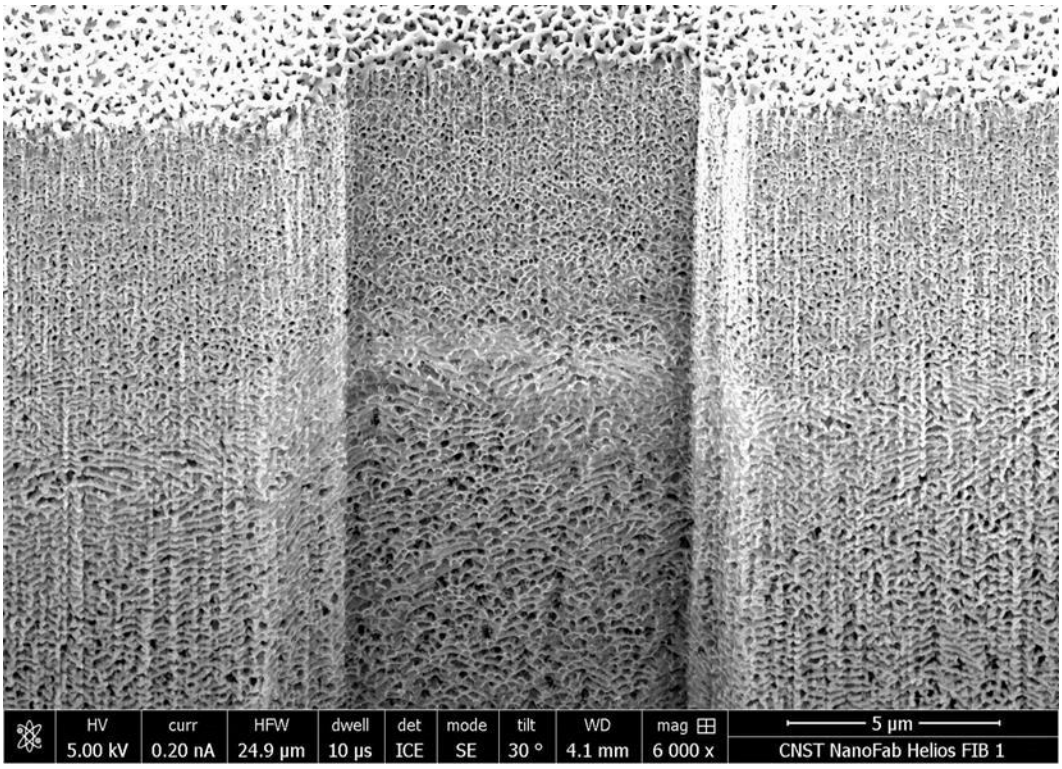

Figure 4.4: The characteristic crust of low porosity at an anodized sample's surface and its interface with the higher porosity material underneath. A comparison of the resultant porosity measurements is shown in figure 5.4.

This denser layer is not ideal for this project, which aims to maximize mass loss. A comparison of the mass density loss of these two levels of porosity shows a difference of about 20%, with the greater density layer typically yielding only ~50% mass reduction and the lower density layer ~70%. Consequently a processing step must be introduced that removes this crust layer of variable depth while leaving a sufficient amount of the less dense material with which to create cantilevers. Additionally, the final surface must be flat. This is so that the produced cantilevers have a uniform cross-sectional area, unlike the cantilever shown in figure 4.5.

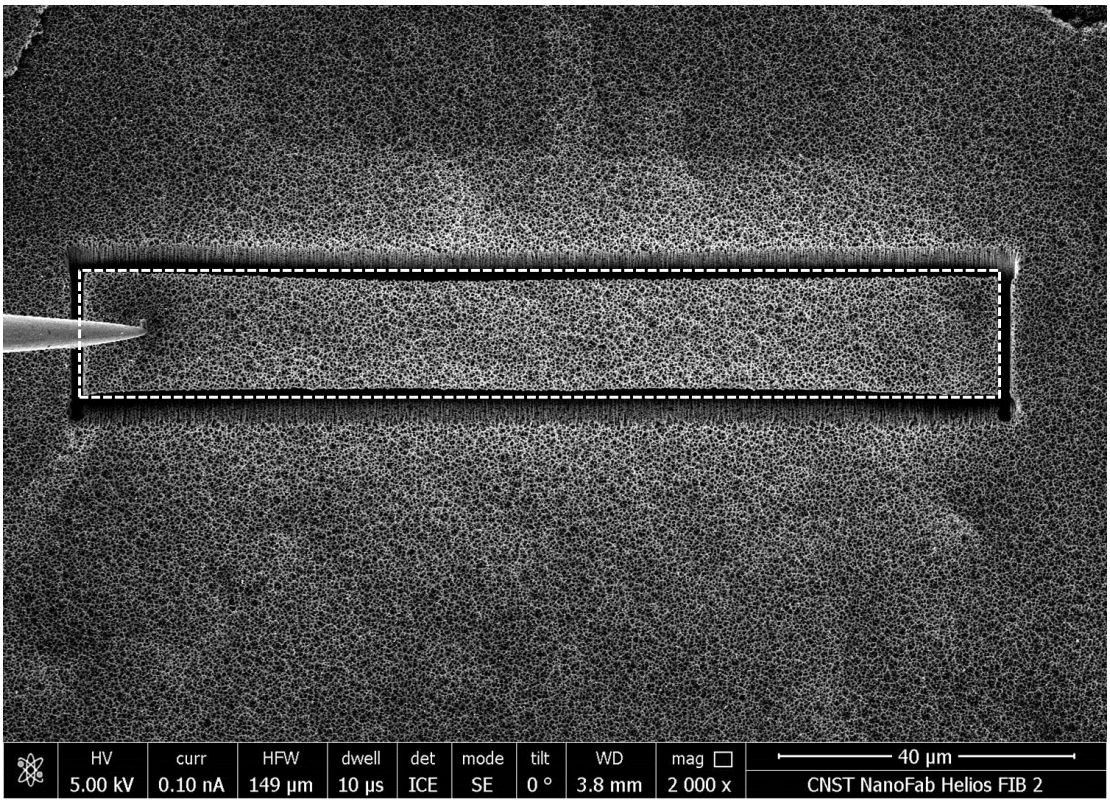

Figure 4.5: A cantilever formed from a surface varying in height. Not only does the thickness of this cantilever vary with the height of the surface, but the two-dimensional perspective of the FIB results in a "wavering" of the milled sides. The dashed box outlines the uniformly shaped cantilever that would have been formed from a flat surface.

Successfully removing the dense material so that it terminates in a flat surface can be done in a sophisticated way, such as using reactive ion etching (RIE), or a less sophisticated way, such as taking advantage of naturally delaminated areas on the sample surface. RIE is a highly variable process that removes different amounts of material from sample to sample. It takes many trials to perfect and does not guarantee a flat surface in the case of porous samples. This is because the empty spaces of the pores allow the etching reaction to reach material at the back of the pore in addition to the material at the immediate surface level.

Delamination, in contrast, is a dependable consequence of the abrupt change between the more and less dense layers. It is believed that the change in density is indicative of a change in the atomic structure, which generates a boundary that is more weakly bonded than the rest of the material. In fact, this interface is so weak that the surface is often unintentionally separated when removing the sample from the tape package. Figure 4.6 shows an example of the distinct demarcation between the more and less porous layers that can occur. The linearity often extends into the plane, so that separation results in significant areas of surfaces that are flatter than is achievable by other methods. While this practice still does not guarantee perfect results, it is efficient and is more often than not satisfactory.

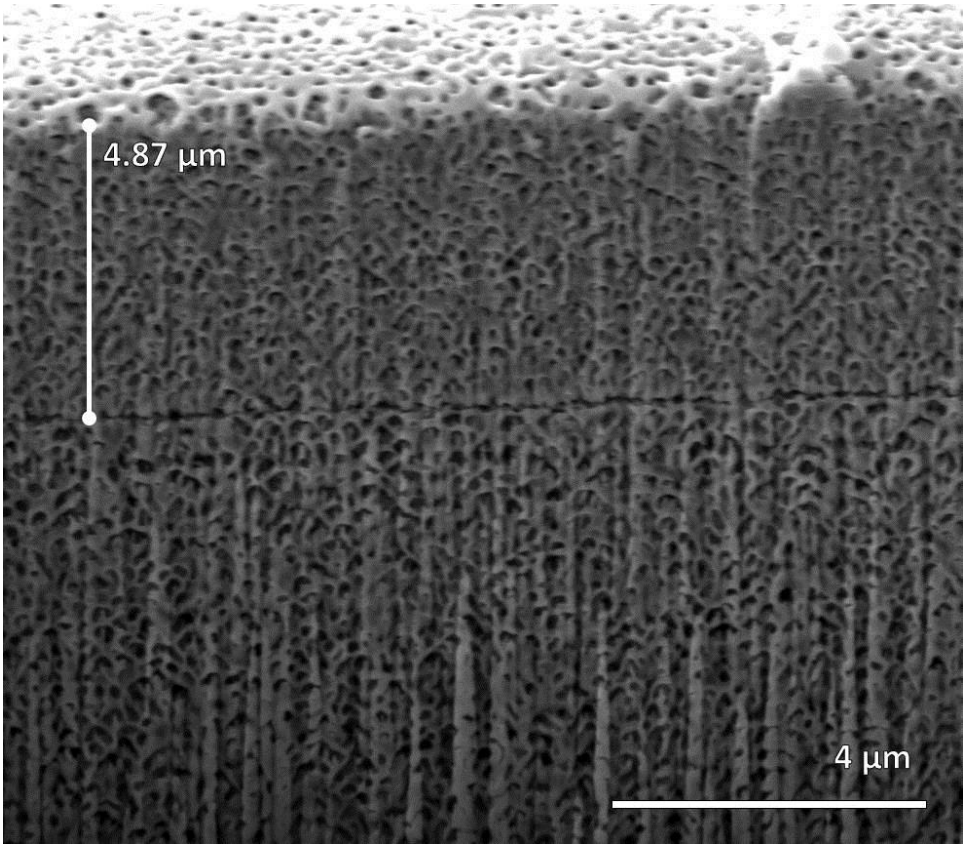

Figure 4.6: An example of how the interface between the less and more dense layers can be very flat. The crust layer of this sample would be easy to remove by delamination and would result in a flat lower surface.

4.2 Cantilever fabrication using FIB

Industrial cantilever fabrication methods typically utilize a series of masking and etching steps to allow highly controlled mass production. This project was interested in more directly visualizing and individually handling the cantilevers. The focused ion beam (FIB) is ideal for these purposes. This section describes this instrument and the methods adopted for creating the AFM cantilevers.

4.2.1 Introduction to FIB

The FIB is a nanofabrication instrument that is particularly popular in the semiconductor industry for its ability to precisely cut and rewire microscale circuits [73, 74]. FIB is often compared to scanning electron microscopes (SEM) because, like the SEM, it uses a focused beam of particles to gain information about a sample. However, while the SEM uses a focused beam of electrons to nondestructively image a sample, a FIB uses a focused beam of much heavier ions—often gallium—to ablate or deposit material as well as image. It is therefore an inherently destructive technique, not only because it is constantly milling away the material it is imaging but additionally because the gallium ions are embedded into the surface of the sample. Fortunately, the FIB is an open platform that can accommodate an SEM or other imaging tools, so that it is easy to image and prepare the sample nondestructively until it is time to employ the FIB.

The most powerful practical benefit of this instrument is that it can simultaneously image and manipulate a sample on a nanoscale. These manipulations not only include its ability to deposit or remove material at a large angular range (the stage can be tilted from 0^o to 52^o, plus offers the option to use a 90^o mount for further

access), but also its ability to pick up and move microscale objects. This is done with a manipulator that can be brought into contact with and attached to the sample using a platinum deposit (often referred to as a "Pt-weld"). The sample can then be altered or transferred as desired and freed by milling away the platinum tacking. To avoid contaminating the sample, a sacrificial digit can be formed beforehand and removed along with the manipulator.

4.2.2 Forming the cantilever

For this project, forming cantilevers from a wafer of bulk or porous SiC was done using a 7-step method:

1. Choose a large, flat area of desired material (either bulk or porous).
2. Make two cuts at a 45^{o} angle into the material, taking care that the cuts meet in the middle.
3. Make contact with the manipulator and Pt-weld it to what will become the clamped end of the cantilever.
4. Simultaneously mill two cuts at either end of the cantilever, cutting the cantilever free.
5. Carry the cantilever to a prepared industrial AFM chip.
6. Pt-weld the cantilever to the chip.
7. Cut free and remove the manipulator.

This method results in a cantilever with an equilaterally triangular cross section. Figure 4.7 illustrates the process and figure 4.8 shows an example of the final product.

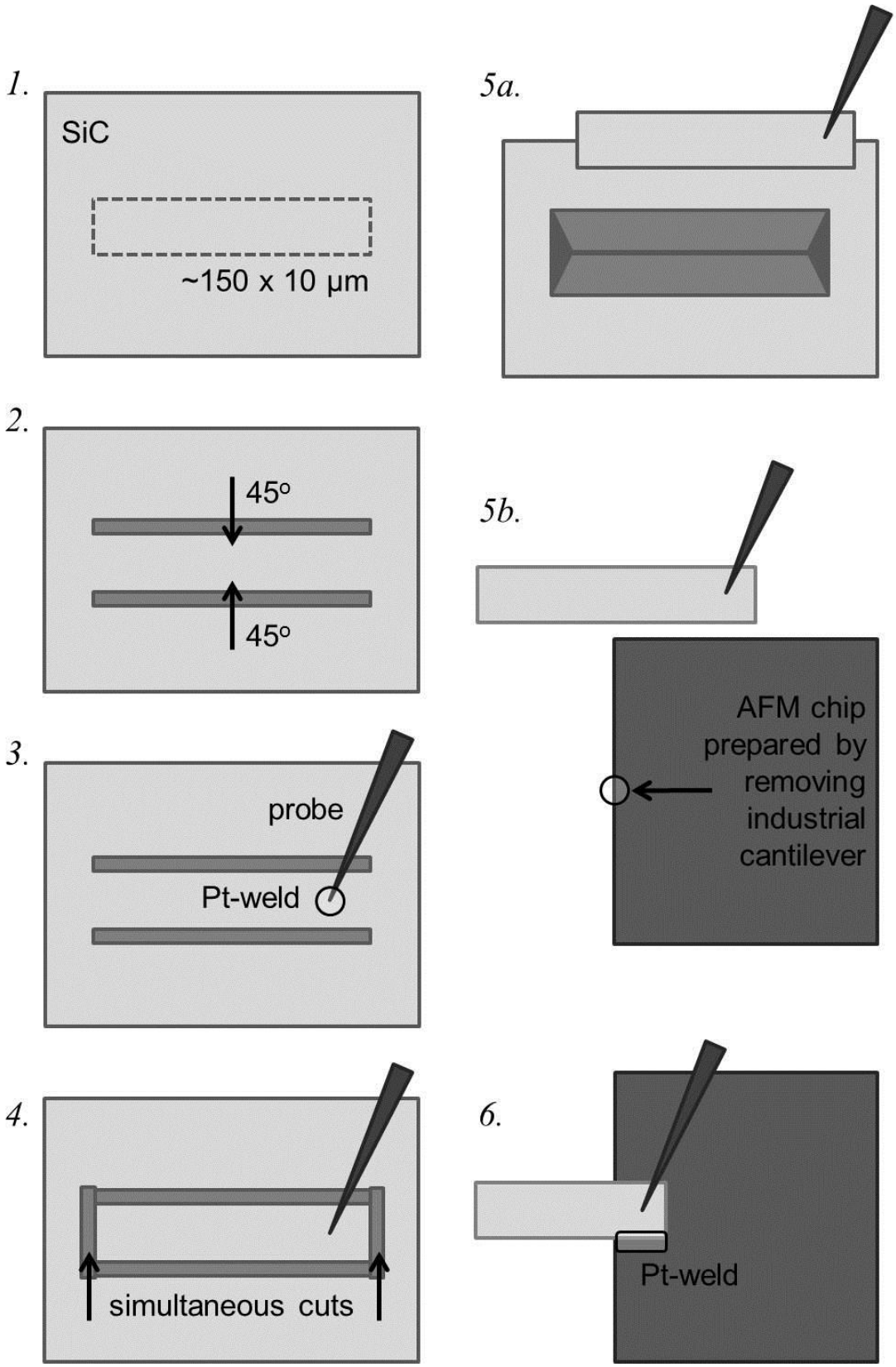

Figure 4.7: Illustration of the cantilever fabrication procedure adopted by this project.

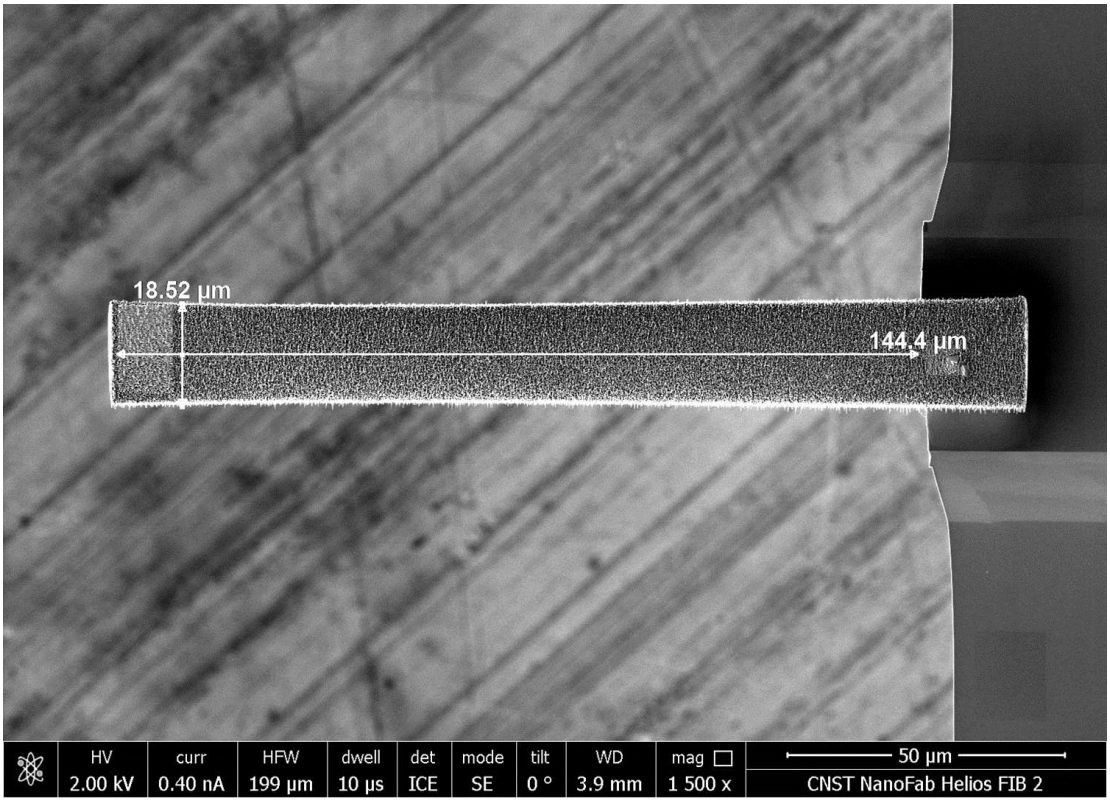

Figure 4.8: An example of a successfully made porous cantilever.

4.2.3 Problems achieving sufficient clamping

The most significant challenge associated with this method for cantilever formation is that the resultant cantilever is not well clamped. The quality of the clamping is significant, as the Euler-Bernoulli beam theory used to analyze the cantilever dynamics assumes perfect clamping. Imperfect clamping changes the dynamic behavior and adds error to measurements, and so must be corrected.

The clamping of this method is weakened due to two reasons. First of all, the Pt-weld is not independently strong enough to keep the cantilever in place under high energy inputs. To remedy this, epoxy is added to the cantilevers outside of the FIB using a micromanipulator equipped with ultra-thin tungsten wire. While evidence

suggests this does not completely rectify the issue, it is shown in section 5.3.1 that it improves the clamping significantly.

The second problem obstructing good clamping is that the cantilever made this way has an equilaterally triangular cross section and is attached to the chip at its apex. This is not a stable position. Three potential solutions were considered: to remove material from the apex to make a trapezoidal cross-sectioned cantilever; to remove a notch from the industrial Si chip in which the apex can fit; or to try to resituate the cantilever so that a flat face is lying against the chip.

By the first idea, milling away the apex of the cantilevers would not only be easier to clamp, but would allow us to approximate a rectangular cross-section, which are preferred in general. However, creating a rectangular cantilever in the FIB requires introducing many more steps, quickly coming to unreasonably long process times. Furthermore, cross-sections produced this way would not be uniform. The FIB suffers some defocusing at great lengths and, while the effect is negligible for most applications, would at best result in uneven surfaces along the dimension from which material was ablated or possibly remove the cantilever entirely. For these reasons this solution was not successful.

The second idea, to create a notch in which to fit the apex of the cantilever, was also unsuccessful. It is in practice very difficult to dependably create a straight and even home for the cantilever and to additionally land the cantilever securely inside it.

The final idea was to attempt to resituate the cantilever on the probe before attaching it to the chip, allowing it to lay with a face against the chip. To do this, the

cantilever would be made as usual through step 4, at which point the cantilever would be severed from the probe, allowing the cantilever to fall and settle face-down. Then, the probe could be reattached at the apex, and the procedure could be continued. Unfortunately, while this is macroscopically intuitive, the microscale cantilever does not behave so predictably. Most often the cantilever is lost altogether. If it does land nearby, it is often at an angle, so that it is skewed when attached to the chip. Ultimately, this idea was decided to result in more failure than improvement.

A dependable solution was not found to land the cantilever in a more stable position. It is believed that imperfect clamping is thus a significant source of error to the analysis. However, the epoxy applied outside of the FIB surrounds the clamped end of the cantilever so that the structure is supported by a case of glue, which adds sufficient stability for a dynamic analysis.

4.2.4 Gas assisted etching

A particularly nefarious problem associated with FIB milling is the redeposition of sputtered material, in which some number of removed atoms reattach to a sidewall rather than escaping the volume [75-77]. SiC is particularly prone to this. Redeposition results in longer process times and "gummy" edges, which in the case of porous SiC means that the porous structures are melted together and erased, reducing the mass reduction so to speak.

Gas-assisted etching is a technique that mitigates these effects [78, 79]. During the milling process, a reactive gas is introduced into the chamber to aid in carrying away sputtered material before it redeposits. There are many gases to choose from for this, and their effectiveness depends on the material to be sputtered. For our

case, xenon difluoride (XeF_2) yields the best results as it both keeps the porous structures clean and intact while also speeding up the milling process by as much as a factor of ten. An illustration of this is given in figure 4.9.

Gas-assisted etching was used for both cantilever fabrication and porosity measurement imaging. However, it was not considered as a way to remove the dense crust layer (section 4.1.3), as a shadowing effect of gas-assisted etching results in an uneven floor level.

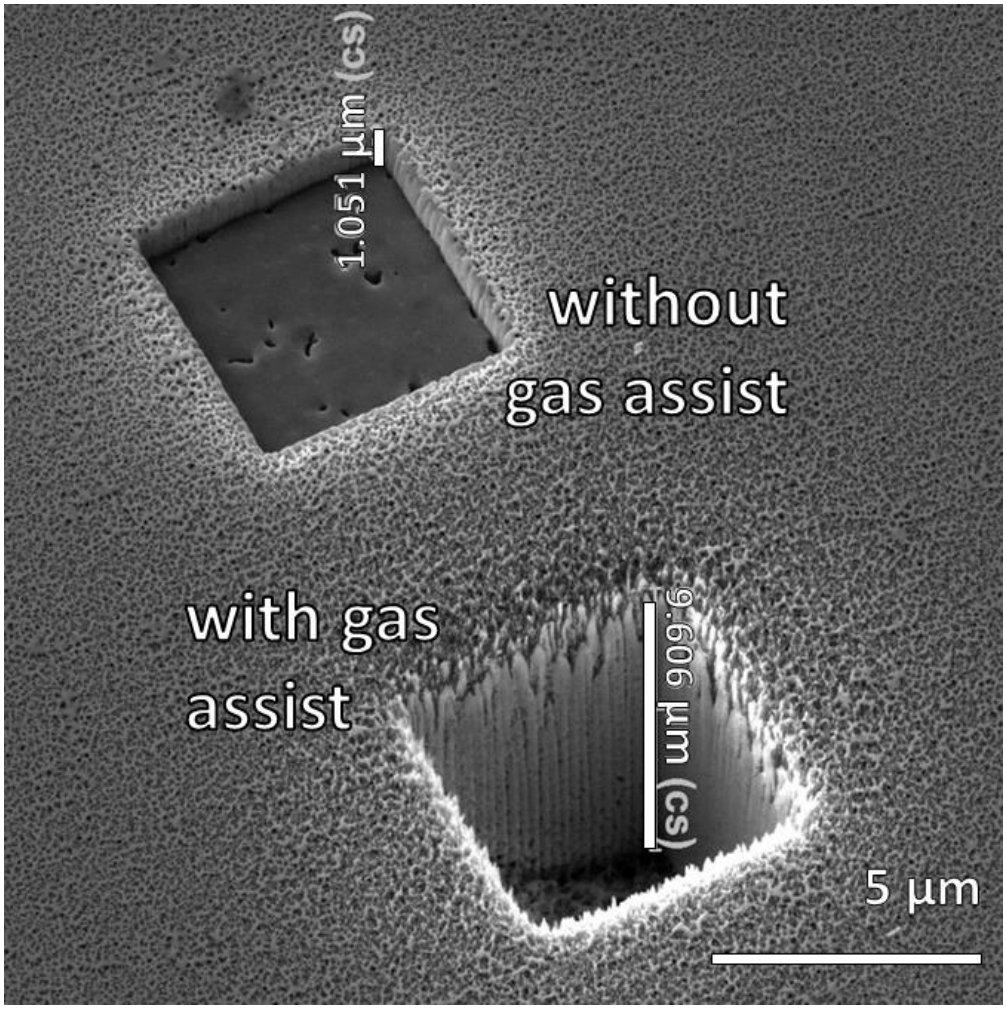

Figure 4.9: Comparison of milling with and without gas-assist. Each trench was milled for the same amount of time. Milling without gas-assist results in a "gummy" surface as a consequence of redeposition, wherein the porous structures of the anodized material are obliterated. Milling with gas-assist yields 10x the depth and preserved porous structures, but an angled floor as a consequence of shadowing.

4.2.5 Note on reflectivity

The backside of an AFM cantilever must be reflective in order to redirect the AFM laser off of the end of the cantilever and onto the PSD. If a cantilever material is not naturally reflective, a thin coating of a reflective material is usually applied to correct it. Porous SiC has an extremely rough surface, scattering light rather than reflecting. It was convenient to use the FIB to deposit a layer of Pt at the free end of the cantilever, where the laser is usually focused to best capture tip motion. This was also originally preferred because mass would only be added to the relevant area, rather than the whole backside, avoiding adding unnecessary mass. Unfortunately, Pt is very heavy; it has a density nearly seven times that of bulk silicon carbide. Moreover, FIB deposition does not produce high quality thin films, meaning that more is required to produce a sufficiently flat, reflective surface. As a consequence, in an effort to create a reflective area on the cantilever surface, a large amount of mass was added to many of the cantilevers. Section 5.3.2 provides an analysis of the Pt deposit's impact on the dynamics. A better option would have been to use a physical vapor deposition tool to deposit a thin layer of material that is less dense than SiC, such as aluminum($\rho_{Al} = 0.82\rho_{SiC}$).

4.3 Cantilever dynamics properties quantification

The force constants, resonance frequencies, quality factors, and geometric properties were measured for each cantilever. The success of the hypothesis is determined by comparing the mechanical properties of a porous cantilever to those of one made from bulk material. A combination of noncontact and contact techniques

was used to measure these properties, including laser Doppler vibrometry (LDV) [80], thermal driving [81], and the reference cantilever method [82, 83].

4.3.1 Noncontact methods: LDV and thermal driving

Two methods that do not require contact were used to take preliminary measurements of the cantilever mechanical properties. This way, measurements could be taken before and after epoxy was added to investigate effects of poor clamping. Both methods extract information from a reflected laser, and so require the cantilever to have a reflective surface.

Laser Doppler vibrometry (LDV) is a noncontact method of measuring cantilever properties with an associated error of below 5%. The method reflects a laser beam off of the end of a cantilever and measures the vibrational spectrum, from which a resonance peak curve can be analyzed to calculate the resonance frequency, its quality factor, and the force constant.

The cantilevers were also thermally driven using the AFM. This method is similar in principle to LDV, as it also analyzes the thermally driven vibrational spectrum to measure the mechanical properties.

The results of these two methods were compared to check accuracy and precision. However, it is believed that the measurements for resonance frequency and quality factor, while accurate, were compromised due to the added mass of the Pt. This is discussed further in section 5.3.2.

4.3.2 Contact method: Reference cantilevers

The reference cantilever method is a technique to extract the force constant of an unknown cantilever by pushing it in series against a well-known cantilever. The method as applied by our system is governed by the equation

$$k_{unknown} = \frac{k_{known} \cdot InvOLS_{unknown}}{InvOLS_{known} - InvOLS_{unknown}} \tag{4.1}$$

InvOLS is a measurement taken by the AFM. It is the inverse optical lever sensitivity in units of nm/V. The stiffness of the known cantilever must be roughly comparable but less than that of the unknown for accuracy. The method is performed by pressing the known cantilever against an "infinitely hard surface" (or, to good approximation, silicon) and then, maintaining similar conditions, pressing it against the unknown cantilever. Error in this method is on the order of 10 to 20%.

Chapter 5: Results and Analysis

5.1 Restatement of Objectives

There are two main goals of this project. First, we want to develop a method for forming qualitatively consistent, highly porous silicon carbide in a room temperature process. We want this process to use for the most part resources that would be available to a typical academic research laboratory—that is, to produce high quality material without relying on highly specialized equipment. To do this we have studied the parameters most influential in the formation of the desired porous structures, attempting to understand how different process recipes affect the qualitative results of the product and to optimize them towards creating as high quality a material as we can. For this application, "high quality" indicates material with clean pores that extend through the volume and significantly (>50%) reduce the bulk mass density, while also providing sufficiently robust structure so that a microcantilever formed from the material can withstand high frequency vibrations and moderately high force impacts.

By avoiding expensive processing equipment, we hope to show that this interesting material is accessible with only a few crucial instruments. It also provides promise that if a simplified process such as the one developed here can produce a sufficient proof of the presented concept, later efforts that introduce specialized equipment will certainly enjoy even better results.

The second objective is to create AFM cantilevers that have a combination of both a high resonance frequency and a low force constant while maintaining

compatible sizes, which are currently unavailable. Contemporary industrial fabrication methods inherently result in one value being compromised for the other. Mass density reduction by introducing porosity could provide a solution to this problem, but has not been greatly explored as it often leads to structural instability. This project argues that reducing the mass density of silicon carbide (SiC) will produce a structurally stable porous foam that does not require sacrificing ideal mechanical properties.

This chapter provides the results of these studies and discusses their implications. It begins with an analysis of the parameters tested while investigating the anodization process, and how the process was ultimately optimized for this application. It then proceeds with a discussion of the theoretical and experimental results of a few successfully fabricated AFM cantilevers.

5.2 Goal one: Anodization process development

5.2.1 Hall measurements

Hall measurements quantify the carrier concentrations specific to each SiC wafer sample, which vary in highly doped semiconductors. The carrier concentration affects the resistivity of the sample, as well as the electrochemical process. Therefore, checking the carrier concentration of each sample is meant to ensure consistent behavior across samples during anodization.

Figure 5.1 displays typical Hall measurements taken at current values ranging from 0.1 to 10 mA for a selection of the samples used for anodization tests. Samples are distinguished by a number and their size, “5” indicating the smaller 5x5 mm wafers and “10” the larger 10x10 mm wafers. The purpose of noting the two sizes is

to see if the doping depends on size. It can be observed that noise significantly affects concentration measurements at low currents, but stabilizes to a consistent value at currents greater than 1 mA.

The range of carrier concentrations for all anodized samples was 1- to 2E15 carriers per cubic millimeter. A larger sample size considering a total of 60 wafers confirms this range. Figure 5.2 illustrates that higher carrier concentrations result in lower electrical resistivity, and vice versa.

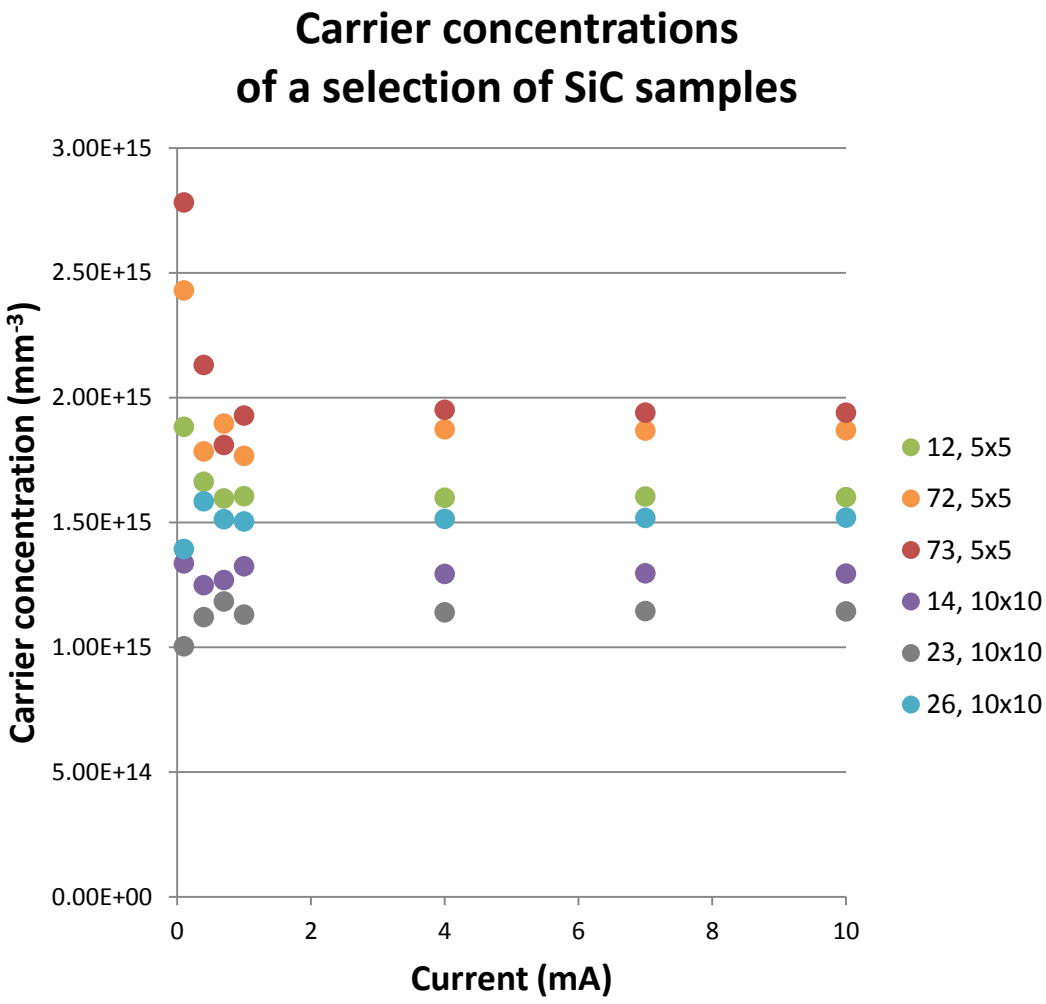

Figure 5.1: A selection of Hall measurements that captures the range of the carrier concentration across all 60 samples. Each sample is labeled by a distinguishing number and its size in millimeters.

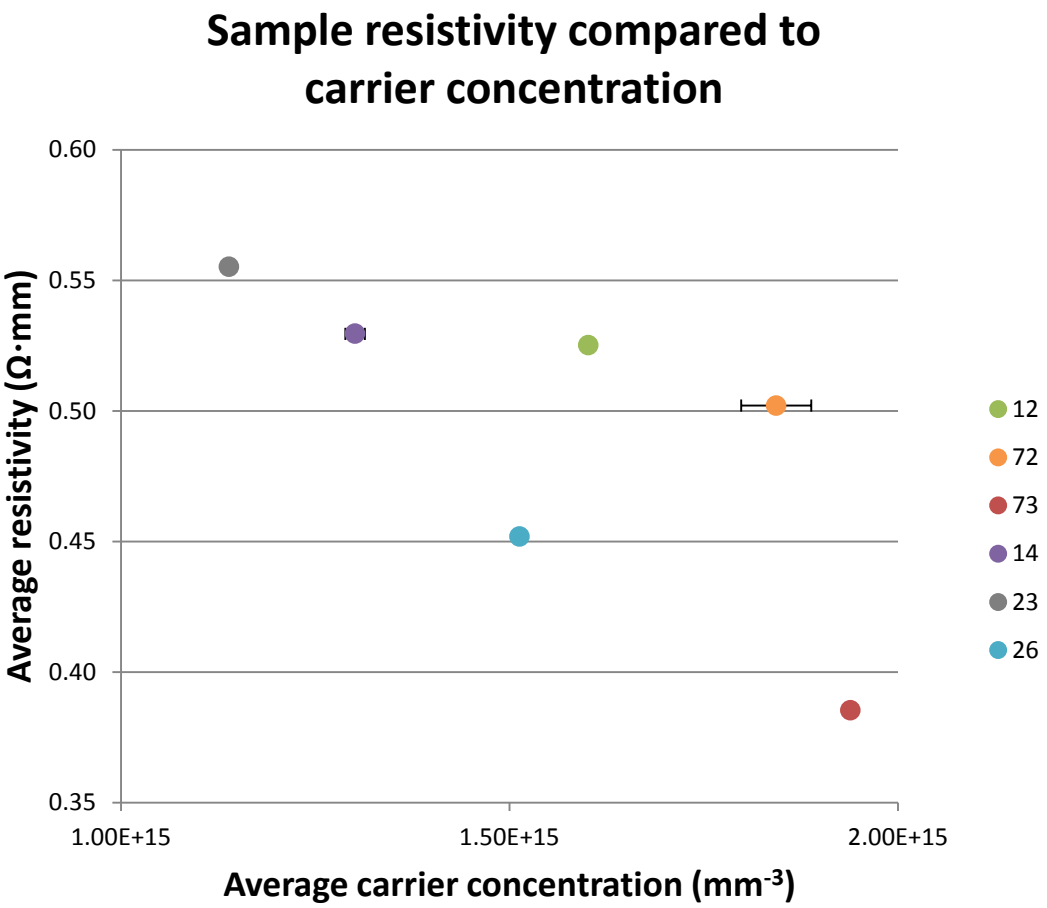

Figure 5.2: The relative resistivities of the selected samples compared to their carrier concentrations. This illustrates the trend that lower carrier concentration results in higher resistivity. Error in the form of standard deviations is included for both axes, although for most measurements the error is smaller than the markers on the graph.

Part of the purpose of these Hall experiments was to investigate how the resistivity may depend on sample size. A compilation of the data organized by size reveals that the 10x10 mm wafers tend to have lower carrier concentrations. Larger samples have a range of carrier concentrations of 0.75- to 1.5E15 carriers per mm^3 while smaller samples have a range of 1.0- to 2.0E15 carriers per mm^3. Because samples were chosen for having low resistivity to aid the anodization process, the consequence of the above trend is that a majority of the anodized samples are the smaller wafers.

These tests offer two conclusions. First, the carrier concentrations are satisfactorily consistent to provide repeatable anodization results. Resistance across samples varies only by 0.2 Ω·mm, which can be mitigated further by choosing samples within a particular range. The samples used in the anodization experiments primarily have carrier concentrations of 1.7E15 mm^{-3} or higher. Second, smaller samples have a slight tendency towards higher carrier concentrations. By choosing samples with higher carrier concentrations, mostly smaller samples were anodized and ultimately used to make cantilevers.

5.2.2 Anodization parameters

Electrochemical etching is a sensitive process that depends on many factors. Different recipes can result in significant qualitative differences in the pore structures, such as creating dendrites or irregularly-spaced pores rather than an organized foam. However, slight recipe variations can also result in improving the qualities of a specific pore morphology, such as pore spacing, diameter, or wall size. To provide a regular, stable structure for a microcantilever, the ideal porous structure is a homogeneous foam. By focusing on fabricating this, many of the anodization parameters can be eliminated, so that only a handful need to be studied to optimize the process for the present application.

To this end, the following parameters were selected to be varied: the concentrations of electrolyte ingredients, the amount of voltage applied, the duration of the process, which sample face was anodized, and the ohmic quality of the anodic electrical junction. By investigating how varying these parameters affected the final product, an optimized processing recipe was developed.

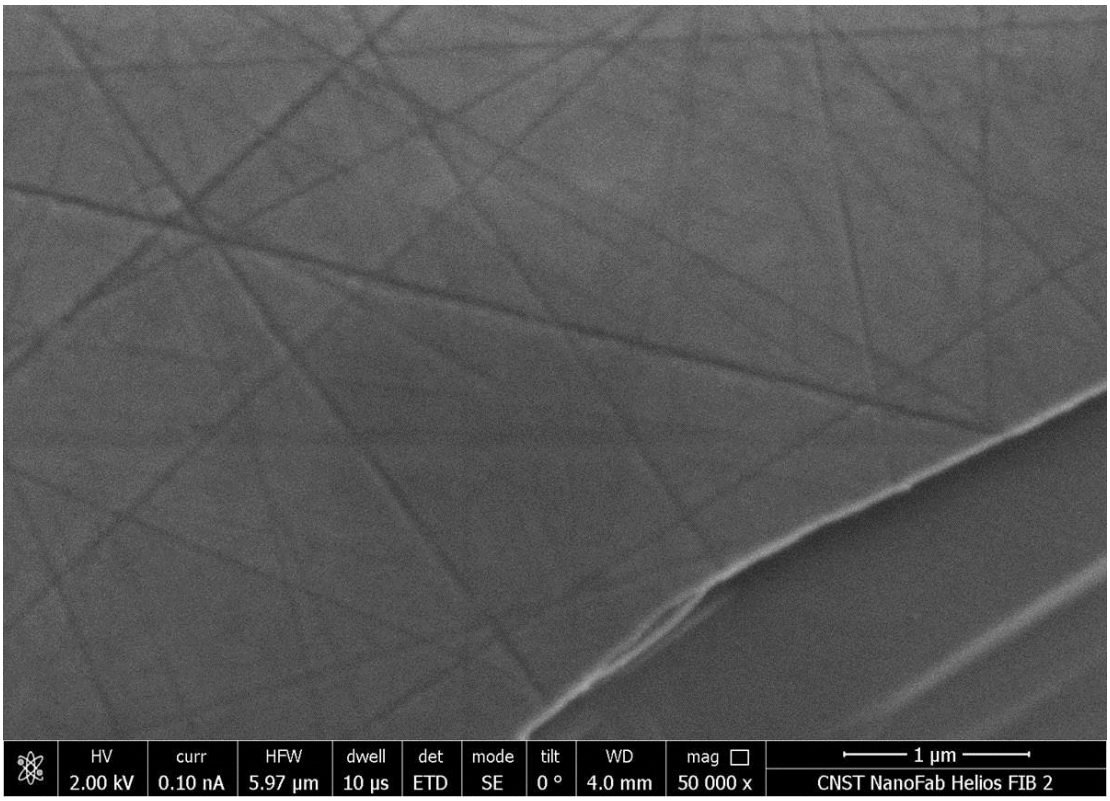

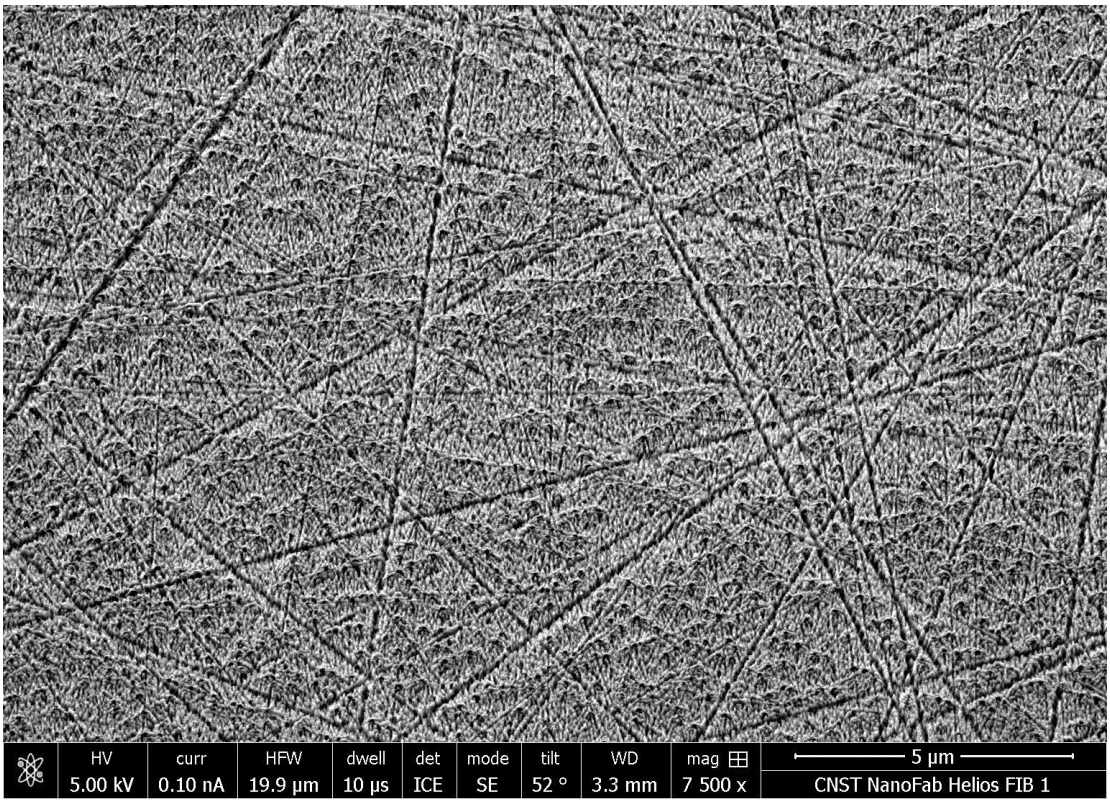

Figure 5.3: A comparison of a SiC wafer surface pre- (top) and post- (bottom) anodization. The intersecting lines are likely artefacts of the crystal structure.

The ingredients of the electrolyte are ethanol, hydrofluoric acid (HF), and deionized water (DI-H_2O). The concentration of ethanol was held at 5% by volume while the concentration of HF was varied in a range of 2 to 20%. The results indicate that the HF concentration affects the diameter of the pores as well as the etching rate. Low HF concentrations formed relatively dense material, such as the blooms from figure 3.8b, that did not extend deeply into the volume. Concentrations above 15% produced structures that were difficult to control, with very large pore sizes and fragile pore walls, and many stratified layers that delaminated while etching. A final recipe that used 10% HF by volume with 5% ethanol and 85% DI-H_2O was ultimately determined to generate pores that were stable and regularly spaced while maximizing mass loss.

The applied voltage during the electrochemical reaction was varied from 5 to 30 V. Experiments showed that low voltages are insufficient to achieve the desired porous structures, while high voltages deteriorate the sample. Furthermore, the optimal voltage is dependent on the resistivity (and thus the carrier concentration) of the SiC sample. By choosing wafers of similar resistivity, the influence of this fact was avoided. For samples with carrier concentrations within the range of 1.7- to 2.0E15 mm^{-3}, a voltage of 20 V formed the desired structures most effectively.

The duration of the process was also tested. The depth of the created porous material is not linearly dependent on time. After the initial 5 minutes the propagation of pores slows down very quickly. However, the quality of the produced material does not significantly change. A duration of 25 to 30 minutes created a sufficient amount of porous material with which to make cantilevers.

The last tests investigated whether it is optimal to etch the silicon-terminated or the carbon-terminated face of the wafer. Results of these tests were considered to simultaneously demonstrate how the ohmicity of the anodic electrical junction affected the sample, as the Si-face provided significantly improved ohmic contact than the C-face. Examining each side showed that etching the C-face produces a deeper porous layer by nearly three times while etching the Si-face produces larger pore diameters. This is believed to be related to the resistivity. Etching the Si-face means that the electrical junction is on the C-face, which is more resistive. This reduces the effective voltage and limits the process from etching deeper but is believed to allow prolonged etching along the pore walls. In contrast the electrical junction to the Si-face is purely ohmic, so that there is no additional boundary adding to the effective resistance. Etching the C-face thus results in greater depth for the same duration. Table 5.1 displays these results.

Face etched	**Porous material depth (μm)**	**Pore diameter (nm)**
C-terminated	87 ± 7	72 ± 8
Si-terminated	29 ± 4	196 ± 14

Table 5.1: A comparison of averaged depth and pore diameter results from anodizing the carbon-terminated face and the silicon-terminated face.

The implications of these results are that anodizing the silicon-face produces greater mass loss but with weaker walls. Anodizing the carbon-face produces more material in the same amount of time. For this reason, most of the cantilevers are formed from anodizing the C-terminated face.

Table 5.2 gives the final process recipe used to make the porous SiC from which the microcantilevers were formed as a result of these tests.

Anodization process recipe	
Electrolyte recipe (by volume)	10% HF; 5% ethanol; 85% DI-H_2O
Voltage	20 V, constant current
Duration	25-30 mins
Sample face etched	C-face

Table 5.2: The finalized process recipe optimizing porous material quality for this project. Anodized samples in future references were made using the recipe.

5.2.3 Depth-dependence of porosity

As described in section 4.1.3, a phenomenon characteristic of these anodizations is the formation of a "crust" layer of relatively dense porous material at the surface. This is believed to be a consequence of the surface chemistry associated with using deionized water in the electrolyte [52].

Using high resolution SEM images, this layer has been found to extend 5 to 15 μm into the larger volume, depending primarily on the duration of the electrochemical etching process. Longer process times result in thicker dense layers, although it is not a linear relationship. Production of the denser layer slows down considerably past depths of 10 μm, and appears to terminate by depths of 15 to 20 μm regardless of very long process times. This denser layer is not ideal for this project, which aims to maximize mass loss. Comparing the mass density loss of these two porous layers shows a difference of between 20 to 25%; the greater density surface layer yields only 49 ± 4% mass reduction and the lower density layer 72 ± 6%. These comparisons were done across six samples anodized using the finalized process recipe from table 5.2. Figure 5.5 shows a typical porosity gradient into the sample.

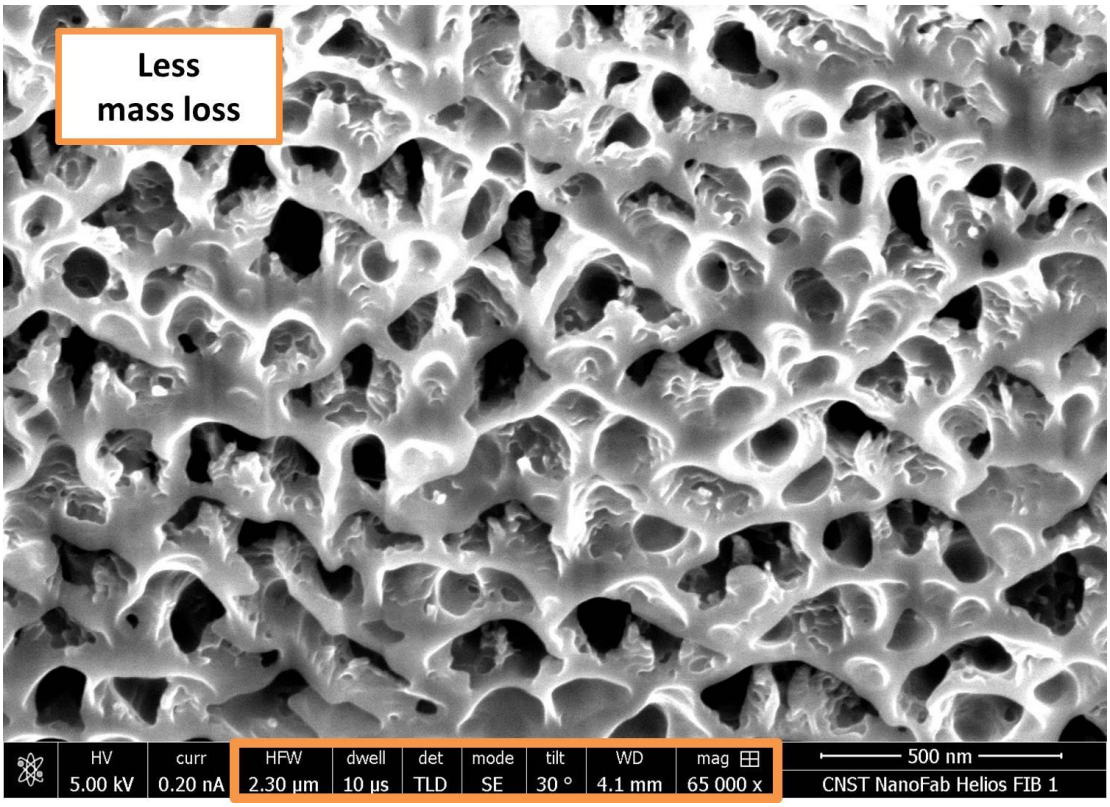

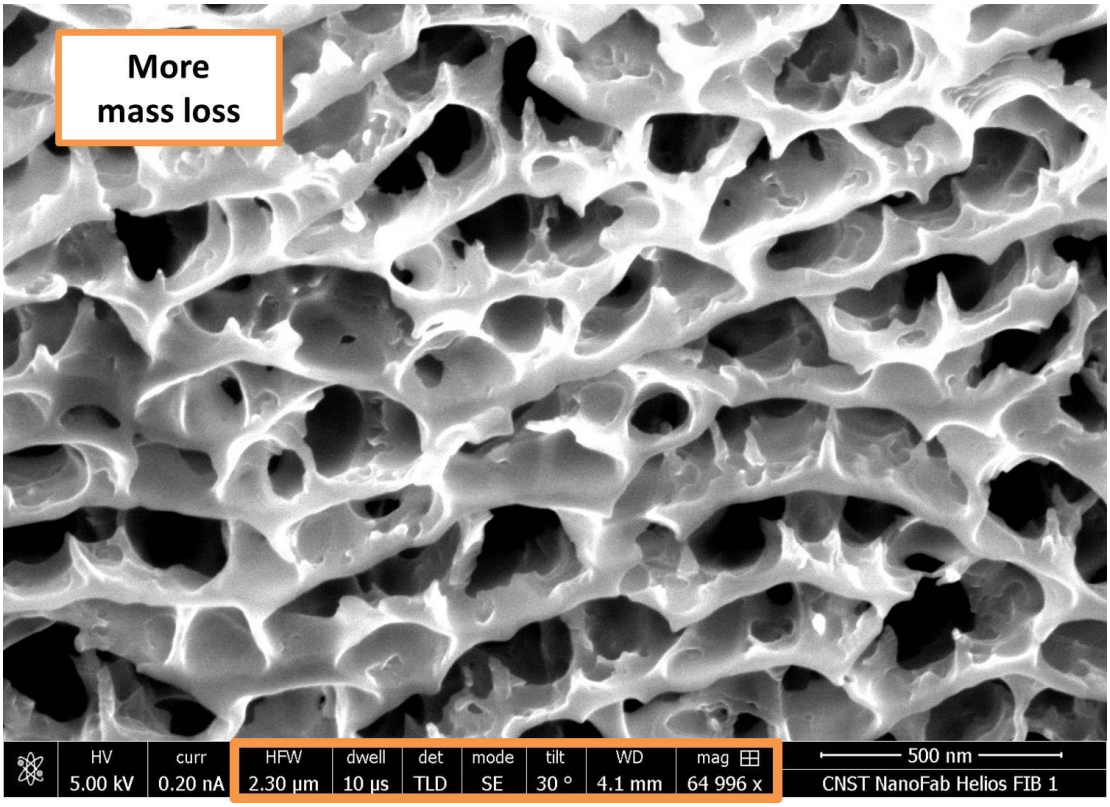

Figure 5.4: A direct comparison of the two different porosity layers shown in figure 4.4. All optical parameters were held constant so that this is a one-to-one comparison.

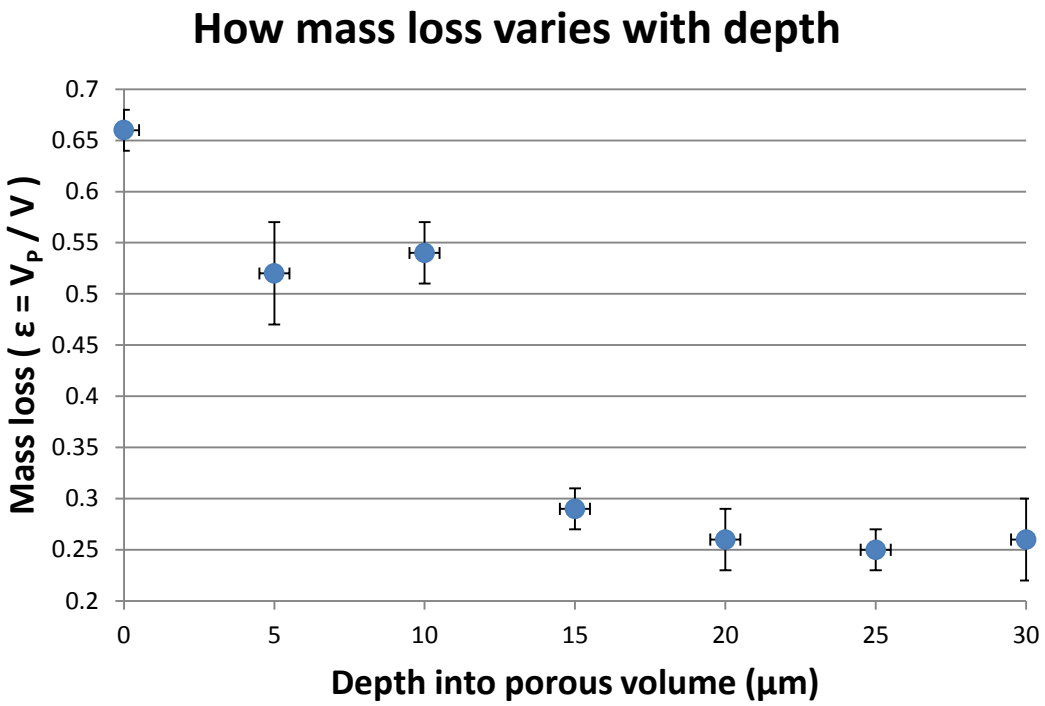

Figure 5.5: A typical porosity gradient into the depth of the porous material. Once past the dense surface layer, porosity reduces dramatically.

5.2.4 Mass reduction results

During parametric trials, mass reduction experiments produced a large range from 55 to 87% of original mass lost. The finalized process dependably created material with 60 to 75% mass loss, from which cantilevers were made. Porosity measurements for the cantilevers are given in table 5.3. Investigating using the SEM, which provides a resolution of nearly 2 nm, there are no discernable features roughening the walls. This indicates that the pores are very clean and thus offer good quality structures for our purposes.

Many of the anodized samples had highly variable pore diameters (standard deviation $\sigma > 30\%$). Areas chosen for cantilever formation were specifically chosen for having relatively low variance ($\sigma < 15\%$). Pore walls have even smaller variation

($\sigma \approx 10\%$). The combination of these indicates that the porosity is homogeneous to good approximation and that the assumption of uniformity is thus reasonable.

Mass reduction of cantilevers			
Lever	**$\varepsilon = V_{por}/V_{bulk}$**	**Pore diameter (nm)**	**Pore wall size (nm)**
Porous 1	0.28	249 ± 33	87 ± 8
Porous 2	0.36	218 ± 28	96 ± 10
Porous 3	0.33	204 ± 12	92 ± 7
Porous 7	0.27	242 ± 32	83 ± 9
Porous 9	0.29	208 ± 19	72 ± 6
Porous 11	0.24	254 ± 38	78 ± 6
Porous 13	0.39	198 ± 30	94 ± 13

Table 5.3: Porosity measurements for a selection of the fabricated cantilevers.

Cross-sectional analysis shows that the anodization process etches away mass at a consistent rate across the entire interface, with only a small decrease in achievable depth near the edge of the exposed area before dropping off completely where the surface is unexposed.

A defect in the crystal structure appears to be impassable by the anodization process, causing hillocks where the porous material meets the bulk material substrate (illustrated in figure 5.6). These defects compromise the regularity of the porous structures in the immediate surrounding area and so should be avoided within the cantilever material. This can easily be done, as they only appear near the substrate at the lower limit of the porous volume.

Other interruptions in the porous material are rare. The most dramatic ones are large pits that are visible at the surface, and so are easily avoided.

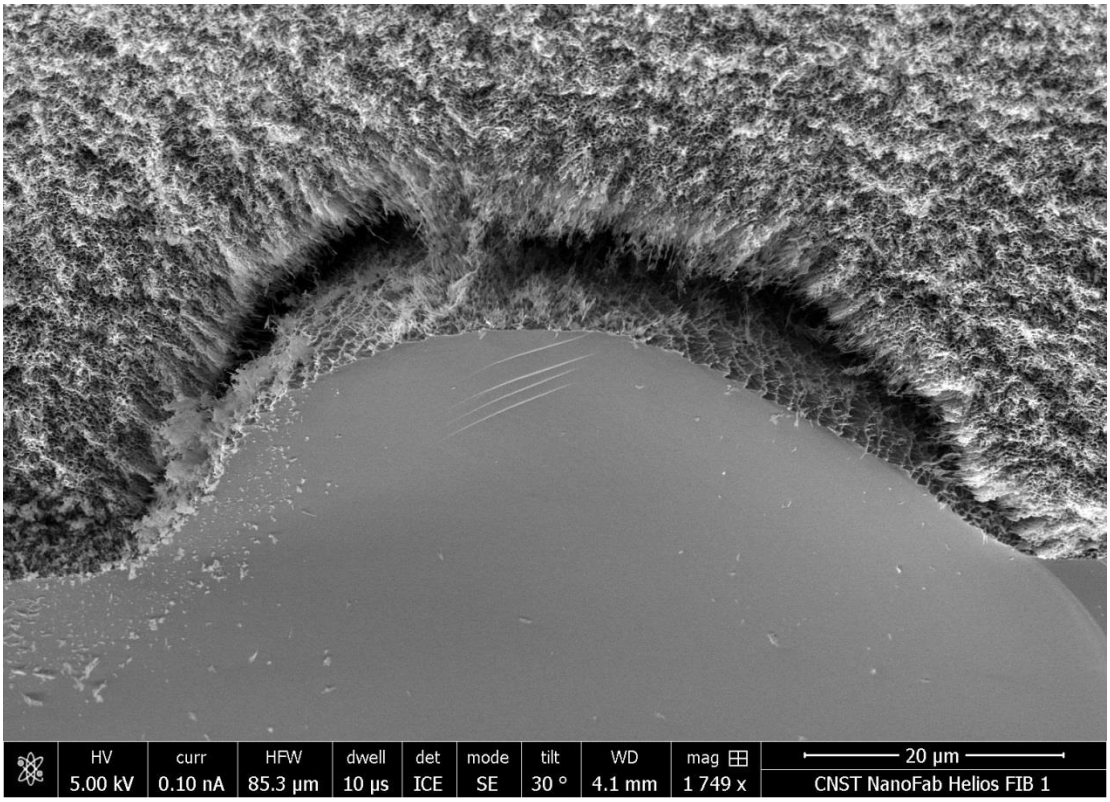

Figure 5.6: A defect in the anodization process at the limit of the anodized material and the substrate. The homogeneity of the surrounding area is compromised and so should not be used for cantilever fabrication.

In conclusion, high mass reduction with relatively little variation was achieved for the production of several porous cantilevers. It is believed that a well-developed process using specialized equipment could easily create large quantities of effectively homogeneous material to manufacture AFM cantilevers for use within a variety of applications.

5.2.5 Anodization conclusions

Hall measurements were taken to affirm consistent dopant levels in silicon carbide samples. Proving small variation in charge carriers across samples eliminates the major variable between samples that influences the electrochemistry. Thus the following experiments can focus on studying the consequences of varying parameters

of the electrochemical process. These measurements not only successfully prove that dopant levels and resistance varied only within a small range, but they also allowed samples to be specifically chosen according to where they fell in that range. In this way, the resistance of samples anodized varied by only 10%.

Subsequent experiments testing the electrochemical parameters included investigating the electrolyte recipe, the voltage applied, the duration of the process, and the sample face etched. The results of these tests informed the process that was ultimately chosen for the cantilevers to be produced, given in table 5.2.

A significant characteristic of the anodization process was a relatively dense crust layer that formed atop the first ~10% of the porous material. This denser layer is not recommended for cantilever material, as it is more massive compared to the less dense material below.

Mass reduction quantification showed that the finalized process recipe consistently reduced the material mass density by 68 ± 8 %. Additionally, the structures below the aforementioned crust were highly regular and closely-spaced, with diameters of nearly a quarter of a micron and wall sizes less than 100 nm. The consistency of these results suggests that the cantilevers can be assumed to be homogeneous to a reasonable approximation.

At this point we have completed our first goal of developing a process for the production of high quality porous SiC using only a few specialized tools and materials. Table 5.4 lists and describes the purpose of the most important equipment in the process. Most of it is available to standard research facilities and the rest is available with access to a fabrication laboratory.

Special equipment	Purpose
A physical vapor deposition tool	To deposit the thin conductive layer of the anodic junction. In this project, a sputter tool was used.
Annealing furnace	To encourage ohmicity of conductive layer. Must reach temperatures of at least 500^{o}C.
Power supply	To drive the electrochemical reaction
Fume hood	To safely house the electrolyte
Hydrofluoric acid	Hazardous ingredient in the electrolyte

Table 5.4: The few specialized tools and materials necessary for fabricating porous SiC.

5.3 Goal two: Low k, high f_0 AFM cantilever fabrication

Using a combination of LDV, thermal driving, and reference cantilever methods, the resonance frequency f_0 and force constant k of several porous and bulk SiC cantilevers were measured. A few iterations of analysis were required to properly understand the dynamics, as will be described below.

5.3.1 Consequences of poor clamping

The preliminary results from the noncontact methods are given below in table 5.5. By optically measuring the cantilever dimensions to calculate the volume V, the effective mass density can be found using equation 3.20. This can then be compared to the known bulk density to produce a ratio describing the density loss, which can further be compared to predicted mass loss ratios from table 5.3.

Lever	f_0 (kHz)	k (N/m)	ρ_{calc}/ρ_{bulk}	ρ_{pred}/ρ_{bulk}
Porous 1	243	7	0.84	0.28
Porous 3	321	12.6	0.33	0.33
Porous 9	362	8.9	0.44	0.29
Bulk 10	572	33.2	0.96	1.00
Porous 11	193	6	0.58	0.24

Table 5.5: Preliminary results of noncontact methods.

These results agree closely with predicted values for cantilevers 3 and 10, the latter of which is made from bulk material. However, the mechanical properties of cantilevers 1, 9, and 11 seem to overestimate the mass. A likely suspect for this inconsistency is a softening of the measured force constant due to poor clamping. The cantilevers were connected to the silicon AFM chip first by tacking them on using platinum (Pt) deposited by the FIB. Outside of the FIB, the cantilevers were additionally glued using an epoxy. However, it was difficult to control the glue application and most were still not very well clamped, as is illustrated in figure 5.7.

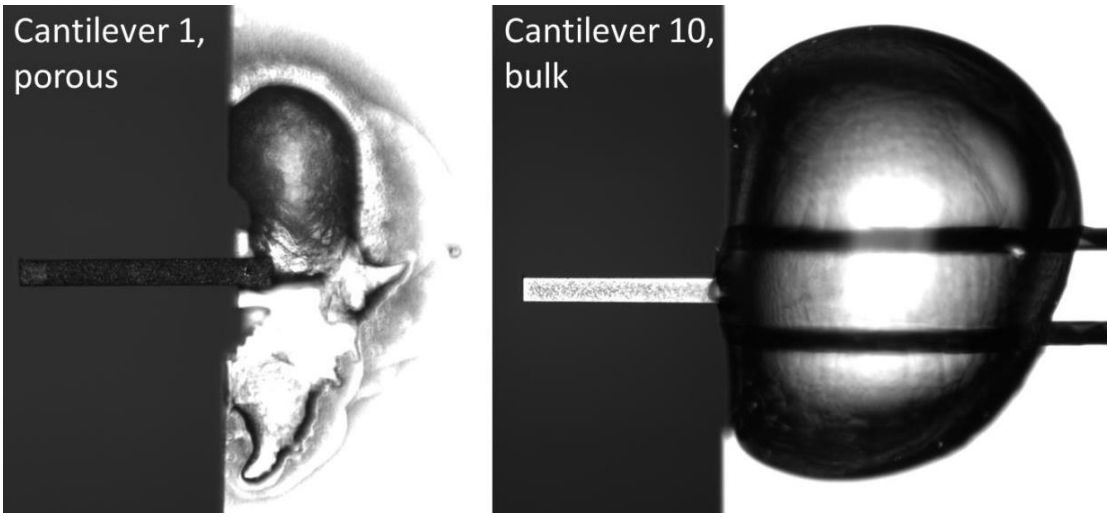

Figure 5.7: Initial gluing of two cantilevers. Cantilever 10 appears to be well clamped while cantilever 1 requires a second attempt.

In an effort to correct this, a second round of glue was applied and properties were measured again. The results of the secondary noncontact measurements are given in table 5.6. The two sets of measurements are compared in figure 5.8. Cantilever 10 was already sufficiently well glued, so it serves as a check that measurements are consistent. It is apparent how improved clamping results in higher force constants which likewise raise the resonance frequency.

Lever	f_0 (kHz)	k (N/m)	ρ_{calc}/ρ_{bulk}	ρ_{pred}/ρ_{bulk}
Porous 1	292	9.6	0.80	0.28
Porous 3	362	17	0.35	0.33
Porous 9	362	8.9	0.44	0.29
Bulk 10	571	34	0.99	1.00
Porous 11	212	6.7	0.54	0.24

Table 5.6: Secondary results of noncontact methods.

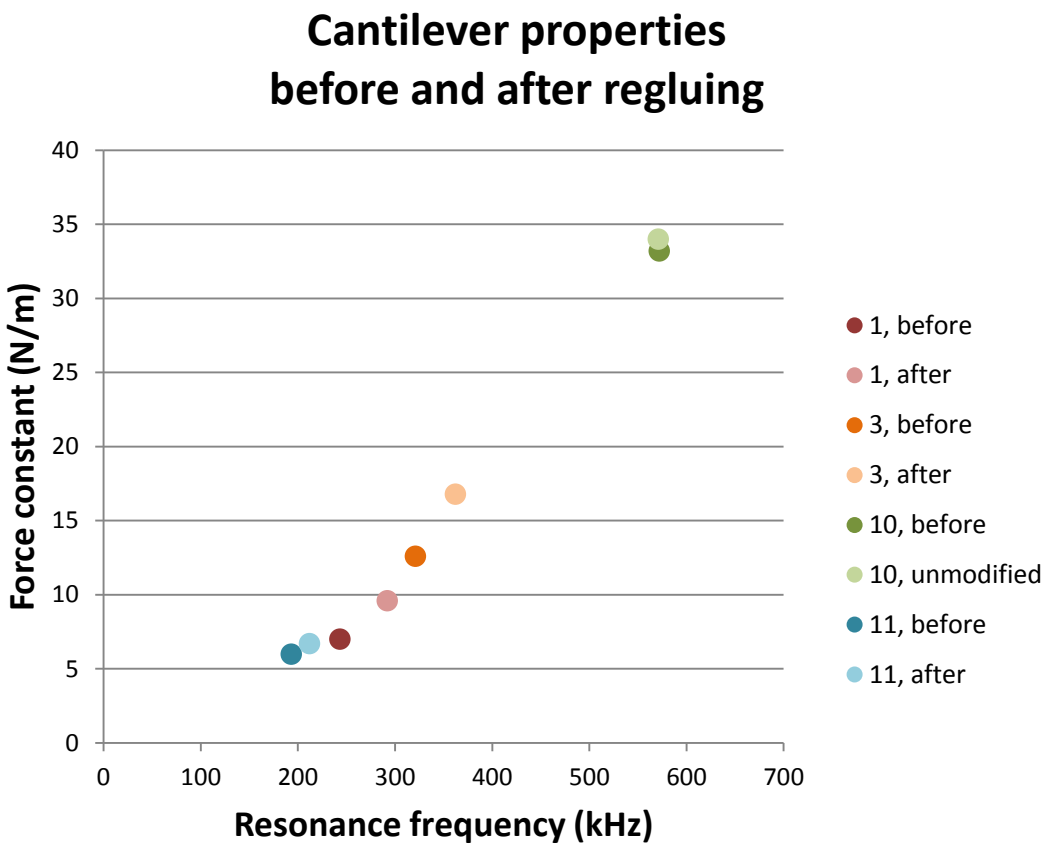

Figure 5.8: A comparison of property values before and after regluing. Cantilevers 10 and 11, which had already been relatively well glued for the first measurement, do not show significant change, as expected. Cantilever 9 was not glued a second time and so does not appear here.

Attempts to provide better clamping to the cantilevers do not resolve the inconsistency between our measured and expected mass densities. However, the quality of the clamping clearly impacts the cantilevers' mechanical properties. The

dynamics of the cantilever described by Euler-Bernoulli beam theory assumes perfect clamping; if our cantilevers are insufficiently clamped, the theory inaccurately relates to our results [84, 85]. Therefore, while the curiosity of the overestimated masses requires further investigation, investing efforts into improving the cantilever clamping is worthwhile for our analysis.

5.3.2 Impact of platinum deposit

Thermal and LDV measurements require that the cantilever have a somewhat reflective surface off of which a laser can reflect. Cantilever 1 from figure 5.7 illustrates how the porous SiC material has too rough a surface to be reflective on its own, compared to the bulk SiC material of cantilever 10. Therefore, as was described in section 4.2.5, a layer of Pt was deposited at the free end of some of the porous cantilevers, such as is shown below.

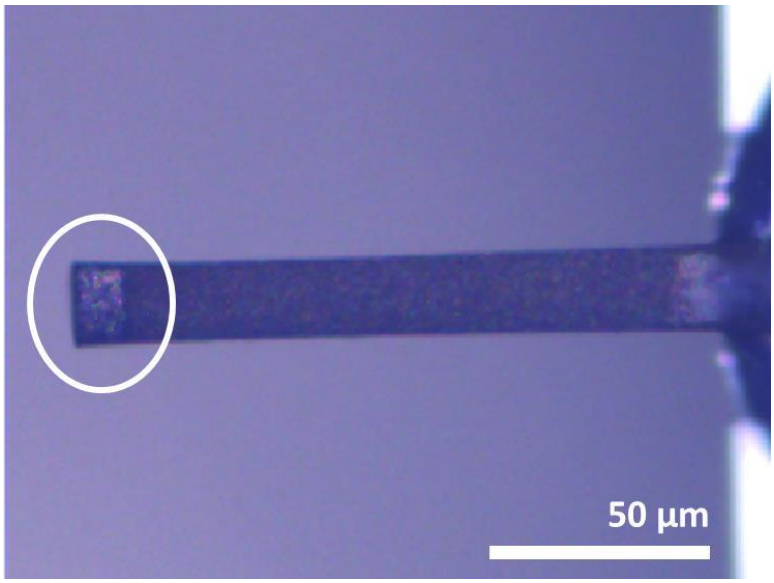

Figure 5.9: Pt deposited on the free end of cantilever 11, intended to enhance reflectivity.

This was not originally expected to greatly impact the dynamics. However, Pt is denser than bulk SiC by a factor of seven, suggesting that even a small amount

could be significant. Therefore, after noncontact measurement methods consistently overestimated the cantilevers' mass, the contribution due to the Pt was considered.

To include the mass of the Pt, the deposited volume was measured optically and confirmed by notes taken during deposition. Then, the effective mass density attributed to just the cantilever was calculated by removing the contribution from the Pt. These results are displayed in table 5.7.

Lever	m_{calc} (kg)	m_{Pt} (kg)	ρ_{calc}/ρ_{bulk}	ρ_{pred}/ρ_{bulk}
Porous 1	3.57E-11	1.39E-11	0.49	0.28
Porous 3	4.11E-11	1.12E-11	0.26	0.33
Porous 9	2.15E-11	0.43E-11	0.35	0.29
Bulk 10	3.31E-11	0	0.99	1.00
Porous 11	4.72E-11	2.14E-11	0.29	0.24

Table 5.7: Corrected mass density ratios after accounting for added Pt.

Initially, this appears to improve our analysis. The mass density ratios calculated from the noncontact measurements agree more closely with the predicted values. However, upon closer inspection, the mass of the Pt apparently makes up a significant portion of the cantilever's mass, by as much as ~50% in the case of cantilever 11. For this reason, the noncontact methods do not accurately capture the dynamic behavior of the cantilevers, but more likely that of the mass at the end. Additionally, the estimated contributions of the Pt have significant associated uncertainty (±0.5E-11 kg), and therefore these results are prone to error.

Ultimately, while this exercise does not offer accurate results, it reveals why these noncontact methods produced measurements that did not relate to each other in expected ways. Fortunately, the added Pt does not impact the measurements made using contact methods, as will be explained in the next section. Therefore, the final

analysis will rely on contact measurements of the force constants and the mass loss ratios predicted from table 5.3.

5.3.3 Effect of porosity on elastic modulus

In addition to the noncontact methods, the reference cantilever method was used to take contact measurements of the cantilevers' force constants. For a cantilever with an equilaterally triangular cross-section, the force constant is related to fundamental parameters by

$$k = \frac{\sqrt{3}Ew^4}{32L^3} \tag{5.1}$$

Because it does not depend on the cantilever's mass, the force constant is unaffected by the added Pt.

It is unclear to what degree introducing porosity affects the material's elasticity *E*. From equation 5.1 we can calculate the effective *E* of each of the porous cantilevers and compare it to that of the bulk cantilever. Table 5.8 shows the results of these calculations.

Lever	E_{calc} (GPa)	E_{calc}/E_{bulk}	ρ_{pred}/ρ_{bulk}
Porous 1	5.73	0.18	0.28
Porous 3	9.31	0.30	0.33
Porous 9	4.62	0.15	0.29
Bulk 10	31.0	1.00	1.00
Porous 11	3.46	0.11	0.24

Table 5.8: Calculated values for elastic moduli, with comparisons between *E* and ρ of the porous cantilevers and bulk cantilever.

These calculations show expected relationships between the density loss and the elasticity loss, as visualized in figure 5.10. However, the bulk cantilever was

expected to come closer to the elastic modulus given in the literature, ≈ 450 GPa. The fact that it does not ($E_{10} = 0.07E_{sic}$) is likely a residual consequence of imperfect clamping. By normalizing the analysis to the bulk cantilever we eliminate the influence of poor clamping in this analysis and can compare porous and bulk cantilevers directly. This assumes that the quality of clamping is the same for each cantilever. This assumption is reasonable for cantilevers 1, 3, 10, and 11; cantilever 9, however, may not be well glued and therefore has higher associated error.

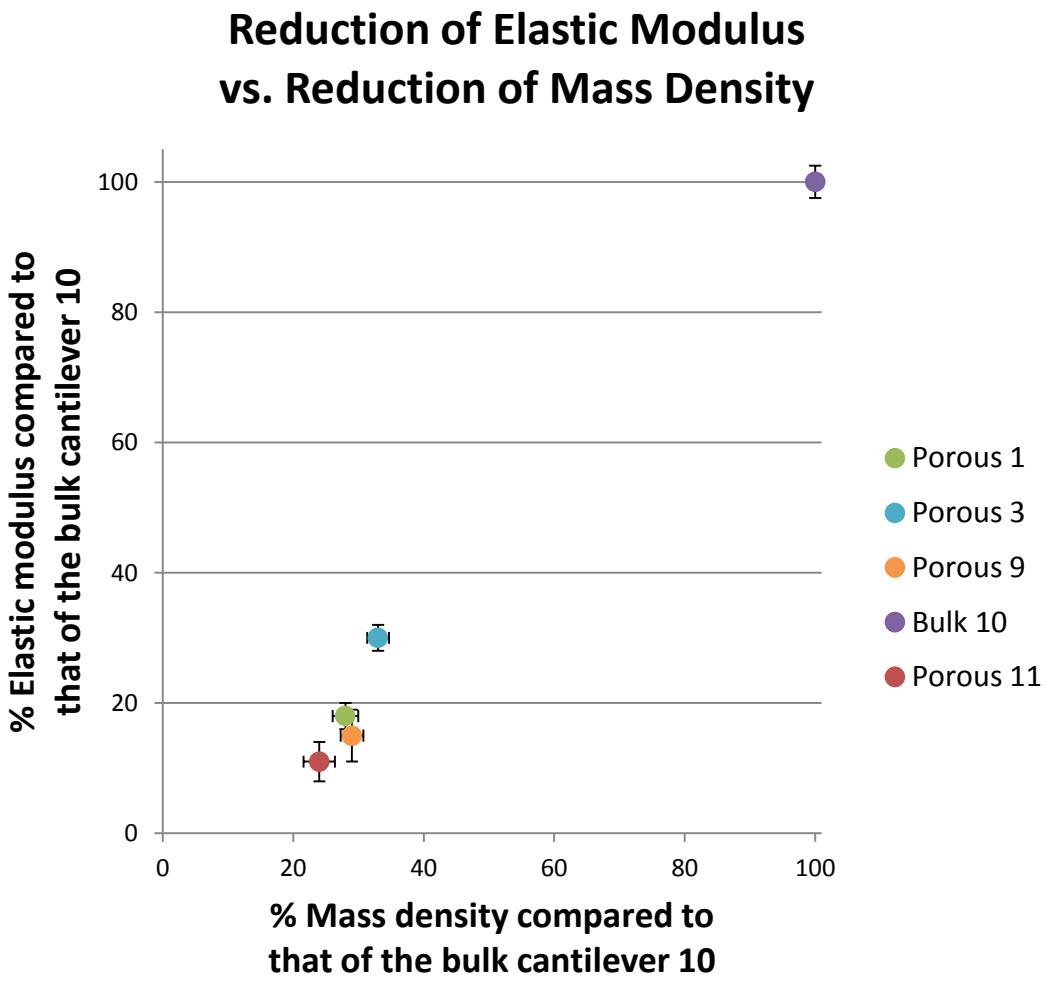

Figure 5.10: Visualization of how introducing porosity reduces material elasticity.

At this point we have confirmed that introducing porosity not only reduces a cantilever's mass, but additionally its force constant as a consequence of the reduced elastic modulus. The next section explores how the combination of these reductions impacts the cantilever's resonance frequency, which is dependent on both.

5.3.4 Porous and bulk cantilever dynamics

Equipped with measured and calculated values for each of the fundamental parameters, we can finally draw some conclusions regarding how introducing porosity affects the cantilever dynamics. To do this, we invent imaginary cantilevers made from bulk SiC that are identically sized to the porous ones. The dynamic properties of these imaginary bulk cantilevers are calculated by replacing the values for E and ρ of the porous cantilevers with those of the bulk cantilever 10. These values are given in table 5.9.

Lever	L (μm)	k_p (N/m)	f_{0p} (kHz)	k_b (N/m)	f_{0b} (kHz)	k_p/k_b	f_{0p} / f_{0b}
Porous 1	120	9.6	494	54	617	0.18	0.80
Porous 3	176	15.8	361	54	384	0.29	0.94
Porous 9	121	8.8	445	62	633	0.14	0.70
Bulk 10	116	X	X	35	577	1.00	1.00
Porous 11	153	6.8	320	62	472	0.11	0.68

Table 5.9: Dynamic property calculations of porous cantilevers and analogous bulk cantilevers using measurements of fundamental parameters. Subscript *p* refers to "porous" and *b* refers to "bulk."

First, it is worthwhile to directly compare the real values found for cantilevers 1 and 10, which have similar lengths ($L_1 = 1.03L_{10}$). The resonance frequency of the porous cantilever is comparable ($f_{0,1} = 0.86f_{0,10}$) while the force constant is greatly reduced ($k_1 = 0.27k_{10}$). This shows directly the difference in the dynamics of a bulk

cantilever and porous cantilever of similar sizes without depending on extrapolated values.

Secondly, the invention of analogous bulk cantilevers shows that the mass density reduction is not enough to completely counteract the elastic modulus reduction. In other words, the cantilevers made from porous material experience some reduction in their associated resonance frequencies. However, while bulk cantilevers have the advantage of having higher resonance frequencies, they also have much higher force constants. Figure 5.11 illustrates the differences in the factors by which porous cantilevers suffer a reduction in f_0 but enjoy a lower k.

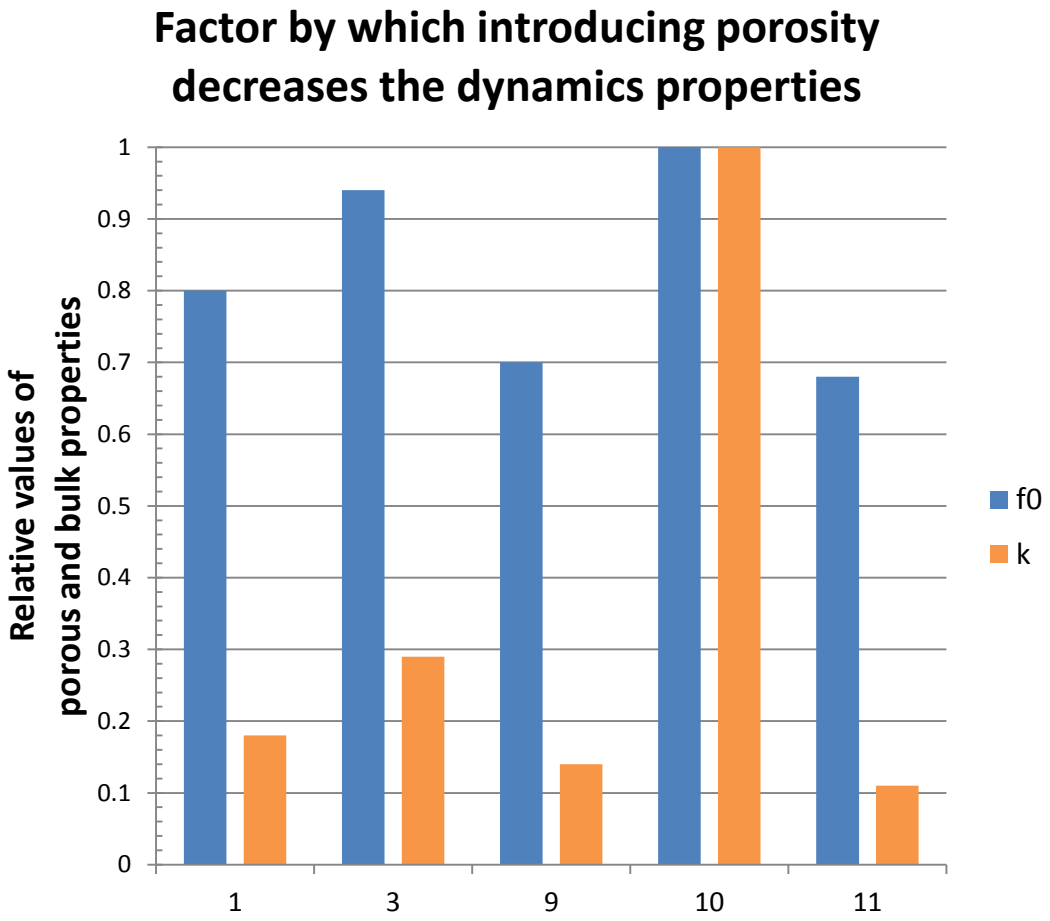

Figure 5.11: Porosity decreases the cantilever dynamic properties. However, the force constants are much more dramatically reduced than the resonance frequencies.

This proves that fabricating cantilevers from porous SiC would produce AFM probes with significantly lower force constants than probes made from bulk SiC for the same resonance frequency. A slight reduction in size could compensate for the frequency reduction while maintaining compatible geometries and dramatically softening the cantilever. This offers a way to provide AFM probes that have a combination of low k and high f_0, which are otherwise not available and would be a significant improvement for many important AFM modes of operation.

Chapter 6: Conclusions

6.1 Summary of results

This thesis describes the process undertaken to fabricate and analyze porous silicon carbide AFM cantilevers. The goal is to prove that reducing the material's mass density would produce cantilevers with simultaneously low force constants and high resonance frequencies while maintaining detectable sizes, a previously inaccessible combination of properties.

The first task for this project was to develop a method for creating porous SiC that produced the highest quality porosity according to the needs of this application. In this case, this requires a combination of maximizing mass reduction while maintaining structural integrity. For this purpose, a porous foam was deemed the most promising pore morphology, of the many that can be produced by porosification. To do this, an electrochemical etching procedure well-established in the literature was assembled and the parameters most influential to the quality of the porous structures were systematically optimized. The results of this analysis informed the process recipe ultimately used to create the porous material for the cantilevers.

The next task was to quantify the mass lost as a result of the anodization event. It was critical to implement a method that could measure the porosity of a local area rather than the averaged porosity of the whole wafer. By taking localized measurements, the mass reduction for a particular cantilever could be more accurately quantified. Additionally, the quality and regularity of the porous structures could be analyzed, as it is important that porous cantilevers maintain structural robustness and

homogeneity (to maintain the validity of assuming uniformity in the analysis). For these reasons, quantifying mass loss was done using a dual scanning electron microscope (SEM) and focused ion beam (FIB), to take advantage of high resolution imaging capabilities in conjunction with the freedom to manipulate the sample. This latter point was pertinent due to a known depth-dependence of the porosity that could be quantified using the FIB.

After this, cantilevers could be formed. While photolithographic processes are most popular for AFM cantilever fabrication, this project again employed the FIB in order to maintain control over individual structures. Many cantilevers were formed out of both bulk and porous material, although many were lost due to insufficient clamping. Ultimately four porous cantilevers and one bulk cantilever survived to the completion of the analysis.

The issue of insufficient clamping demonstrated the need for further preparation before conducting a final comparison of the mechanical properties. This is because the Euler-Bernoulli model applied to analyze the dynamic behavior of the cantilevers assumes perfect clamping. Epoxy was therefore added to the clamped end of the cantilevers in an effort to provide additional support. Tests show that the added epoxy improves the clamping significantly.

A variety of noncontact and contact methods were employed to measure the mechanical properties of the cantilevers. Noncontact methods determined the force constant, resonance frequency, and quality factor of the cantilevers. These results generally followed the trend of the expected behavior, but significantly overestimated the mass of a few of the cantilevers compared to predicted values. It is demonstrated

that this is likely due to an added mass of platinum. Adding the platinum had been intended to create a reflective area at the free end of the cantilever, which is necessary for the noncontact measurements. While correcting for this yields more expected relationships between the mass, force constant, and resonance frequency, it is ultimately decided that the resultant associated error compromises the validity of the noncontact methods' results.

Subsequently, contact methods were employed to take measurements of the force constants using a method that is unaffected by the added platinum. These measurements agree with those from the noncontact methods to within 5% error, as expected. Because the force constant of the structure is not affected by the added mass, these values can be considered accurate for the cantilever structure independently. Using the relationship of the force constant with fundamental parameters, the effective elastic moduli of the porous and bulk SiC cantilevers could be calculated. In this way, it is shown that introducing porosity reduces the elastic modulus to approximately 10% that of the bulk cantilever's. Equipped with these results in addition to estimations for the mass, the resonance frequencies of the cantilevers without the added platinum were determined.

Finally, values of the mechanical properties for the porous cantilevers could be compared to those of the bulk cantilever, as well as imaginary bulk cantilevers analogous in size to the porous ones. Results proved that forming cantilevers out of porous material reduced the force constants 82±7% compared to the analogous bulk cantilevers, while only reducing the resonance frequencies by 22±10%. Furthermore, the real bulk cantilever was compared directly to a porous cantilever of similar size,

confirming these results with less error ($L_1 = 1.03L_{10}$ proving similar sizes, $f_{0,1} = 0.86f_{0,10}$ proving small reduction in resonance frequency, and $k_1 = 0.27k_{10}$ proving large reduction in force constant). This confirms the hypothesis that simultaneously low *k* and high f_0 AFM cantilevers can be created without compromising size.

6.2 Future work

This project easily has the capacity to become a larger scale project with the potential to yield a dissertation or a patent. There are a multitude of directions one can go towards the ultimate goal of perfecting a process for the industrialization of porous silicon carbide AFM cantilevers.

For example, while optimizing the anodization process was studied, it certainly was not exhausted. The range most consistently achieved here was between 60 to 75% mass reduction. However, higher porosity could be achievable. Continued research into both the anodization process (to maximize mass loss) and the cantilever fabrication process (to protect the clarity of the pores so that mass is not regained) could further improve the degree to which the force constant is reduced.

In this vein, the reduction of the elastic modulus can also be much more thoroughly studied. By experimentally demonstrating how porosity relates to the cantilever's elasticity in the case of silicon carbide, the force constant and resonance frequency could be controlled—perhaps not independently, but in a way that has not been previously possible.

Moreover, if very high porosity (>80%) cantilevers are pursued, it is unclear how it would affect the structural integrity. Even assuming that higher porosity cantilevers are strong enough to withstand impact forces, there is a limit to how much

mass is removable before the structure no longer functions as an AFM probe. For example, at a certain amount of mass loss the remaining material would not form a continuous structure and it would no longer be possible to assume that the material properties are uniform through the cantilever. Another aspect is that some substance must exist of the cantilever in order for the laser to have a surface off of which to reflect. Deeper research would be able to quantify the limit at which porosity compromises the cantilever's structure, perhaps by employing finite element analysis or other computer simulation.

A significant improvement that should be investigated is how to fabricate cantilevers with rectangular cross sections. "Diving board" cantilevers are favored in the AFM community and so ones made from a new material would easily conform to numerous existing applications. A process for fabricating these would likely utilize established photolithographic methods similar to those used for bulk silicon or silicon nitride cantilevers. Development of such a process would have to consider how to best protect the clarity of the porous material, in order to avoid inadvertently raising the mass when applying photolithographic masks, such as photoresist. However it is likely that nanoporous features are too small to be contaminated and, if they are, any masking material that leaks into the pores will also be accessible to standard removal processes.

A crucial task related to improving the cantilever fabrication method is to develop a way to produce a porous SiC cantilever monolithically from a SiC chip. Monolithic cantilevers are significantly superior structurally as they provide perfect clamping to the cantilever. Additionally, the AFM tip could be monolithically

fabricated to capitalize on SiC properties like low wear and low stiction that make it an intriguing AFM probe material. Again, methods for creating the entire chip-lever-tip structure out of porous or a combination of bulk and porous SiC could be adapted from already established methods for making monolithic silicon probes.

A final improvement would be to apply a reflective surface to the backside of the cantilever without adding excessive mass. This would be most efficiently done by depositing a thin film of aluminum using physical vapor deposition (PVD).

6.3 Intellectual contributions and anticipated benefits

The success of this project offers a significant contribution to the AFM community by making possible the fabrication of cantilevers that are relatively soft while maintaining resonance frequency and compatible sizes. Many AFM modes of operation must sacrifice resolution or tip and sample preservation for scanning speed or low noise, due to the nature of the influence of the fundamental parameters on the mechanical properties. These fundamental parameters can be organized as geometric (L, w, t) and material (E, ρ). Up to this point, material properties could not be altered without compromising the cantilever's robustness. Therefore, only the geometric properties could be extensively modified, and they affect k and f_0 in such a way that precludes cantilevers from being both low k and high f_0.

This project offers a demonstration that silicon carbide, already considered a promising AFM probe material, retains its structure even after introducing significant porosity. Thus, the material properties can be modified, making available a previously inaccessible parameter with which to adjust the cantilever's mechanical properties. The result of reducing mass density and consequently the elastic modulus is a

cantilever with slightly reduced f_0 and greatly reduced k, thus proving the possibility of low k, high f_0 cantilevers.

The benefits of this project are far-reaching. The atomic force microscope is an essential tool for the nanoscale characterization of materials. The cantilevers described in this project would allow many AFM operative modes to better optimize experimental parameters. These applications include classic contact mode, which is the original mode of operation and one of the most widely used; lateral force microscopy, which is a popular method for measuring nanoscale friction forces; and fast tapping mode, which is crucial for faithfully imaging soft samples in the biological and medical sciences. By using porous silicon carbide probes, experiments would be able to achieve higher resolution, cause less sample damage, and beat sample deterioration, all with less noise and without purchasing expensive modifications to standard equipment.

Appendix: Error Analysis

The project was largely intended as a proof of concept, and so a rigorous error analysis is not crucial. However, it is worthwhile to discuss significant sources of error and how they might impact the final results, to ensure no false conclusions were made.

The first part of the project, which was a series of parametric experiments exploring the anodization process, was for the most part simply qualitative. Error was mitigated where possible, such as choosing samples with resistivities that varied within 15% and maintaining consistent anodization parameters. The most significant source of variance between anodized samples was likely the quality of the anodic electrical junction, which is affected by the ohmicity of the metal-deposit on the sample and the area of contact between the foil and the metal-deposit. The latter varies with the size of the strip of foil and when air bubbles are trapped between the foil and the sample in the anodization package.

Porosity measurements are taken directly using the SEM and FIB. Contributions to error include uncertainty in the measurements (<5%) and variance in the pore qualities (~15%).

The largest source of error in the final analysis of the cantilever mechanical properties is due to imperfect clamping. Using LDV, the resonance peaks of the second mode were detected and shown to be lower than predicted by the theory. This indicates that the cantilevers still are not perfectly clamped, even after a second application of glue. The true force constants of the cantilevers with perfect clamping would likely be an additional 30% higher. However, since the force constant would

simply scale all calculations up, for both the porous and imaginary bulk cantilevers, this does not impact the final conclusion of the analysis in any way.

The most significant issue that could potentially detract from the quality of the analysis due to error is in the case of underestimation of the predicted mass. The difference between f_0 for the porous and bulk cantilevers depends directly upon the mass prediction. For example, while it was ultimately concluded that porous resonance frequencies only suffer an averaged 25% reduction compared to those of the bulk, an error of 10% in the predicted porosity would result in a comparative reduction of 35% between the porous and bulk resonance frequencies. Fortunately, the directness of the porosity measurements leads to a low associated error of ±8%, further implying that the mass could be overestimated as easily as underestimated. Furthermore, while it is possible that the cantilever fabrication process suffered some erasure of the pores due to redeposition, an improved process using specialized equipment would allow for the maintenance of clear pores, eliminating this issue.

Bibliography

[1] Binnig, G., Quate, C. F., & Gerber, C. (1986). Atomic force microscope. Physical review letters, 56(9), 930.

[2] Albrecht, T. R., Grütter, P., Horne, D., & Rugar, D. (1991). Frequency modulation detection using high-Q cantilevers for enhanced force microscope sensitivity. Journal of Applied Physics, 69(2), 668-673.

[3] Zhong, Q., Inniss, D., Kjoller, K., & Elings, V. B. (1993). Fractured polymer/silica fiber surface studied by tapping mode atomic force microscopy. Surface Science Letters, 290(1), L688-L692.

[4] Frisbie, C. D., Rozsnyai, L. F., Noy, A., Wrighton, M. S., & Lieber, C. M. (1994). Functional group imaging by chemical force microscopy. Science, 265(5181), 2071-2074.

[5] Meyer, G., & Amer, N. M. (1990). Simultaneous measurement of lateral and normal forces with an optical-beam-deflection atomic force microscope. Applied physics letters, 57(20), 2089-2091.

[6] Martin, Y., Abraham, D. W., & Wickramasinghe, H. K. (1988). High-resolution capacitance measurement and potentiometry by force microscopy. Applied Physics Letters, 52(13), 1103-1105.

[7] Rief, M., Oesterhelt, F., Heymann, B., & Gaub, H. E. (1997). Single molecule force spectroscopy on polysaccharides by atomic force microscopy. Science, 275(5304), 1295-1297.

[8] Bhushan, B., & Koinkar, V. N. (1994). Nanoindentation hardness measurements using atomic force microscopy. Applied physics letters, 64(13), 1653-1655.

[9] Martin, Y., & Wickramasinghe, H. K. (1987). Magnetic imaging by ‘‘force microscopy’’with 1000 Å resolution. Applied Physics Letters, 50(20), 1455-1457.

[10] Nonnenmacher, M., o’Boyle, M. P., & Wickramasinghe, H. K. (1991). Kelvin probe force microscopy. Applied Physics Letters, 58(25), 2921-2923.

[11] Majumdar, A. (1999). Scanning thermal microscopy. Annual review of materials science, 29(1), 505-585.

[12] Minne, S. C., Adams, J. D., Yaralioglu, G., Manalis, S. R., Atalar, A., & Quate, C. F. (1998). Centimeter scale atomic force microscope imaging and lithography. Applied Physics Letters, 73(12), 1742-1744.

[13] Piner, R. D., Zhu, J., Xu, F., Hong, S., & Mirkin, C. A. (1999). " Dip-pen" nanolithography. science, 283(5402), 661-663.

[14] AC10FS Olympus AFM probe. Retrieved October 29, 2014, from www.asylumresearch.com/Probe/AC10FS,Olympus

[15] AC10DS Olympus AFM probe. Retrieved October 29, 2014, from www.asylumresearch.com/Probe/AC10DS,Olympus

[16] Boubekri, R., Cambril, E., Couraud, L., Bernardi, L., Madouri, A., Portail, M., ... & Gauthier, S. (2014). Electrothermally driven high-frequency piezoresistive SiC cantilevers for dynamic atomic force microscopy. Journal of Applied Physics, 116(5), 054304.

[17] Cimalla, V., Pezoldt, J., & Ambacher, O. (2007). Group III nitride and SiC based MEMS and NEMS: materials properties, technology and applications. Journal of Physics D: Applied Physics, 40(20), 6386.

[18] Michaud, J. (2014). Silicon carbide (SiC) for high power electronics. Retrieved October 29, 2014, from greman.univ-tours.fr/activities/silicon-carbide-sic--283292.kjsp

[19] Binnig, G., Rohrer, H., Gerber, C., & Weibel, E. (1982). Surface studies by scanning tunneling microscopy. Physical review letters, 49(1), 57.

[20] Radmacher, M. (1997). Measuring the elastic properties of biological samples with the AFM. Engineering in Medicine and Biology Magazine, IEEE, 16(2), 47-57.

[21] Fotiadis, D., Scheuring, S., Müller, S. A., Engel, A., & Müller, D. J. (2002). Imaging and manipulation of biological structures with the AFM. Micron, 33(4), 385-397.

[22] Kasas, S., Thomson, N. H., Smith, B. L., Hansma, P. K., Miklossy, J., & Hansma, H. G. (1997). Biological applications of the AFM: from single molecules to organs. International journal of imaging systems and technology, 8(2), 151-161.

[23] Burton, Z., & Bhushan, B. (2006). Surface characterization and adhesion and friction properties of hydrophobic leaf surfaces. Ultramicroscopy, 106(8), 709-719.

[24] Vericat, C., Vela, M. E., Benitez, G. A., Gago, J. M., Torrelles, X., & Salvarezza, R. C. (2006). Surface characterization of sulfur and alkanethiol self-assembled monolayers on Au (111). Journal of Physics: Condensed Matter, 18(48), R867.

[25] Poon, C. Y., & Bhushan, B. (1995). Comparison of surface roughness measurements by stylus profiler, AFM and non-contact optical profiler. Wear, 190(1), 76-88.

[26] Garcia, R., & San Paulo, A. (1999). Attractive and repulsive tip-sample interaction regimes in tapping-mode atomic force microscopy. Physical Review B, 60(7), 4961.

[27] Kopycinska-Müller, M., Geiss, R. H., & Hurley, D. C. (2006). Contact mechanics and tip shape in AFM-based nanomechanical measurements. Ultramicroscopy, 106(6), 466-474.

[28] Atamny, F., & Baiker, A. (1995). Direct imaging of the tip shape by AFM. Surface science, 323(3), L314-L318.

[29] Radmacher, M., Tillamnn, R. W., Fritz, M., & Gaub, H. E. (1992). From molecules to cells: imaging soft samples with the atomic force microscope. Science, 257(5078), 1900-1905.

[30] Berglund, B., Hassmen, P., & Job, R. S. (1996). Sources and effects of low-frequency noise. The Journal of the Acoustical Society of America, 99(5), 2985-3002.

[31] Eaton, P. J., & West, P. (2010). Atomic force microscopy (Vol. 10). Oxford: Oxford University Press.

[32] How to choose AFM probes: Composition. Retrieved October 29, 2014, from www.spmtips.com/how-to-choose-afm-probes-by-experiment-composition.html

[33] Reitsma, M. G. (2007). Lateral force microscope calibration using a modified atomic force microscope cantilever. Review of Scientific Instruments, 78(10), 106102.

[34] Morita, S., Wiesendanger, R., & Meyer, E. (Eds.). (2002). Noncontact atomic force microscopy (Vol. 1). Springer.

[35] Martin, Y., Williams, C. C., & Wickramasinghe, H. K. (1987). Atomic force microscope–force mapping and profiling on a sub 100-Å scale. Journal of Applied Physics, 61(10), 4723-4729.

[36] Grütter, P., Zimmermann-Edling, W., & Brodbeck, D. (1992). Tip artifacts of microfabricated force sensors for atomic force microscopy. Applied physics letters, 60(22), 2741-2743.

[37] Ivanov, D. A., Amalou, Z., & Magonov, S. N. (2001). Real-time evolution of the lamellar organization of poly (ethylene terephthalate) during crystallization from the melt: high-temperature atomic force microscopy study. Macromolecules, 34(26), 8944-8952.

[38] Neumeister, J. M., & Ducker, W. A. (1994). Lateral, normal, and longitudinal spring constants of atomic force microscopy cantilevers. Review of Scientific Instruments, 65(8), 2527-2531.

[39] Russel, P., & Krause, O. (2008). AFM Probe Manufacturing. NanoWorld Services.

[40] Wolter, O., Bayer, T., & Greschner, J. (1991). Micromachined silicon sensors for scanning force microscopy. Journal of Vacuum Science & Technology B, 9(2), 1353-1357.

[41] Choose from available probes. (2014). Retrieved October 29, 2014, from www.asylumresearch.com/ProbeStore/MODEL_FAMILY

[42] Meirovitch, L., & Parker, R. G. (2001). Fundamentals of vibrations. Applied Mechanics Reviews, 54, 100.

[43] Morrison, S. R. (1980). Electrochemistry at semiconductor and oxidized metal electrodes.

[44] Bagotsky, V. S. (Ed.). (2005). Fundamentals of electrochemistry (Vol. 44). John Wiley & Sons.

[45] Memming, R. (2008). Semiconductor electrochemistry. John Wiley & Sons.

[46] Shor, J. S., Grimberg, I., Weiss, B. Z., & Kurtz, A. D. (1993). Direct observation of porous SiC formed by anodization in HF. Applied physics letters, 62(22), 2836-2838.

[47] Shor, J. S., & Kurtz, A. D. (1994). Photoelectrochemical Etching of 6 H-SiC. Journal of the Electrochemical Society, 141(3), 778-781.

[48] Lauermann, I., Memming, R., & Meissner, D. (1997). Electrochemical properties of silicon carbide. Journal of The Electrochemical Society, 144(1), 73-80.

[49] Zangooie, S., Woollam, J. A., & Arwin, H. (2000). Self-organization in porous 6H–SiC. Journal of Materials Research, 15(09), 1860-1863.

[50] Zangooie, S., Jansson, R., & Arwin, H. (1998). Microstructural control of porous silicon by electrochemical etching in mixed HCl/HF solutions. Applied surface science, 136(1), 123-130.

[51] Feenstra, R. M., & Wood, C. E. (2008). Porous silicon carbide and gallium nitride: epitaxy, catalysis, and biotechnology applications. John Wiley & Sons.

[52] Kang, M. G., Lezec, H. J., & Sharifi, F. (2013). Stable field emission from nanoporous silicon carbide. Nanotechnology, 24(6), 065201.

[53] Ke, Y. (2007). Formation and Characterization of Columnar Porous SiC Fabricated by Photo-electrochemical Etching (Doctoral dissertation, University of Pittsburgh).

[54] Wu, C. C., Xu, H., Otto, C., Reinhoudt, D. N., Lammertink, R. G., Huskens, J., ... & Velders, A. H. (2009). Porous multilayer-coated AFM tips for dip-pen nanolithography of proteins. Journal of the American Chemical Society, 131(22), 7526-7527.

[55] Pikul, J. H., Dai, Z., Yu, X., Zhang, H., Kim, T., Braun, P. V., & King, W. P. (2014). Micromechanical devices with controllable stiffness fabricated from regular 3D porous materials. Journal of Micromechanics and Microengineering, 24(10), 105006.

[56] Cullis, A. G., & Canham, L. T. (1991). Visible light emission due to quantum size effects in highly porous crystalline silicon.

[57] Lehmann, V., & Gösele, U. (1991). Porous silicon formation: A quantum wire effect. Applied Physics Letters, 58(8), 856-858.

[58] Wolkin, M. V., Jorne, J., Fauchet, P. M., Allan, G., & Delerue, C. (1999). Electronic states and luminescence in porous silicon quantum dots: the role of oxygen. Physical Review Letters, 82(1), 197.

[59] Cullis, A. G., Canham, L. T., & Calcott, P. D. J. (1997). The structural and luminescence properties of porous silicon. Journal of Applied Physics, 82(3), 909-965.

[60] Lin, V. S. Y., Motesharei, K., Dancil, K. P. S., Sailor, M. J., & Ghadiri, M. R. (1997). A porous silicon-based optical interferometric biosensor. Science, 278(5339), 840-843.

[61] Klobes, P., Meyer, K., & Munro, R. G. (2006). Porosity and specific surface area measurements for solid materials. US Department of Commerce, Technology Administration, National Institute of Standards and Technology.

[62] Levinshtein, M. E., Rumyantsev, S. L., & Shur, M. S. (Eds.). (2001). Properties of Advanced Semiconductor Materials: GaN, AIN, InN, BN, SiC, SiGe. John Wiley & Sons.

[63] Harris, G. L. (Ed.). (1995). Properties of silicon carbide (No. 13). Iet.

[64] Courtney, T. H. (2005). Mechanical behavior of materials. Waveland Press.

[65] Gurtin, M. E. (1982). An introduction to continuum mechanics. Academic press.

[66] Lehmann, V., & Grüning, U. (1997). The limits of macropore array fabrication. Thin Solid Films, 297(1), 13-17.

[67] Lehmann, V., & Föll, H. (1990). Formation mechanism and properties of electrochemically etched trenches in n-type silicon. Journal of The Electrochemical Society, 137(2), 653-659.

[68] Masuda, H., & Fukuda, K. (1995). Ordered metal nanohole arrays made by a two-step replication of honeycomb structures of anodic alumina. Science, 268(5216), 1466-1468.

[69] Nielsch, K., Choi, J., Schwirn, K., Wehrspohn, R. B., & Gösele, U. (2002). Self-ordering regimes of porous alumina: the 10% porosity rule. Nano letters, 2(7), 677-680.

[70] Föll, H., Carstensen, J., & Frey, S. (2006). Porous and nanoporous semiconductors and emerging applications. Journal of Nanomaterials, 2006.

[71] Föll, H., Langa, S., Carstensen, J., Christophersen, M., & Tiginyanu, I. M. (2003). Pores in III–V semiconductors. Advanced Materials, 15(3), 183-198.

[72] Pettinger, B., Schöppel, H. R., & Gerischer, H. (1976). Electroluminescence at semiconductor electrodes caused by hole injection from electrolytes. Berichte der Bunsengesellschaft für physikalische Chemie, 80(9), 849-855.

[73] Giannuzzi, L. A., & Stevie, F. A. (Eds.). (2005). Introduction to focused ion beams: instrumentation, theory, techniques and practice. Springer.

[74] Melngailis, J. (1987). Focused ion beam technology and applications. Journal of Vacuum Science & Technology B, 5(2), 469-495.

[75] Rubanov, S., & Munroe, P. R. (2004). FIB-induced damage in silicon. Journal of Microscopy, 214(3), 213-221.

[76] Prenitzer, B. I., Urbanik-Shannon, C. A., Giannuzzi, L. A., Brown, S. R., Irwin, R. B., Shofner, T. L., & Stevie, F. A. (2003). The correlation between ion

beam/material interactions and practical FIB specimen preparation. Microscopy and Microanalysis, 9(03), 216-236.

[77] Wirth, R. (2004). Focused Ion Beam (FIB) A novel technology for advanced application of micro-and nanoanalysis in geosciences and applied mineralogy. European Journal of Mineralogy, 16(6), 863-876.

[78] Utke, I., Hoffmann, P., & Melngailis, J. (2008). Gas-assisted focused electron beam and ion beam processing and fabrication. Journal of Vacuum Science & Technology B, 26(4), 1197-1276.

[79] Young, R. J., Cleaver, J. R. A., & Ahmed, H. (1993). Characteristics of gas-assisted focused ion beam etching. Journal of Vacuum Science & Technology B, 11(2), 234-241.

[80] Gates, R. S., & Pratt, J. R. (2012). Accurate and precise calibration of AFM cantilever spring constants using laser Doppler vibrometry. Nanotechnology, 23(37), 375702.

[81] Hutter, J. L., & Bechhoefer, J. (1993). Calibration of atomic-force microscope tips. Review of Scientific Instruments, 64(7), 1868-1873.

[82] Torii, A., Sasaki, M., Hane, K., & Okuma, S. (1996). A method for determining the spring constant of cantilevers for atomic force microscopy. Measurement Science and Technology, 7(2), 179.

[83] Gibson, C. T., Watson, G. S., & Myhra, S. (1996). Determination of the spring constants of probes for force microscopy/spectroscopy. Nanotechnology, 7(3), 259.

[84] Guillon, S., Saya, D., Mazenq, L., Perisanu, S., Vincent, P., Lazarus, A., ... & Nicu, L. (2011). Effect of non-ideal clamping shape on the resonance frequencies of silicon nanocantilevers. Nanotechnology, 22(24), 245501.

[85] Åkesson, H., Smirnova, T., & Håkansson, L. (2009). Analysis of dynamic properties of boring bars concerning different clamping conditions. Mechanical Systems and Signal Processing, 23(8), 2629-2647. [86]

[87] Kittel, C., & McEuen, P. (1976). Introduction to solid state physics (Vol. 8). New York: Wiley.

[88] Giessibl, F. J. (2003). Advances in atomic force microscopy. Reviews of modern physics, 75(3), 949.